

Utah State University

DigitalCommons@USU

All Graduate Theses and Dissertations, Fall
2023 to Present

Graduate Studies

12-2024

Engineered Microalgae Cultivations Systems: Conversion of Wastewater Nutrients Into Biofuels and Bioplastics

Jacob Watkins
Utah State University

Follow this and additional works at: <https://digitalcommons.usu.edu/etd2023>

 Part of the [Biological Engineering Commons](#)

Recommended Citation

Watkins, Jacob, "Engineered Microalgae Cultivations Systems: Conversion of Wastewater Nutrients Into Biofuels and Bioplastics" (2024). *All Graduate Theses and Dissertations, Fall 2023 to Present*. 334.
<https://digitalcommons.usu.edu/etd2023/334>

This Thesis is brought to you for free and open access by the Graduate Studies at DigitalCommons@USU. It has been accepted for inclusion in All Graduate Theses and Dissertations, Fall 2023 to Present by an authorized administrator of DigitalCommons@USU. For more information, please contact digitalcommons@usu.edu.



ENGINEERED MICROALGAE CULTIVATIONS SYSTEMS: CONVERSION OF
WASTEWATER NUTRIENTS INTO BIOFUELS AND BIOPLASTICS

by

Jacob Watkins

A thesis submitted in partial fulfillment
of the requirements for the degree

of

MASTER OF SCIENCE

in

Biological Engineering

Approved:

Ronald C. Sims, Ph.D.
Major Professor

H. Scott Hinton
Committee Member

Richard D. Cutler, Ph.D.
Committee Member

Janis L. Boettinger, Ph.D.
Senior Vice Provost

UTAH STATE UNIVERSITY
Logan, Utah

2024

Copyright © Jacob Watkins 2024

All Rights Reserved

ABSTRACT

Engineered Microalgae Cultivations Systems: Conversion of
Wastewater Nutrients into Biofuels and Bioplastics

by

Jacob Watkins, Master of Science

Utah State University, 2024

Major Professor: Dr. Ronald C. Sims
Department: Biological Engineering

Rotating Algae Biofilm Reactors (RABRs) are a developing microalgae cultivation technology that can be used to recover dissolved Nitrogen and Phosphorus from wastewater. The biomass produced from RABRs treating wastewater can be used to produce fertilizers, soil conditioners, biofuels, and bioplastics. This thesis (1) investigates the effects of four environmental factors on the biomass productivity and phosphorus removal efficiency of a wild microalgae-bacteria biofilm consortia found at Central Valley Water Reclamation Facility (CVWRF) in Salt Lake City, UT, (2) quantifies the biochemical composition and hydrothermal liquefaction product yields of microalgae biomass cultivated using a RABR at the Central Valley Water Reclamation Facility (CVWRF) in Salt Lake City, Utah, and (3) assesses the economic viability of producing bioplastics and biofuels from the same biofilm.

The effects of the four environmental factors (temperature, light intensity, harvesting period, and hydraulic retention time (HRT)) were investigated using a factorial

design which allowed the estimation of the main effects and two-way interaction effects of each factor and factor combination. Three two-way interactions had significant effects on biomass productivity (harvesting period*temperature, harvesting period*light intensity, and light intensity*HRT), and one two-way interaction had a significant effect on phosphorus removal (light intensity*temperature). The main effects of all four factors aligned with literature: increasing light intensity and increasing HRT increased phosphorus removal, and increasing temperature, increasing light intensity, and decreasing HRT increased biomass productivity. The main effects of harvesting period were nonsignificant. Phosphorus removal was exceptionally rapid during the first two days HRT, which may suggest precipitation contributed significantly to phosphorus removal. The optimized conditions identified this study were applied to a 11,400-liter pilot RABR operating at CVWRF and used to help determine operating conditions for use in a full-scale model (600,000 gallons of wastewater per day) of the RABR system.

Techno-economic assessment of upgrading processes for the microalgae biofilm cultivated at CVWRF included three conversion processes: 1) the production of bioplastics, 2) the production of bioplastics with a lipid-extraction pretreatment, and 3) the production of biocrude via hydrothermal liquefaction. Of these processes, the bioplastic production process had the most cost-competitive pricing and the highest carbon and energy efficiency.

PUBLIC ABSTRACT

Engineered Microalgae Cultivations Systems: Conversion of
Wastewater Nutrients into Biofuels and Bioplastics

Jacob Watkins

Dissolved Nitrogen and Phosphorus in wastewater can contribute to harmful algae blooms if released into the environment. One technology that can be used to recover dissolved nutrients from wastewater is the Rotating Algae Biofilm Reactor (RABR), which supports microalgae growth in an easily-harvested biofilm and produces nitrogen- and phosphorus-rich biomass that can be used to produce slow-release fertilizers, biofuels, and compostable bioplastics. This thesis (1) examines the effects of several environmental factors on the biomass production rate and nutrient removal efficiency of RABRs treating municipal wastewater, (2) quantifies the composition and biofuel yields of microalgae biomass cultivated using a RABR at the Central Valley Water Reclamation Facility (CVWRF) in Salt Lake City, Utah, and (3) evaluates the cost of producing biofuels and bioplastics from the same biofilm.

The effects of four environmental factors (temperature, light intensity, harvesting period, and hydraulic retention time) on biofilm growth and phosphorus removal were evaluated using a statistical design that allows the estimation of changes in the effect of each factor in response to the other factors. This study found that the effect of harvesting period on biofilm growth was influenced by temperature and by light intensity, the effect

of light intensity on biofilm growth was influenced by HRT, and the effect of light intensity on phosphorus removal was influenced by temperature. Phosphorus removal could be accounted for primarily by chemical precipitation, with relatively small contributions from direct uptake by the microalgae biofilm. Results from this study were applied to a 11,400-liter pilot RABR operating at CVWRF and used to help determine operating conditions for use in a full-scale model (600,000 gallons of wastewater per day) of the RABR system.

Products like compostable bioplastics, biofuels, and slow-release fertilizers are produced from wastewater-grown microalgae biomass and can be sold to offset wastewater treatment costs. To determine which product should be produced from the algae grown at CVWRF, the biochemical composition and biocrude yields of the CVWRF algae were characterized. Based on this characterization, the technical and economic feasibility of three biomass upgrading processes were selected for evaluation. These processes are (1) the production of bioplastics, (2) the production of bioplastics with a lipid-extraction pretreatment, and (3) the production of biocrude via hydrothermal liquefaction. The production of slow-release fertilizer (dried algae with no further treatment) is also described. Of these processes, the bioplastic production process had the most cost-competitive pricing and the highest carbon and energy efficiency.

ACKNOWLEDGMENTS

I give thanks to my committee members, Richard Cutler, Scott Hinton, and Ronald Sims, and to my family for their support and assistance throughout my educational experience at Utah State University.

Additionally, I give thanks to my many colleagues at the Sustainable Waste-to-Bioproducts Engineering Center who have given me advice and support, namely Jaden Storrer, Clayton Lords, Julissa van Renselaar, Hamza Abdellaoui, Caleb Barton, Abiela Meek Bradley, Elise Barton, Pascal Watson, Joshua Wintch, and Gerald B. Jones. Special thanks go to Pacific Northwest National Laboratory employees Peter Valdez and Yunhua Zhu, who helped tremendously with the techno-economic analysis of bioplastic and biofuel production included in this thesis. Finally, I express my gratitude to the U.S. Department of Energy Bioenergy Technology Office and the Huntsman Corporation Endowed Professorship occupied by Ronald Sims for supporting my research.

Jacob Watkins

CONTENTS

	Page
Abstract.....	iii
Public Abstract.....	v
Acknowledgments.....	vii
Table of Contents.....	viii
List of Tables.....	xii
List of Figures.....	xiii
List of Symbols, Notations, and Definitions.....	xiv
CHAPTER I Introduction and literature review.....	1
1.1 Wastewater reclamation.....	1
1.2 Rotating Algae Biofilm Reactors.....	2
1.3 DE Project EE0009271.....	3
CHAPTER II Effects of light intensity, temperature, harvesting period, and hydraulic retention time on the biomass productivity and nutrient removal efficiency of a native microalgae-bacteria biofilm.....	5
2.1 Abstract.....	5
2.2 Highlights.....	6
2.3 Introduction.....	6
2.4 Methods.....	9
2.4.1 Microalgae inoculum.....	9
2.4.2 RABR design and operation.....	10
2.4.3 Biomass harvesting and quantification.....	13
2.4.4 Nutrient analysis.....	14
2.4.5 Experimental Design.....	15
2.4.6 Statistical analysis.....	16
2.5 Results and Discussion.....	17
2.5.1 Biomass productivity.....	17
2.5.2 Total phosphorus removal.....	25
2.6 Conclusions.....	33
2.7 Acknowledgments.....	33
2.8 Author contributions.....	33

2.9	Funding	34
2.10	Conflicts of interest.....	34
CHAPTER III Compositional analysis and hydrothermal liquefaction of a high-ash microalgae-bacteria biofilm		35
3.1	Abstract	35
3.2	Value of the data.....	36
3.3	Background.....	36
3.4	Data description	37
3.5	Experimental design, materials and methods.....	41
3.5.1	Microalgae feedstock	41
3.5.2	Biofilm moisture content	42
3.5.3	Ash content	42
3.5.4	Hydrothermal Liquefaction.....	43
3.5.5	Elemental Analysis.....	44
3.5.6	Inductively-coupled plasma spectrophotometry	44
3.5.7	Bomb Calorimetry	44
3.5.8	Protein content	45
3.5.9	Lipid Content	45
3.5.10	Carbohydrate content	46
3.6	Author Contributions.....	47
3.7	Acknowledgments	48
3.8	Declaration of competing interests.....	48
3.9	Data availability	48
CHAPTER IV Techno-economic analysis of biofuel and bioplastic production from a high-ash microalgae-bacteria biofilm		49
4.1	Graphical Abstract	49
4.2	Abstract	49
4.3	Keywords	50
4.4	Highlights.....	50
4.5	Introduction.....	51
4.6	Materials and Methods.....	54
4.6.1	Process Inputs and Assumptions for Algae Production	57
4.6.2	Production of Bioplastics	59

4.6.3	Production of Bioplastics with Lipid Extraction	61
4.6.4	Hydrothermal Liquefaction (HTL)	64
4.6.5	Economic Analysis.....	66
4.7	Discussion.....	67
4.7.1	Bioplastic conversion system.....	68
4.7.2	Bioplastic conversion system with lipid extraction pretreatment	70
4.7.3	Hydrothermal Liquefaction.....	71
4.7.4	Sustainability Metrics	74
4.8	Conclusions.....	74
4.9	Funding	75
4.10	Declaration of Competing Interests	76
4.11	Author Contributions	76
CHAPTER V Conclusions.....		78
CHAPTER VI Recommendations for future work		79
6.1	Future research pertaining to Chapter II	79
6.1.1	Bioaugmentation	79
6.1.2	Light intensity	79
6.1.3	Harvesting period.....	80
6.1.4	Hydraulic Retention Time.....	80
6.2	Future research pertaining to Chapter IV.....	80
6.2.1	Production of polyurethanes and high-value lipid products:	80
6.2.2	Treatment of hydrothermal liquefaction aqueous products:	81
References.....		82
Appendixes		94
Appendix A: Statistical design, biomass productivity data, and effluent phosphorus data for Chapter I.....		94
Appendix B: Mineral compositions data for microalgae biofilm and biochar samples.....		98
Appendix C: Techno-economic analysis results for the hydrothermal liquefaction conversion process		99

Appendix D: Considerations for future research based on observations during experimental testing of laboratory RABR productivity	100
Appendix E: Standard Operating Procedures.....	103
E.1 Bomb Calorimetry.....	103
E.2 Parr Pressure Vessel	106
E.3 Hydrothermal Liquefaction.....	109
E.4 Analyzing HTL Products	110
E.5 Lyophilization	111
E.6 Dry Weight - 60°C	112
E.7 Ash Free Dry Weight with a ramp-capable muffle furnace	113
E.8 Ash Free Dry Weight in a non-ramping muffle furnace	114

LIST OF TABLES

	Page
Table 1. Differences in RABR operating conditions between trials.	13
Table 2. Comparison of effluent phosphorus concentrations and TP removal rates	30
Table 3. Contents of the dataset	38
Table 4. Abbreviations used to label samples within the dataset.	39
Table 5. Elemental composition (CHNS-O) and higher heating value (HHV)	40
Table 6. Yield in each phase after hydrothermal liquefaction.....	40
Table 7. Properties of aqueous products obtained after HTL reactions.	41
Table 8. Biochemical composition of biofilm samples.....	41
Table 9. Seasonal averages for daily algae production rate	58
Table 10. Process parameters for the production of bioplastic	61
Table 11. Process parameters for lipid extraction	63
Table 12. Process parameters for HTL conversion	66
Table 13. Economic parameters for analysis	67
Table 14. Microalgae feedstock composition	68
Table 15. TEA results of WW-algae conversion to bioplastic system	69
Table 16. TEA results of WW-algae lipid extraction and bioplastic production system ..	71
Table 17. Conversion sustainability metrics	74
Table 18. Harvest-harvest productivity variations for RABRs in Trial 1.	101

LIST OF FIGURES

	Page
Figure 1. 5-L Rotating Algae Biofilm Reactors.....	11
Figure 2. Two-way interaction plots for microalgae biomass productivity	18
Figure 3. Main effect analysis plots for total biomass productivity and ash-free biomass productivity	20
Figure 4. Interaction plots for the effects of temperature*light intensity.....	26
Figure 5. Main effect plots for effluent phosphorus concentrations, biofilm ash content, and mineral sorption rate	28
Figure 6. Conceptual block diagram for WW-algae conversion to bioplastic system..	60
Figure 7. Conceptual block diagram for the WW-algae lipid extraction and bioplastic production system	63
Figure 8. Conceptual block diagram for WW-algae HTL conversion to biocrude system.....	65
Figure 9. Potential profit margin values for the proposed conversion processes	73

LIST OF SYMBOLS, NOTATIONS, AND DEFINITIONS.

AD	Anaerobic Digester
AFDW	Ash Free Dry Weight
AP	Aqueous Phase
BBOT	25-(Bis(5-tert-butyl-2-benzo-oxazol-2-yl) thiophene
BETO	Bioenergy Technology Office
CHNS-O	Carbon, Hydrogen, Nitrogen, Sulfur, Oxygen
COD	Chemical Oxygen Demand
CVWRF	Central Valley Wastewater Reclamation Facility
DCM	Dichloromethane
DOE	Department of Energy
DTT	Dithiothreitol
DW	Dry Weight
EPS	Extracellular Polymeric Substance
GGE	Gallon Gasoline Equivalent
HHV	Higher Heating Value
HRT	Hydraulic Retention Time
HTL	Hydrothermal Liquefaction
LCA	Life Cycle Analysis
LEA	Lipid-extracted Algae
LHSV	Liquid hourly space velocity
LHV	Lower heating value
MBTH	3-methyl-2-benzothiazolinone hydrazone
MFSP	Minimum Feedstock Selling Price
MGD	Million Gallons per Day
MPaG	Megapascal (Gauge pressure)
MPaA	Megapascal (Absolute pressure)
MPSP	Minimum Plastic Selling Price
NH ₃	Ammonia
ORP	Open Raceway Pond
PBR	Photobioreactor

PLA	Polylactic Acid
PNNL	Pacific Northwest National Laboratory
PPFD	Photosynthetic Photon Flux Density
RABR	Rotating Algae Biofilm Reactor
SPV	Sulpho-phospho-vanillin
SWBEC	Sustainable Waste-to-Bioprocess Engineering Center
TEA	Techno-economic Analysis
TN	Total Nitrogen
TOC	Total Organic Carbon
TP	Total Phosphorus
USU	Utah State University
WRRF	Water Resource Recovery Facility
WSP	Waste Stabilization Pond
WSU	Washington State University
wt%	Weight percent
WW-Algae	Wastewater-grown algae

CHAPTER I

Introduction and literature review

1.1 Wastewater reclamation

High concentrations of nitrogen and phosphorus in wastewater can lead to significant environmental and health problems, including eutrophication of lakes and rivers [1], [2], toxic algae blooms [3], [4], and infant methemoglobinemia [5], [6]. State and federal governments recognize this and have continuously tightened water treatment requirements for decades to address this problem [7]. These increasingly stringent effluent standards require the implementation of expensive reclamation processes, incurring large tax burdens on states and municipalities [8].

To combat the increasing costs of nutrient removal, water reclamation facilities are encouraged to offset nutrient removal costs by upgrading wastewater nutrients into value-added bioproducts [8], [9], [10], [11]. Developing technologies for wastewater reclamation with value-added bioproducts incomprehensively include hydrothermal liquefaction of anaerobic sludge to produce biocrude, soil conditioners, and sterile nutrient media [12], methanotroph cultivation to transform anaerobic digester gas into bioplastic and ectoine [13], [14], [15], and microalgae cultivation to absorb nitrogen and phosphorus and generate protein- or lipid-rich biomass for biofuels [16], [17] and bioplastics [10], [18]. Particularly, the United States Department of Energy has recognized microalgae water reclamation systems as a source of sustainable energy, stating that “inevitably, wastewater treatment and recycling must be incorporated with algae biofuel production” [9]. Microalgae systems are considered a strong candidate for

efficient wastewater valorization because they can couple nitrogen and phosphorus removal with the generation of high-value biomass, which can be used to produce biofuel [11], [19], [20], bioplastic [10], [18], [20], [21], and slow-release fertilizer [21], [22], [23]. These systems can also significantly reduce energy requirements and carbon emissions compared to conventional wastewater reclamation techniques [24] and reduce global phosphorus depletion by redirecting phosphorus away from landfills and water bodies [25], [26], [27].

1.2 Rotating Algae Biofilm Reactors

Photobioreactors (PBRs) used for microalgae cultivation can be categorized into two modes of operation: planktonic PBRs, such as open raceway ponds and tubular photobioreactors, and biofilm PBRs, which promote the growth of microalgae on a solid substratum [28], [29]. Examples of biofilm PBRs include flat-plate PBRs [30], [31], [32], porous substrate PBRs [33], [34], [35], and Rotating Algae Biofilm Reactors (RABRs) [12,16,23,24]. Suspension cultures are currently the most common microalgae cultivation technology for large-scale applications. However, these systems are inherently challenged by high harvesting energy requirements, inefficient land use and nutrient delivery, and low light penetration through liquid media [36], [37].

Biofilm-associated microalgae are differentiated from planktonic microalgae by the production of an extracellular polymeric substance (EPS) matrix of proteins, polysaccharides, nucleic acids, and lipids [38], [39], [40] that bind cells in the biofilm to one another and contain functional groups that help transfer dissolved nutrients to cells from liquid media [41], [42], [43], [44]. These properties lead to faster wastewater reclamation compared to planktonic cultures [45], [46], [47] and facilitate harvesting by

mechanical scraping, which can significantly reduce dewatering energy costs compared to centrifugation or filtration [48]. In addition, biofilm photobioreactors can be designed with a substratum growth area : reactor footprint area higher than 1:1, which contributes to significantly higher areal biomass productivities than those typically achieved in WSPs and ORPs [36], [49]. Considering these advantages, a preliminary economic assessment indicates that biofilm photobioreactors may reduce the total cost of algae cultivation by 8-10 times compared to planktonic cultivation [49].

1.3 DE Project EE0009271

Effective January 1, 2020, the Utah Division of Water Quality requires a Technology-Based Phosphorus Effluent Limit of 1.0 mg/L for all wastewater treatment facilities in the state. Central Valley Water Reclamation Facility (CVWRF) in Salt Lake City, Utah, has been granted a five-year variance to the requirement and is incorporating several processes to meet these effluent requirements by January 2025.

CVWRF is designed to treat 75 million gallons per day (MGD) of municipal wastewater and is the largest wastewater treatment plant in the state of Utah. This facility incorporates an anaerobic digester into its reclamation plan and 0.6 MGD of anaerobic digester effluent is filtered by belt press and recycled to CVWRF headworks. This recycle stream contains approximately 470mg/L total nitrogen, 24mg/L total phosphorus, 50mg/L magnesium, and 92mg/L calcium [22].

CVWRF is currently undergoing renovations to meet the new state water quality guidelines. One added technology (AirPrex) facilitates side stream phosphorus removal by sparging recycled belt press filtrate from anaerobic digestion with nitrogen gas, which removes dissolved CO₂ to increase the pH of the system and encourage struvite

precipitation. Controlled struvite precipitation can remove dissolved ammonium and phosphate and prevent downstream clogging due to nuisance precipitation. Struvite is a mineral with an equimolar ratio of ammonia, phosphorus, and magnesium, and would typically require magnesium supplementation for this process to be successful. However, due to local geography, water at CVWRF is rich in magnesium and additional supplementation is not required. For nitrogen removal, bacteria-based reactors (Annamox) are being considered to convert dissolved ammonia into nitrogen gas.

Pilot-scale Rotating Algae Biofilm Reactors (RABRs) are in operation at CVWRF to test the ability of RABRs to supplement these existing processes by absorbing dissolved nitrogen and phosphorus from recycled anaerobic digester effluent. RABRs facilitate microalgae growth in an attached biofilm, enabling rapid and efficient harvesting by mechanical scraping and reducing microalgae harvesting energy demands by over 90% compared to suspension ponds [50], [51], [52]. This harvested biofilm is typically 12-16% solids content, which is high enough biofuel and bioplastic production without additional dewatering [53], [54], [55]. If CVWRF RABRs operate successfully, the new system will reduce plant energy requirements and generate biomass for the production of bioplastics and biofuel.

To avoid potential issues with contamination, CVWRF RABRs are inoculated with a naturally-forming microalgae-bacteria biofilm collected from the trickling filter aeration windows at CVWRF. This biofilm contains unicellular green algae (*Chlorella*), diatoms (*Nitzschia*, *Navicula*), filamentous green algae (*Ulothrix*, *Klebsormidium*) and filamentous cyanobacteria (*Pseudoanabaena*), and has previously been observed to encourage struvite precipitation in pilot RABR biofilms [22], [56].

CHAPTER II

Effects of light intensity, temperature, harvesting period, and hydraulic retention time on the biomass productivity and nutrient removal efficiency of a native microalgae-bacteria biofilm

2.1 Abstract

Rotating Algae Biofilm Reactors (RABRs) can reduce energy requirements for wastewater reclamation but require further optimization for implementation at wastewater resource recovery facilities (WRRF). Optimizing RABR operation at WRRF is challenging because disregarding interaction terms which involve the constantly-changing environmental conditions at WRRF can lead to incorrect conclusions about RABR behavior. Optimizing RABR operation is challenging because conditions at WRRF change frequently, and disregarding interaction terms related to these changes can produce incorrect conclusions about RABR behavior. This study evaluated the two-way interaction and main effects of four factors (temperature, light intensity, harvesting period, and hydraulic retention time (HRT)) on biomass productivity and phosphorus removal efficiency of a microalgae-bacteria biofilm grown in municipal wastewater, with factor levels and operating conditions selected to mimic a pilot RABR at a WRRF in Utah. The main effects of all four factors aligned with literature: increasing light intensity and increasing HRT increased phosphorus removal, and increasing temperature, increasing light intensity, and decreasing HRT increased biomass productivity. The main effects of harvesting period were nonsignificant, although harvesting period had significant two-way interactions with temperature and light intensity: at high temperature

and low light intensity, the highest biomass productivity was achieved with a 14-day harvesting period, but at medium temperature and high light intensity, the highest biomass productivity was achieved with a 7-day HRT. The two-way interaction light intensity*HRT was also significant: the highest biomass productivity at high HRT occurred at low light intensity, but the highest biomass productivity at low HRT occurred at high light intensity. Phosphorus removal was strongly influenced by LI and occurred most rapidly during the first 2 days HRT, which may suggest precipitation contributed significantly to phosphorus removal. These observations provide insight for further RABR optimization.

2.2 Highlights

- A native microalgae biofilm was cultivated in anaerobic digester centrate
- Two-way interaction and main effects of temperature, light intensity, hydraulic retention time, and harvesting period were studied
- Two-way interactions light intensity*harvesting period, temperature*harvesting period, and light intensity*HRT were significant
- Phosphorus removal rates were consistent with mineral precipitation models

2.3 Introduction

Phosphorus recovery from municipal and agricultural wastewater prevents downstream eutrophication of water bodies and reduces agricultural dependence on finite mineral phosphorus reserves [25]. Microalgae have emerged as a promising technology for economical phosphorus recovery at water resource recovery facilities (WRRF) due to their ability to efficiently absorb dissolved phosphorus and couple wastewater treatment

with the production of valuable bioproducts, such as biofuel, bioplastic, and slow-release fertilizer [22], [57].

Currently, waste stabilization ponds (WSPs) and open raceway ponds (ORPs) are the most common microalgae cultivation methods at WRRF [58]. These systems can be constructed at low cost, but are inherently challenged by high harvesting energy requirements, limited gas exchange, and low light penetration through colored and sediment-rich liquid media [36], [38], [48]. Rotating algae biofilm reactors (RABRs) resolve these issues by cultivating algae in an easily harvestable biofilm, which is periodically submerged in liquid for nutrient absorption and exposed to the atmosphere for direct access to light and carbon dioxide [36]. RABRs demonstrate higher nutrient removal rates than suspension cultures [45], [46] and can be designed with a substratum growth area: reactor footprint area higher than 1:1, which contributes to significantly higher areal biomass productivities than those typically achieved in WSPs and ORPs [36], [49].

However, RABRs are still in the early stages of development, and more research is needed before they can reliably be used for microalgae cultivation [38], [48]. Optimizing RABR operation at WRRF is particularly challenging because disregarding interaction terms which involve the constantly-changing environmental conditions (e.g. temperature, light intensity, etc.) at WRRF may lead to incorrect conclusions about RABR behavior.

Currently, many long-term RABR pilot operations at WRRF cultivate native microalgae-bacteria biofilm communities [22], [59]. Native communities can improve nutrient removal rates and contamination resistance compared to monocultures [60], [61],

but fluctuate in response to environmental conditions [62], [63]. Consequently, as biofilm community compositions change in response to one factor, the optimum values and magnitude of the effects of other factors may change. For example, nutrient concentration (influenced by HRT [64]) can influence community compositions in microalgae biofilms [63], and the optimal light intensity for organisms which dominate a native community in low-nutrient conditions may be higher or lower than the optimal light intensity for organisms which dominate a native microalgae-bacteria community in nutrient-replete conditions.

Biofilm growth dynamics can further complicate interaction terms for these factors: for example, as biofilm growth rate increases in response to temperature, the biofilm may reach its maximum thickness more quickly, decreasing the optimal harvesting period for maximum biomass productivity [65]. However, if increasing temperature also increases the maximum thickness of the biofilm, this effect may reverse, increasing the optimal harvesting period for maximum biomass productivity. Similarly, light penetrates further into the biofilm at higher light intensities. Mathematical models suggest that biofilm thickness is influenced by how far light and nutrients penetrate into the biofilm [66], [67]; therefore, increasing light intensity or decreasing HRT may increase the maximum thickness of a biofilm and consequently influence the effects of temperature and harvesting period on biomass productivity. Alternatively, increasing light intensity excessively may lead to photoinhibition and cell death [68], [69] or promote the growth of biofilm community members which grow more rapidly, but form a thinner biofilm.

Based on the discussion above, light intensity, temperature, HRT, and harvesting period are selected as candidates for potential interaction effects and are investigated in this study. These factors have demonstrated significant effects on biomass productivity or nutrient removal efficiency in previous microalgae-bacteria biofilm studies [29], [63], [64], [70], [71] and have demonstrated interactive effects on the growth dynamics of microalgae grown in suspension [72], [73], but the influence of these interaction effects on the growth of wild-type microalgae-bacteria biofilm cultures is uncertain. Quantification of these interactions will improve our understanding of wild-type microalgae-bacteria biofilm growth dynamics and will allow better optimization of RABR operations at WRRF. Biomass productivity and nutrient removal efficiency are two of the most significant factors affecting the economics of algae biofilm cultivation at WRRF and are selected for further investigation in this study [60], [74], [75].

2.4 Methods

2.4.1 Microalgae inoculum

The microalgae biofilm used in this study was collected from trickling filter aeration windows at Central Valley Water Reclamation Facility (CVWRF) in Salt Lake City, Utah. Hillman et. al determined that this biofilm contains unicellular green algae (*Chlorella*), diatoms (*Nitzschia*, *Navicula*), filamentous green algae (*Ulothrix*, *Klebsormidium*), and filamentous cyanobacteria (*Pseudoanabaena*) [22]. Comprehensive genetic characterization of community members within this biofilm is ongoing: preliminary 16S/18S/23S/ITS sequencing efforts have identified community members from *Chlorella*, *Pleurocapsa*, *Tychonema*, *Stigeoclonium*, *Oedogonium*,

Dictyosphaerium, and *Micractinium*, among others [76]. This inoculum was selected because it is currently being used in pilot studies for sidestream nutrient recovery from a 0.6 million gallons per day (MGD) nutrient recycle stream (anaerobic digester centrate) at Central Valley Water Reclamation Facility (CVWRF), which treats 60 MGD of municipal wastewater in Salt Lake City, Utah [76].

2.4.2 RABR design and operation

RABRs (1 L and 5 L) were constructed by wrapping 4-ply hard duck cotton (Murdock Industrial, Akron, Ohio, USA) around 2" ABS piping to form columns with a total surface area of 300 cm². Columns were attached to steel rods, submerged 40% in undiluted anaerobic digester (AD) centrate, and rotated constantly at 6 rotations per minute. Cotton substratum was used in this study to mimic the pilot RABR at CVWRF as closely as possible. Cotton substratum exhibits significantly higher biomass productivity than other substrates [29], [77] and can be composted after use, but must be replaced every 4-12 months due to biological degradation [51], [77] and is more expensive per square foot than some alternatives.

Inoculation was performed by smearing 10 - 15 ml of trickling filter microalgae over the entire cotton surface of each RABR. Following inoculation, all RABRs were operated for a 3-week homogenization period to increase inter-RABR biofilm homogeneity. During this period, RABRs were operated with 600 $\mu\text{mol photons/m}^2/\text{s}$, a 7-day hydraulic retention time (HRT), and mechanical biofilm harvesting, homogenization with other RABRs, and partial reapplication every 4-7 days. Data collection commenced after completion of the homogenization period. Representative

images of the RABRs used in this study immediately after inoculation and after biofilm formation are provided in Figure 1.



Figure 1. 5-L Rotating Algae Biofilm Reactors immediately after inoculation (left) and after biofilm formation (right).

Untreated anaerobic digester (AD) centrate from CVWRF was used as the nutrient source in this study. This AD centrate contains approximately 470 mg/L total nitrogen, 45 mg/L total phosphorus (TP), 30 mg/L magnesium, and 90 mg/L calcium [22], [78]. HRT was simulated in batch mode: every 2, 4, or 6 days (as specified by the experimental design), the entire AD centrate volume was removed and replaced with fresh centrate from CVWRF. AD centrate was collected every 7 – 14 days from CVWRF and stored in sealed barrels until use. AD centrate samples were collected from each

RABR immediately prior to each media change. Note that average influent phosphorus concentrations measured in this study (Table 1) were 10 - 25 mg/L lower than those reported previously, which may have been due to precipitation during shipping from the WRRF to Utah State University (USU) and storage before treatment with RABRs.

Testing was performed in three trials (Trial 1, Trial 2, and Trial 3). In the first Trial, RABRs were inoculated at the operating temperature determined by the experimental design (10°C, 20°C, or 25°C). However, some differences were seen between RABRs inoculated at the lowest temperature and the other temperatures in this trial, and all RABRs were inoculated at room temperature in the remaining two trials. In addition, RABR volume was increased from 1 L to 5 L after Trial 1 because it was observed that phosphorus was below CVWRF's objective of 15 mg/L for all HRT at the 1-L scale.

At the end of Trial 1 and Trial 2, it was observed that the cotton substratum used for algae growth was significantly softer and more frayed than at the beginning of each Trial. This degradation has been noted in other studies [51], [77], but to our knowledge, interactions between this degradation and other factors had not been previously studied. Therefore, in Trial 3, the cotton belts which were partially degraded in Trial 2 were randomly shuffled and reused in Trial 3. Factor levels and different specifications among the trials are outlined in Table 1.

Table 1. Differences in RABR operating conditions between trials.

Variable	Trial 1	Trial 2	Trial 3
Number of experimental units	81 (3 ⁴)	36 (3 ⁴⁻¹ + 3 ⁴⁻²)	36 (3 ⁴⁻¹ + 3 ⁴⁻²)
Total growth period	50 days	28 days	28 days
Volume	1 Liter	5 Liters	5 Liters
Substratum surface area (cm ²)	300 cm ²	300 cm ²	300 cm ²
Light intensity ($\mu\text{mol photons m}^{-2} \text{s}^{-1}$)	200, 600, 1200	80, 800, 1600	80, 800, 1600
Temperature (°C)	10, 20, 25	10, 20, 30	10, 20, 30
HRT (days)	2, 4, 6	2, 4, 6	2, 4, 6
Average influent [P] (mg TP/L)	31.63	19.35	36.6
Harvesting Period (days)	4, 7, 10	2, 7, 14	2, 7, 14
Inoculation temperature	10°C, 20°C, or 25°C	20°C	20°C
Cotton quality	Fresh	Fresh	Degraded during Trial 1

Light intensity was controlled using full-spectrum dimmable LED grow lights and monitored using an MQ-200X quantum meter (Apogee Instruments, Logan, UT).

Lighting was supplied in a 16 hours on, 8 hours off cycle. Temperature was controlled using a refrigerated temperature control chamber (10°C), radiative heating (20°C and 25°C), and submersible aquarium heaters (30°C). Waterproof sensors were used to continuously monitor water temperature, air temperature, and humidity over the course of the experiment, and box fans were used to keep lights from overheating and maintain constant air exchange for all RABRs except the 10°C and 25°C RABRS in Trial 1, which had passive air exchange. Fans were used for all RABRs in Trial 2 and Trial 3.

2.4.3 Biomass harvesting and quantification

Harvesting was performed by scraping the entire substratum surface area of each RABR with a metal or rubber spatula at the interval specified in the experimental design (2, 4, 7, 10, or 14 days). All biomass was stored at -20°C and dried for at least 48 h at 60°C before quantification.

Quantification of biomass ash content was performed following a previously described ramping protocol (Van Wychen and Laurens, 2016) and reported as *ash content* (wt%) = $(\text{Dry mass after ashing} - \text{tare}) / (\text{Dry mass before ashing} - \text{tare}) \times 100\%$.

Biomass productivity is reported on an ash-free dry weight (AFDW) basis and was calculated using the equation $\text{AFDW biomass productivity (g AFDW/m}^2\text{/day)} = [\text{Total harvested biomass (g DW)} \times (1 - \text{Ash content (wt)})] / [(\text{Growth period (days)} \times \text{Reactor footprint area (100 cm}^2\text{)}]$. Total mineral sorption rate (g ash/m²/day) was calculated by subtracting AFDW biomass productivity (g AFDW/m²/day) from total biomass productivity (g DW/m²/day). Photosynthetic efficiency (g biomass/mol photons) was calculated by dividing AFDW biomass productivity by photosynthetic photon flux density (PPFD, μmol photons/m²/s) and multiplying by the photoperiod (16 hours of light per day). Biomass yield per liter AD centrate (g AFDW/liter AD centrate) was calculated by dividing AFDW biomass productivity by HRT (days / tank volume) and multiplying by reactor footprint area (m²).

Note that biomass productivity and total mineral sorption rate are reported per unit reactor footprint area and not per unit substratum surface area. Conversion between footprint productivity and substratum productivity is performed by dividing footprint productivity by the substratum packing factor, which is approximately 3.14 for the cylindrical RABRs used in this study.

2.4.4 Nutrient analysis

Total phosphorus concentration in each sample was measured using QuikChem Method 10-115-01-3-A (Lachat QuikChem 8500 Series 2 Flow Injection). In this method, organic phosphorus and polyphosphates are simultaneously converted to orthophosphate

by a UV-catalyzed potassium persulfate digestion and a 125°C sulfuric acid digestion, respectively. Orthophosphate is subsequently complexed with ammonium molybdate and antimony potassium tartrate and then reduced by ascorbic acid to form a blue complex. After this color change, the phosphorus concentration is calculated using the sample's measured absorbance at 880 nm and the Beer-Lambert Law.

At the beginning of each analysis run, a series of potassium phosphate monobasic standards were used to generate a calibration curve with points at 10 mg/L, 4 mg/L, 2 mg/L, 1 mg/L, 0.4 mg/L, 0.2 mg/L, 0.1 mg/L, and 0 mg/L. To preserve the integrity of phosphorus data, analysis was halted if the correlation coefficient of the calibration curve was less than 0.9998. Two check standards were analyzed at 30-sample intervals to assess data quality. AD centrate samples were centrifuged at 5000 rpm and filtered through 5.0 µm nylon syringe filters before analysis.

2.4.5 Experimental Design

Experimentation was performed in three trials. In the first trial (Trial 1), a randomized full-factorial experiment was conducted with four factors: 1) light Intensity, 2) temperature, 3) HRT, and 4) harvesting period, each at three levels for a total of $3^4 = 81$ experimental units. One purpose for carrying out this experiment was to determine if there were any significant interaction effects among the experimental factors.

Based on the results of the first trial, a design using 36 experimental units was used in the second and third trials (Trial 2 and Trial 3). This design comprised a randomized 3^{4-1} fractional factorial design (27 experimental units) and a randomized 3^{4-2} fractional factorial design (9 experimental units) to permit the estimation of second order interactions among the experimental factors. This experimental design requires the

assumption that no three-way interactions have significant effects. Separate randomizations were carried out for Trial 2 and Trial 3. Full details of the experimental designs used in this study are available online in Appendix A.

2.4.6 Statistical analysis

Statistical analysis was performed independently for each trial using SAS 9.4 software (SAS Institute, Inc.). The primary method of analysis was fixed effects analysis of variance with graphics to ascertain whether the statistical assumptions of the methodology were met and to characterize and compare the means for different levels of the factors. Analysis of residual plots showed that the data in all three trials was homoscedastic and approximately normal in distribution without any major outliers. Visual analysis of two-way interactions effects was performed using ggplot2 [79] in the R programming language and environment [80]. A significance level of $p=0.05$ was used to aid in the interpretation of main and higher-order interaction effects. In cases where all two-way or three-way interaction terms were nonsignificant ($p>0.05$), interaction terms were removed from the model and analysis was repeated.

2.5 Results and Discussion

2.5.1 Biomass productivity

2.5.1.1 Two-way interaction effects – biomass productivity

Interaction plots for biomass productivity in Trial 2 are presented in Figure 2.

Discounting temperature*harvesting period, no two-way interactions had a statistically significant effect on biomass productivity in either Trial 1 or Trial 3.

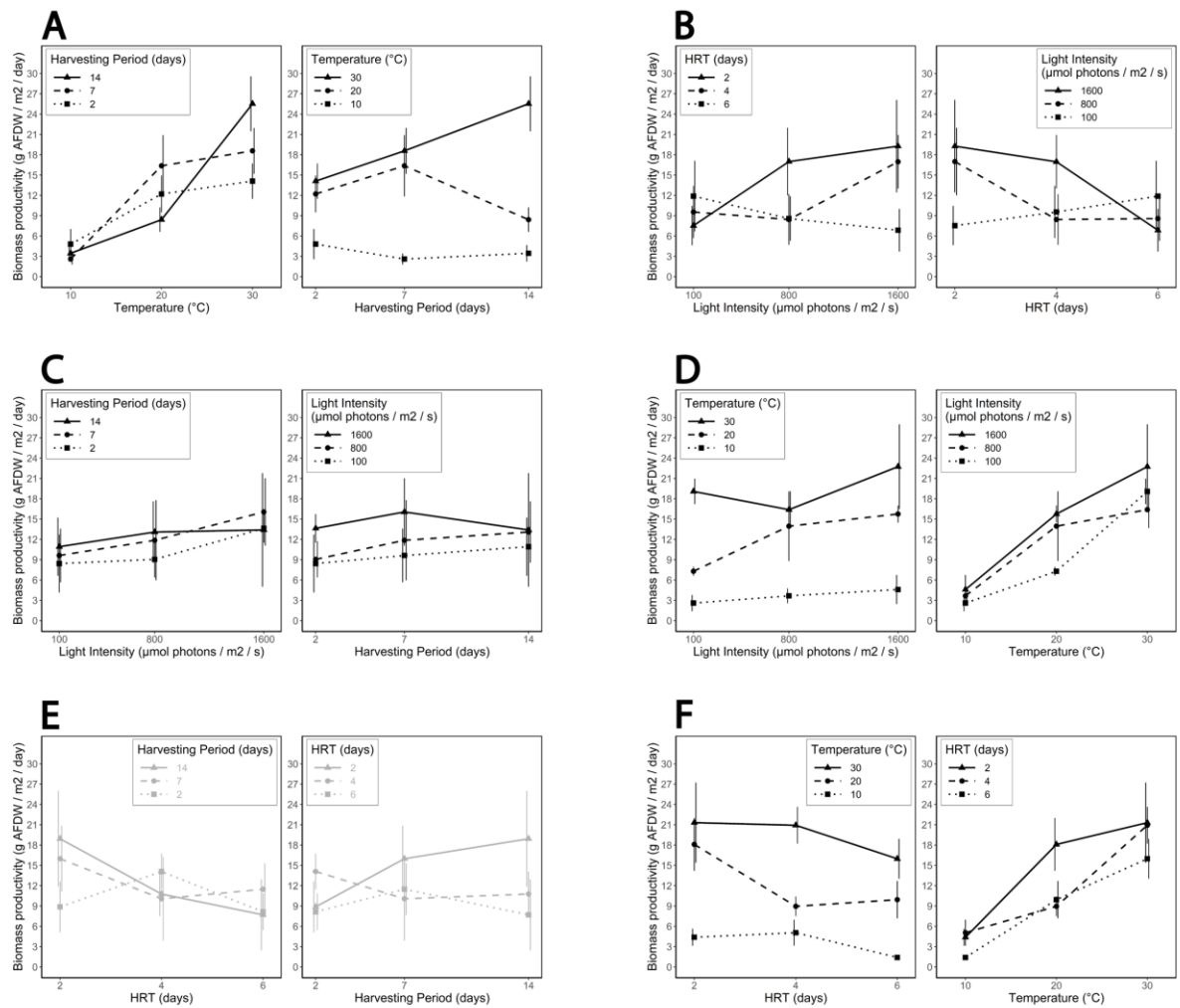


Figure 2. Two-way interaction plots for effects of (A), temperature * light intensity; (B) temperature * HRT; (C), temperature * harvesting period; (D) light intensity * HRT; (E), light intensity * harvesting period; (F), harvesting period * HRT on RABR areal biomass productivity in Trial 2. Line shading represents statistical significance: Black lines: $p < 0.05$, Gray lines: $p > 0.05$. Error bars represent standard error.

Two statistically significant two-way interactions are observed in Figure 2 and caused biomass productivity to increase in ways that differ from phototrophic biofilm growth rates reported for indigestible substrates (e.g. polyethylene, polypropylene, and nylon).

In Figure 2A (harvesting period*temperature), optimal harvesting period increases when temperature (and presumably growth rate) increases. However, microalgae biofilm growth models [66], [67] describe that for biofilms with constant maximum thickness, optimal harvesting period decreases as growth rate increases. To achieve the results seen in this study with a purely autotrophic biofilm, maximum biofilm thickness must increase dramatically in response to increasing temperature and harvesting period. In this case, one potential explanation is that at the highest temperature, the biofilm grew quickly enough to form an aphotic bottom layer before the end of the 14-day harvesting period, which decreased competitive inhibition against cellulolytic microorganisms and increased overall biomass production at the expense of increased cotton degradation.

A similar effect is observed in Figure 2B (light intensity*HRT): typically, RABR productivity is highest with $HRT = 1 - 2$ days [81]. This was observed for RABRs with

800 and 1600 $\mu\text{mol photons/m}^2/\text{s}$, but biomass productivity at 100 $\mu\text{mol photons/m}^2/\text{s}$ was highest with HRT = 6 days. One explanation for this increase is that cellulolytic heterotrophs in the biofilm may have experienced less competitive inhibition from autotrophs and grown more quickly in low light, low nutrient conditions. Effects of nutrient concentration and light intensity on competitive inhibition between phototrophic and heterotrophic organisms have been reported previously [62], [63].

The three remaining statistically significant interaction effects had marginal effects. In Figure 2C (light intensity*harvesting period), the optimal harvesting period is shorter for the highest light intensity (1600 $\mu\text{mol/m}^2/\text{s}$) than for lowest light intensity (100 $\mu\text{mol/m}^2/\text{s}$). However, this effect was small, and it's unclear whether this interaction should be attributed to randomness, to changes in photosynthetic growth kinetics [66], [67], or to an increase in cellulolytic activity in the lower biofilm layers at low light intensities. In Figure 2D (light intensity*temperature), the effect of light intensity is smaller at 10°C compared to 20°C or 30°C. In Figure 2F (HRT*temperature), the effect of HRT appears larger when temperature is higher than 10°C. The final two interactions (HRT*temperature and light intensity*temperature) highlight that when temperature or is too low, microalgae biomass productivity is limited regardless of the other factor levels. In each case, more study is needed before the mechanisms driving the interactions identified in this study can be identified.

2.5.1.2 Main effects – biomass productivity

Apart from harvesting period*temperature and light intensity*HRT, the effects of two-way interactions between factors were marginal compared to the main effects.

Therefore, main effect analysis was considered appropriate and main effect analysis plots for all three trials are presented (Figure 3).

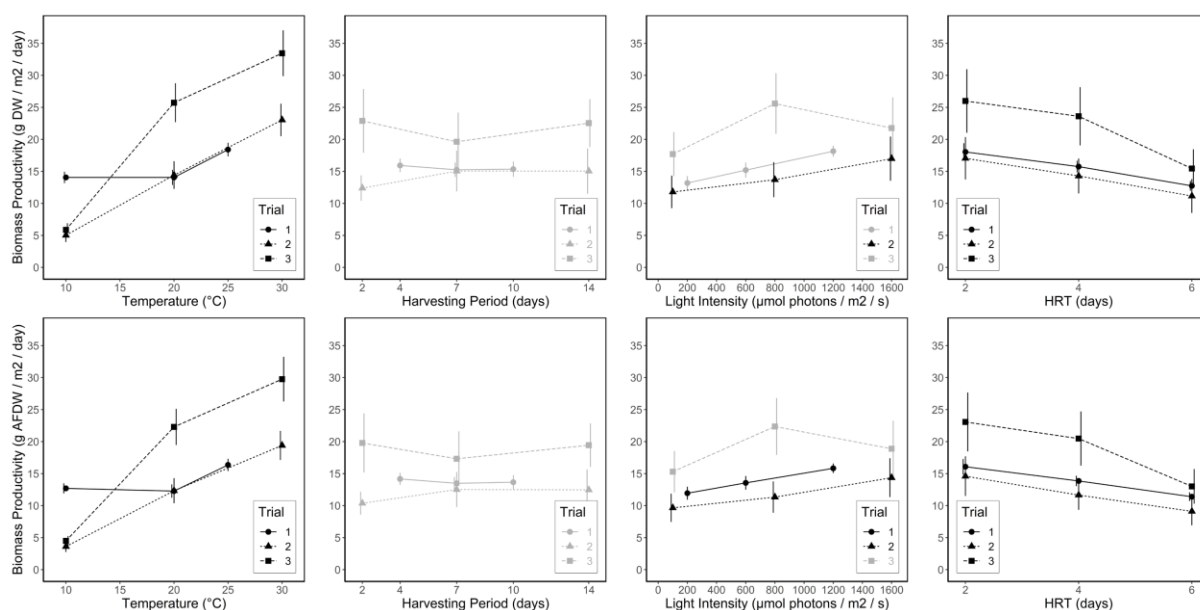


Figure 3. Side-by-side main effect analysis plots for the effects temperature, harvesting period, light intensity, and HRT on total biomass productivity (top row) and ash-free biomass productivity (bottom row) in each trial. Line shading represents statistical significance: Black: $p < 0.05$, Gray: $p > 0.05$. Error bars represent standard error.

Average areal biomass productivity ranged from 3.62 – 29.8 g AFDW/m²/day, which is within the range of areal biomass productivities reported in literature [49]. Average productivity was highest in Trial 3 (partially degraded substratum), followed by Trial 1 (fresh substratum) and then by Trial 2 (fresh substratum). Average productivity in the two trials with fresh substratum (Trial 1 and Trial 2) was similar at 20°C and 30°C but

significantly higher at 10°C in Trial 1. Aside from this difference, average biomass productivities were nearly identical in Trial 1 and Trial 2. Effects of temperature, HRT, and harvesting period on biomass productivity were similar in all three trials, but optimal light intensity was lower in Trial 3 than in the other two trials. No major differences between ash-free biomass productivity and total biomass productivity were observed in any of the three trials.

2.5.1.2.1 Main effect of temperature

Of the four factors evaluated in this study, temperature had the largest effect on biomass productivity. Increasing temperature from 10°C to 25°C (Trial 1) or from 10°C to 30°C (Trial 2 and Trial 3) increased areal biomass productivity from 12.7 to 16.4 g AFDW/m²/day in Trial 1, from 3.62 to 19.4 g AFDW/m²/day in Trial 2 and from 4.5 to 29.8 g/m²/day in Trial 3. Biomass productivity was similar at 20°C and 25°C in Trial 1 and Trial 2 (interpolated), but significantly higher in Trial 1 than Trial 2 at 10°C.

Inoculation method, air circulation rate, and volume were the three largest differences between 10°C RABRs in Trial 1 and Trial 2. Given the similar growth rates at 25°C in Trial 1 (no air circulation) and interpolated productivity at 25°C in Trial 2 (max air circulation), it's unlikely that differences in air circulation rates between Trial 1 and Trial 2 account for the differences in biomass productivity differences at 10°C seen in Figure 3. Similarly, increasing the volume of the media reservoir from 1 L to 5 L had no effect on biomass productivity at 20°C or 30°C and is unlikely to have had a major effect on biomass productivity at 10°C.

Inoculation method differed significantly between Trial 1 and Trial 2 and may account for the difference in biomass productivity at 10°C between the two trials. In Trial

1, RABRs were inoculated and homogenized directly at the temperature specified by the experimental design (10°C, 20°C, or 25°C). However, in Trial 2, all units were inoculated and homogenized at 25°C. Furthermore, RABRs in Trial 2 and Trial 3 were inoculated with microalgae samples that were frozen prior to inoculation, which can have disparate effects on the survival of various species [82]. These two differences may have partially or fully eliminated some psychrotolerant community members in the biofilm, resulting in a lower productivity at 10°C in Trial 2 and Trial 3 compared to Trial 1.

Preliminary 18S rDNA sequencing results for Trial 1 RABRs support this theory: *Micractinium sp.* were among the most abundant species in 10°C and 20°C units but were only sparsely present in 25°C test units in Trial 1 (data in preparation. 10°C: $n=4$; 20°C: $n=5$; 25°C: $n=2$) [76]. *Micractinium sp.* grow relatively quickly at low temperatures and can have growth rates at 10°C similar to the growth rates of some mesophilic organisms growing at 20°C [83]. Given that *Micractinium sp.* was only sparsely present in the 25°C units in Trial 1, it's possible that these psychrotolerant algae were replaced by mesophilic species during the pre-trial homogenization period conducted at 25°C before Trial 2 and Trial 3.

These results suggests that bioaugmentation with psychrotolerant species may reduce winter heating requirements and improve winter biomass productivity at WRRF where heat energy recovery from other processes is not practical. Methods for identifying and isolating biofilm species have been previously reported [59] and may be adapted for the isolation and identification of psychrotolerant species in the CVWRF biofilm. In some cases, it may be possible for WRRF to manage temperature challenges by co-locating RABR units with thermophilic anaerobic digesters and annamox reactors. At

these WRRF, RABR operating temperatures will necessarily remain high year-round and additional measures to circumvent low winter temperatures are unnecessary.

2.5.1.2.2 Main effect of light intensity

The optimal light intensity for microalgae growth varies significantly from species to species and optimal values ranging from 20 $\mu\text{mol photons/m}^2/\text{s}$ to 1600 $\mu\text{mol photons/m}^2/\text{s}$ and higher have been reported [84]. In this study, increasing light intensity from 200 to 1200 $\mu\text{mol photons/m}^2/\text{s}$ (Trial 1) or 100 to 1600 $\mu\text{mol photons/m}^2/\text{s}$ (Trial 2 and Trial 3) increased biomass productivity from 11.9 to 15.8 g AFDW/ m^2/day in Trial 1, from 9.66 to 14.4 g AFDW/ m^2/day in Trial 2, and from 15.3 to 18.9 g/ m^2/day in Trial 3.

Because the effects of light intensity were relatively small, the authors of this paper suggest that substratum surface area: footprint area ratio in large-scale RABRs is optimized for maximum photosynthetic efficiency (g biomass / mol photons) rather than for maximum substratum biomass productivity (g biomass/ m^2 substratum/day). Using this criterion, to justify a 2x increase in light intensity, RABRs must also see a 2x increase in biomass productivity. In this study, increasing light intensity from 200 to 1200 $\mu\text{mol photons/m}^2/\text{s}$ (Trial 1) or 100 to 1600 $\mu\text{mol photons/m}^2/\text{s}$ (Trial 2 and Trial 3) decreased photosynthetic efficiency from 1.03 to 0.22 g biomass/mol photons in Trial 1, from 1.68 to 0.16 g biomass/mol photons in Trial 2, and from 2.66 to 0.21 g biomass/mol photons in Trial 3. The decrease in photosynthetic efficiency at higher light intensity is explained through a combination of several compounding mechanisms, including rapid light attenuation caused by self-shading [65], [85], photosaturation at high light intensities [68], [69], oxygen toxicity at high algal cell densities [86], and photosensitive competition between autotrophic and heterotrophic organisms within the biofilm [62].

Presumably, cellulolytic heterotrophs also contributed significantly to biomass productivity in this biofilm [77], [87].

To reduce costs associated with repeatedly replacing biodegradable substrata, future work should optimize growth at low light intensities using inorganic substrata (e.g. polyethylene, polypropylene, or stainless steel). Based on this results of this study, the potential to supplement mixotrophic biofilm growth on inorganic substrata in low light conditions (e.g. winter conditions) using carbon-rich waste products should also be investigated [87].

2.5.1.2.3 Main effect of harvesting period

The main effect of harvesting period on biomass productivity was not significant in this study and may have been muted by (1) interactions with and temperature (Figure 2A) and light intensity (Figure 2C); (2) mixed culture dynamics, where different biofilm community members dominate growth during late- and early-stage biofilm development [88]; or (3) by minute differences in harvesting intensity between experimental units, which may shift the optimal harvesting period for a given biofilm by several days [66], [67].

Optimal harvesting periods reported for microalgae biofilm cultures are typically between 4 and 8 days for phototrophic biofilms [29], [66], [67], [89]. However, effects of harvesting period on biomass productivity are often small, and several studies have found no statistically significant effects of harvesting period on biomass productivity [90], [91]. In this case, the previously reported 7-day optimum appears in the interaction plot for harvesting period*temperature when $T=20^{\circ}\text{C}$ (Figure 2A) and in the interaction plot for harvesting period*light intensity when light intensity = $1600 \mu\text{mol photons/m}^2/\text{s}$ (Figure

2C). Because the increased growth that was sometimes seen at longer harvesting periods may be linked to increased cotton degradation, harvesting at least every 7 days is recommended for long-term operation of cotton RABRs.

2.5.1.2.4 Main effect of hydraulic retention time

In this study, increasing HRT from 2 days to 6 days decreased AFDW biomass productivity from 16.1 to 13.9 g/m²/day in Trial 1, from 14.6 to 9.11 g/m²/day in Trial 2, and from 23.1 to 13.0 g/m²/day in Trial 3. In terms of water use, HRT had the opposite effect: increasing HRT from 2 to 6 days increased biomass yield per liter from 0.97 to 2.05 g AFDW/L AD centrate in Trial 1, from 0.18 to 0.33 g AFDW/L AD centrate in Trial 2, and from 0.28 to 0.47 g AFDW/L AD centrate in Trial 3. The higher biomass yield per liter in Trial 1 vs. Trial 2 and Trial 3 occurs because reservoir volume was increased from 1 L to 5 L in later trials, increasing the ratio of liquid media to growth substrate by a factor of 5.

Depending on the application, HRT selection can be performed using biomass productivity (g algae/footprint area/day), biomass yield per L (g algae/L nutrient media), or nutrient removal efficiency (mg TP removed/m²/day). For WRRF, biomass production is often a secondary objective, and HRT selection based on nutrient removal efficiency may be more appropriate.

2.5.2 Total phosphorus removal

2.5.2.1 Two-way interaction effects – TP removal

The two-way interaction temperature*light intensity had a statistically significant effect on TP removal in both Trial 2 ($p=0.0063$) and Trial 3 ($p=0.0111$) and is presented

in Figure 4. Similar interactions between light intensity and temperature have been reported previously for microalgae grown in suspension [73], [92].

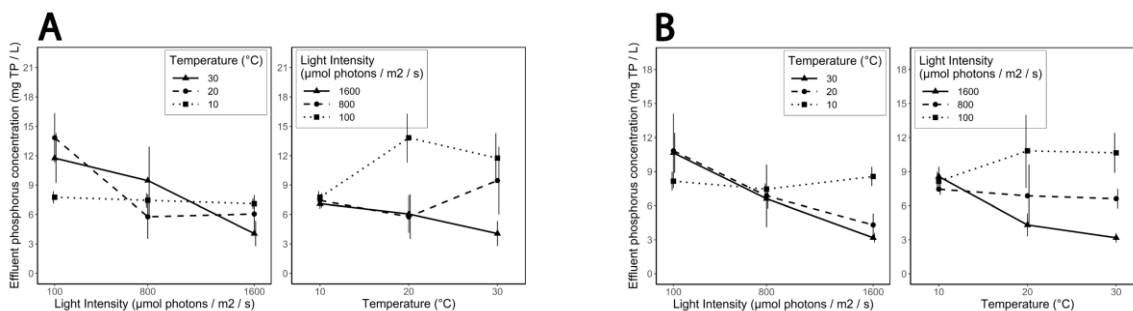


Figure 4. Interaction plots for the effects of temperature*light intensity on effluent total phosphorus concentration in (A) Trial 2 and (B) Trial 3. Line shading represents statistical significance: Black lines: $p < 0.05$, Gray lines: $p > 0.05$. Error bars represent standard error.

The effects of the interaction temperature*light intensity were similar in Trial 2 and Trial 3. At 10°C, biomass growth was severely limited regardless of light intensity (Figure 3). At 20°C and 30°C, biomass growth and photosynthesis were not limited by temperature, and effluent phosphorus concentrations decreased with increasing light intensity. This is most clear in Trial 3 (Figure 4B), as both lines decrease at nearly the same rate over the full range of light intensities. In Trial 2 (Figure 4A), light intensity had the same overall effect, but variation about the mean was large and average effluent TP concentration was lower at 20°C than 30°C for the middle light intensity (800 μmol

photons/m²/s). In both trials, increasing temperature from 10°C to 30°C increased average effluent TP concentration when light intensity was 100 μmol photons/m²/s and decreased average effluent TP concentration when light intensity was 1600 μmol photons/m²/s. This interaction had a much larger effect on effluent TP concentration than on AFDW biomass productivity (Figure 2D), which could be due to an increase in the relative abundance of autotrophic organisms, an increase in photosynthetic activity and pH, or increased phosphorus accumulation at higher light intensities.

2.5.2.2 Main effects – TP removal

Apart from temperature*light intensity, the effects of two-way interactions between factors were marginal compared to the main effects, and main effect analysis was considered appropriate. Previous analysis has determined that precipitation is a major form of nutrient removal for rotating algae bioreactors treating industrial wastewater (36 mg/L influent TP) and municipal wastewater (12 mg/L influent TP) [45]; therefore, plots for ash content and mineral sorption rate are presented alongside effluent phosphorus concentrations in Figure 5.

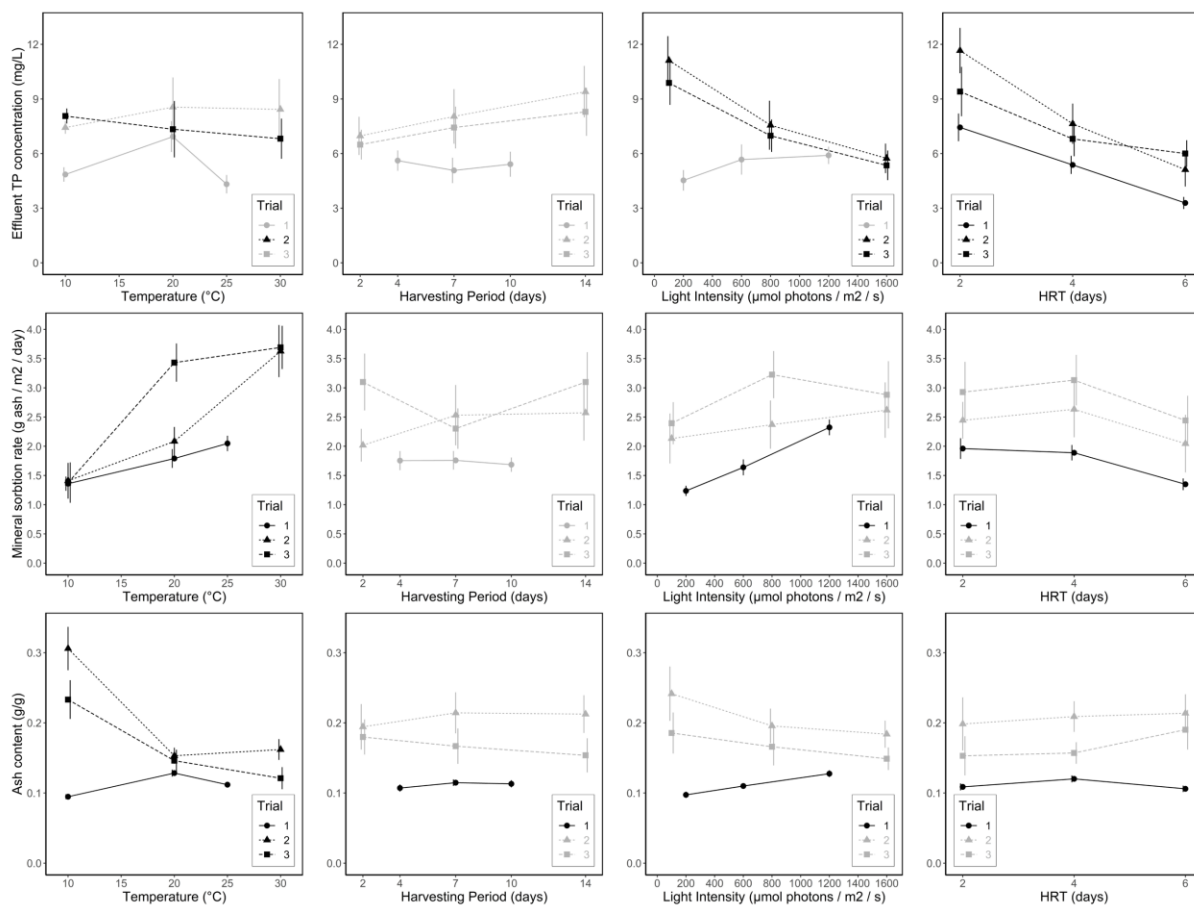


Figure 5. Side-by-side main effect plots for the effects of temperature, harvesting period, light intensity, and HRT on effluent phosphorus concentrations, biofilm ash content, and mineral sorption rate in each trial. Line shading represents statistical significance: Black lines: $p < 0.05$, Gray lines: $p > 0.05$. Error bars represent standard error.

Average effluent phosphorus concentration ranged from 3.29 to 11.7 mg TP/L.

Effluent phosphorus concentrations were lowest in Trial 1 (1-L volume) and approximately equal in Trial 2 and Trial 3 (5-L volume). Average ash content was highest in Trial 2, followed by Trial 3 and then by Trial 1, although total mineral sorption rate was higher in Trial 3 than in Trial 2. Ash content was only marginally affected by harvesting period, HRT, and light intensity, but was significantly influenced by

temperature. Changes in total mineral sorption rate were roughly proportional to changes in biomass productivity.

2.5.2.2.1 Main effect of temperature

The effects of temperature on effluent phosphorus concentration are interesting because decreasing temperature significantly decreased ash-free biomass productivity (and presumably phosphorus consumption and adsorption), but significantly increases phosphorus precipitation and biofilm ash content (g ash / g biofilm). In this case, it appears that these two competing effects were roughly equivalent, and the effect of temperature on effluent phosphorus concentration was marginal. Notably, despite nearly equal effluent phosphorus concentrations, total mineral sorption rate was higher at 30°C than at 10°C. This result implies that a large proportion of precipitated minerals remained in suspension or fell to the bottom of the tank at 10°C. To account for this, large-scale RABR systems treating AD centrate and other high-strength wastewater may benefit from supplementation with clarifiers or other low-cost precipitate recovery technologies.

2.5.2.2.2 Main effect of hydraulic retention time

Increasing HRT from 2 days to 6 days decreased average effluent phosphorus concentrations from 7.44 to 3.29 mg/L in Trial 1, from 11.7 to 5.12 mg/L in Trial 2, and from 9.41 to 6.0 mg/L in Trial 3. Notably, these concentrations were similar in all three trials, despite different volumes, different influent nutrient concentrations, and nearly equal biomass productivities in Trial 1 and Trial 2. Consequently, TP removal rates differed significantly between trials (Table 2).

Table 2. Comparison of effluent phosphorus concentrations and TP removal rates in each trail.

	Influent phosphorus concentration (mg TP/L)	Effluent phosphorus concentration (mg TP/L)			Influent phosphorus concentration (mg TP/m ² substratum)	Phosphorus removal rate (mg TP/m ² /day)		
		HRT = 2 days	HRT = 4 days	HRT = 6 days		Days 0 – 2	Days 2 – 4	Days 4 – 6
Trial 1	31.6	7.44	5.38	3.29	1050	374	34.3	34.8
Trial 2	19.35	11.7	7.64	5.12	3230	638	338	210
Trial 3	36.6	9.41	6.81	6	6100	2270	217	67.5

As shown in Table 2, the highest TP removal rate calculated between day 2 and day 6 was nearly 2x lower than previously reported nutrient removal rates [37] (660 mg TP/m²/day), and the highest calculated rate between day 0 and day 2 was nearly 3x higher. The high initial phosphorus removal rate followed by low removal rates in later periods and the nearly-constant effluent concentrations between trials indicate that precipitation was a major driver of TP removal in this study. AD centrate simulations in Visual MINTEQ [78] and direct measurements [93], [94] confirm that effluent TP concentrations observed in this study could reasonably be achieved primarily through precipitation with relatively small contributions from algal phosphorus consumption.

Currently, the fate of phosphate crystals formed in AD centrate as a result of RABR treatment is unknown. Although crystals can be found in biofilms grown on pilot-scale RABRs [22], these crystals have not been observed in laboratory-scale RABRs [78]. Fine struvite crystals (10 - 100 μ m) can form in AD centrate at pH 8.5 – 9 and be lost in crystallization reactor effluent at low HRT (2 – 11 h / 21 L) [93]; it follows that phosphate crystals of similar size could form in RABRs (which can increase pH to similar levels [22], [78]) and remain suspended when mixing or flow is sufficiently high,

where they could eventually flow out of the reactor. These crystals are too large to pass through the 5.0 μm filters used to prevent equipment clogging prior to phosphorus quantification in this study, but still may contribute to total mineral sorption and shift phosphorus equilibrium toward the liquid phase. Other mechanisms that may explain this decrease in phosphorus removal rate in response to increased HRT include saturation of EPS binding sites within the first two days HRT [44], [45] and metabolic or community changes associated with increased HRT [45], [95].

2.5.2.2.3 Main effect of light intensity

Increasing light intensity from 100 to 1600 $\mu\text{mol}/\text{m}^2/\text{s}$ decreased effluent TP concentrations from 11.10 to 5.74 mg TP/L in Trial 2 and from 9.88 to 5.35 mg TP/L in Trial 3. This optimum value of 1600 $\mu\text{mol}/\text{m}^2/\text{s}$ is significantly higher than the typical optimum light intensities reported for phosphorus removal by suspended cultures (200 to 450 $\mu\text{mol}/\text{m}^2/\text{s}$) [96], but aligns with previous experiments on phosphorus removal by microalgae biofilm reactors [97]. Light intensity directly affects phosphorus removal in two ways: first, increasing light intensity increases biofilm growth and phosphorus uptake per g biomass [86]. Second, increasing light intensity increases the pH of the wastewater by removing dissolved CO_2 during photosynthesis. This pH change decreases the solubility of phosphorus-containing minerals like hydroxyapatite and struvite, which can improve phosphorus removal from solution and increase the total amount of minerals sorbed to the biofilm [22], [78], [97]. Further research is needed to quantify the relative contributions of pH-induced nutrient precipitation, nutrient sorption, and direct uptake into biomass on phosphorus removal from AD centrate by RABRs. In addition, large-scale RABRs are likely to have a higher ratio of surface area to footprint area (packing

factor) than cylindrical RABRs, leading to increased light dilution compared to the RABRs used in this study. Decreased light intensity is associated with higher porosity in algae biofilms [71], which may improve nutrient removal and biomass productivity by allowing better access to nutrients or by increasing the biofilm surface area available for nutrient sorption. More research is needed to optimize RABR packing factor for maximum biomass productivity and phosphorus removal.

2.5.2.2.4 Main effect of harvesting period

Harvesting period had a small, nonsignificant effect on phosphorus removal in Trial 2 and Trial 3: decreasing harvesting period from 14 days to 2 days decreased average effluent phosphorus concentration from 9.40 to 6.97 mg/L in Trial 2 and from 8.29 to 6.49 mg/L in Trial 3. This effect may be related to the crystal redissolution effect discussed in section 3.2.3.3: TDS are separated from the AD centrate more frequently for shorter harvesting periods, which drives crystallization equilibrium toward the solid phase and reduces the concentration of dissolved phosphorus. However, this effect was small and nonsignificant, and investigating this effect further was beyond the scope of this study. Other dynamics that may explain this effect include differences in community composition in response to harvesting period [22], differences in the ratio of cells to EPS as the biofilm progresses through different stages of growth [89], and random variation between units.

2.6 Conclusions

The novelty of this research lies in the quantification of two-way interactions between temperature, harvesting period, hydraulic retention time, and light intensity in regards to the biomass productivity and phosphorus removal efficiency of wild-type microalgae-bacteria biofilms grown in municipal wastewater. Major findings include positive identification of two-way interactions harvesting frequency* temperature, harvesting period*light intensity, and light intensity*HRT and a strong implication that precipitation is the major driver of nutrient removal from untreated anaerobic digester effluent by rotating algae biofilm reactors.

2.7 Acknowledgments

The authors would like to acknowledge the support of Central Valley Water Reclamation Facility, WesTech Engineering, Inc., the Sustainable Waste to Bioproducts Engineering Center (SWBEC), and Dr. Foster Agblevor for the generous access to laboratory facilities, infrastructure, and ongoing support. Biological engineering students Abby Lamborn, Adam Martin, Amanda Moravek, Anna Scribner, Carson Miller, Coldon Malan, Elise Barton, Ellie Siddoway, Emma John, Ethan Rico, Hamza Abdellaoui, Jaden Storrer, Joshua Wintch, Kade Fish, Laurent Saysanavong, Parker Goldsberry, and Shaylynn Cannon and mathematics student Gerald Jones are acknowledged for their supporting functions and technical discussions.

2.8 Author contributions

Jacob D. Watkins: Conceptualization, Methodology, Software, Data curation, Formal analysis, Investigation, Project administration, Supervision, Visualization,

Writing – original draft, Writing – review and editing; **Clayton Lords**: Methodology, Investigation, Data curation, Writing – Original draft, Writing – review and editing, Supervision; **Abiela Meek Bradley**: Investigation, Software, Writing – Original draft, Project administration, Supervision; **D. Richard Cutler**: Conceptualization, Methodology, Software, Validation, Formal analysis, Writing – original draft, Writing – Review and Editing; **Ronald C. Sims**: Conceptualization, Methodology, Writing – Review and editing, Funding acquisition, Resources. All authors have approved the final manuscript.

2.9 Funding

This research was funded by the U.S. Department of Energy Bioenergy Technology Office (BETO) under award number DE-EE0009271. BETO was not involved in the study design; in the collection, analysis and interpretation of data; in the writing of the report; or in the decision to submit the article for publication. Laboratory space and supplemental funding for operation of the Algae Processing and Products facility and laboratory operations of the BioInnovations building were provided by the Utah State University Sustainable Waste-to-Bioprocess Engineering Center and the Huntsman Corporation Endowed Professorship occupied by Dr. Ronald C. Sims.

2.10 Conflicts of interest

The authors declare no conflict of interest.

CHAPTER III

Compositional analysis and hydrothermal liquefaction of a high-ash microalgae-bacteria biofilm

3.1 Abstract

This chapter describes biochemical composition data and hydrothermal liquefaction (HTL) yield results for a high-ash microalgae biofilm which was cultivated in effluent from a mesophilic anaerobic digester using rotating algae biofilm reactors (RABRs). These data are available online [98] and were originally collected for use in a techno-economic analysis of biocrude, biodiesel, and bioplastic production from algae that was cultivated using RABRs for municipal wastewater reclamation.

Biochemical data for the microalgae biomass includes bulk protein, measured both using the Bradford protein assay and by multiplying total N; carbohydrate content, measured using a 3-methyl-2-benzothiazolinone hydrazone / dithiothreitol (MBTH/DTT) assay; total lipid content, measured using a sulpho-phospho-vanillin method; hexane-extractable lipid content, measured by mass difference after extraction with methanol and hexane; ash content, measured by mass difference after incineration at 550°C; moisture content of the harvested biofilm slurry, measured by mass difference after drying at 60°C, mineral composition, measured using an inductively-coupled plasma spectrophotometer; higher heating value, measured using a bomb calorimeter; and CHNS-O elemental composition, measured using an elemental analyzer.

Data reported for the HTL product phases include mass yields for each phase (solid, aqueous, biocrude, gas); higher heating value of the biocrude phase, measured using a bomb calorimeter; elemental composition of the biocrude phase, measured using

an elemental analyzer; and chemical properties of the aqueous phase, including pH, chemical oxygen demand (COD) (HACH method 8000), total nitrogen (TN) (HACH method 10208), total ammonia (NH₃) (HACH method 10301), total phosphorus (TP) (HACH method 10209/10210), and total organic carbon (TOC) (HACH method 10267).

Currently, the effects of ash composition and HTL heating rate on biocrude yields and on N and P partitioning into biocrude, aqueous, and solid phases are not clearly defined. Models used to predict biocrude yields after HTL of microalgae are commonly trained using data collected from numerous studies. This dataset contains the feedstock composition data and ramp rate data necessary to help define the effects of ash content on biocrude yields after HTL and can be reused to help train yield-prediction models for the HTL of microalgae and other feedstocks.

3.2 Value of the data

- This dataset contains microalgae mineral composition data and reports heating ramp rates, both of which are not always reported in microalgae hydrothermal liquefaction studies.
- This dataset can help determine the extents to which ash composition and heating rate affect biocrude yield and HTL process water quality.
- This dataset can be used to help train yield-predictive models for the hydrothermal liquefaction of microalgae biomass.

3.3 Background

This dataset was collected for use in a techno-economic analysis (TEA) study evaluating the economic and technical feasibility of biocrude and bioplastic production

from a microalgae biofilm used for nutrient recovery from municipal anaerobic digester centrate and is presented separately to avoid unnecessarily detracting from the primary focus of the TEA [76], [99]. Quantification of protein, lipid, carbohydrate, and ash content was necessary prior to testing bioplastic production to ensure that the microalgae feedstock would not harm the equipment used in bioplastic production tests.

Quantification of the extractable lipid portion was performed to assess the feasibility of co-producing lipid and bioplastic products from the microalgae feedstock.

Characterization of heavy metals and minerals was performed to ensure that the final compostable bioplastic product and the solid phase leftover after hydrothermal liquefaction (HTL) of the microalgae biomass did not exceed land application toxicity limits set by the United States Environmental Protection Agency. HTL testing was performed to estimate biocrude yields for the feedstock assessed in the study and to determine which temperature to use when building process models for the TEA.

Characterization of the HTL aqueous phase was performed to determine treatment requirements for the aqueous recycle stream.

3.4 Data description

The dataset [98] documents the biochemical and elemental composition of a microalgae biofilm community cultured in untreated anaerobic digester centrate using polyethylene Rotating Algae Biofilm Reactors (RABRs), along with product yields measured after HTL of the same microalgae biofilm samples. The elemental composition of the dataset includes an analysis of heavy metals and trace elements in the biofilm and biochar. The dataset is provided in an Excel spreadsheet on separate sheets. The contents

of the dataset are outlined in Table 3 and summarized below as mean \pm standard deviation.

Table 3. Contents of the dataset

Sheet number	Sheet	Contents
1	Contents	Table of Contents
2	Ultimate_analysis	CHNS data for microalgae biofilm samples and biocrude produced after hydrothermal liquefaction of the biofilm samples
3	ICPS_analysis	Al, As, B, Ba, Ca, Cd, Co, Cr, Cu, Fe, K, Mg, Mn, Mo, Na, Ni, P, Pb, S, Se, Si, Sr, and Zn data for microalgae biofilm samples and biochar samples produced after hydrothermal liquefaction of the biofilm samples
4	HTL_product_yields	Mass in biocrude, solid, and gaseous phases after hydrothermal liquefaction of the biofilm samples
5	Aqueous_phase_analysis	Total nitrogen, total ammonia, total organic carbon, pH, and chemical oxygen demand measured in aqueous phase after hydrothermal liquefaction of the biofilm samples
6	Biochemical_analysis	Protein, lipid, carbohydrate, ash, HHV, and moisture content of the biofilm samples, ash content and HHV of biocrude samples

Biomass samples and products collected after HTL reactions are labelled using the following notation: [biomass source] [HTL product phase] [HTL reaction temperature], where biomass cultivated using either a laboratory RABR (L), pilot RABR (P), or harvested directly from trickling filters at Central Valley Water Reclamation Facility (T); phase is either biomass, biocrude, biochar, gas, or aqueous (Aqueous Phase, AP), and reaction temperature is either 280°C or 350°C. For example, biocrude collected after HTL of biomass cultivated using a laboratory RABR is labelled “L_biocrude_280” for an HTL reaction temperature of 280°C and “L_biocrude_350” for an HTL reaction temperature of 350°C. For biomass samples that have not been subject to an HTL reaction, HTL reaction temperature is not applicable and samples are simply labelled

“L_biomass,” “P_biomass,” or “T_biomass”. These abbreviations and their definitions are listed in Table 4 and on sheet labelled “Contents” in the dataset file.

Table 4. Abbreviations used to label samples within the dataset and throughout this document.

Term	Definition
L_biomass	Biomass harvested from a laboratory-scale Rotating Algae Biofilm Reactor (10-L volume)
P_biomass	Biomass harvested from a pilot-scale Rotating Algae Biofilm Reactor (11,400-L volume)
T_biomass	Biomass harvested from trickling filters at Central Valley Water Reclamation Facility in Salt Lake City, Utah
L_biocrude_280	Biocrude produced by hydrothermal liquefaction of L_biomass at 280°C
L_biocrude_350	Biocrude produced by hydrothermal liquefaction of L_biomass at 350°C
P_biocrude_280	Biocrude produced by hydrothermal liquefaction of P_biomass at 280°C
P_biocrude_350	Biocrude produced by hydrothermal liquefaction of P_biomass at 350°C
L_biochar_280	Solid products produced by hydrothermal liquefaction of L_biomass at 280°C
L_biochar_350	Solid products produced by hydrothermal liquefaction of L_biomass at 350°C
P_biochar_280	Solid products produced by hydrothermal liquefaction of P_biomass at 280°C
P_biochar_350	Solid products produced by hydrothermal liquefaction of P_biomass at 350°C
L_AP_280	Aqueous products produced by hydrothermal liquefaction of L_biomass at 280°C
L_AP_350	Aqueous products produced by hydrothermal liquefaction of L_biomass at 350°C
P_AP_280	Aqueous products produced by hydrothermal liquefaction of P_biomass at 280°C
P_AP_350	Aqueous products produced by hydrothermal liquefaction of P_biomass at 350°C

Elemental compositions data (CHNS-O) and higher heating values for biomass and biocrude samples are summarized in Table 5. Elemental compositions data is provided in the sheet labelled “Ultimate_analysis” in the dataset file. This sheet includes CHNS data measured by ultimate analysis, and the summary table additionally includes oxygen content (O), calculated by mass difference, and higher heating values. Higher heating value data are provided in the sheet labelled “Biochemical_analysis”.

Table 5. Elemental composition (CHNS-O) and higher heating value (HHV) of biofilm samples and biocrude samples collected after hydrothermal liquefaction at 280°C and 350°C.

	Nitrogen	Carbon	Hydrogen	Sulfur	Oxygen*	HHV (MJ/kg)
L_biomass	6.12 ± 0.15	52.15 ± 2.43	6.51 ± 0.18	0.63 ± 0.07	24.73 ± 2.21	16.7
L_biocrude_280	6.7 ± 0.2	74.05 ± 2.03	8.31 ± 0.13	1.01 ± 0.13	5.19 ± 1.8	33.26 ± 0.17
L_biocrude_350	6.46 ± 0.34	79.88 ± 1.43	8.64 ± 0.79	0.7 ± 0.05	3.69 ± 1.57	36.27 ± 0.06
P_biomass	4.01 ± 0.06	26.29 ± 0.29	4.41 ± 0.07	0.54 ± 0.01	26.15 ± 0.39	11.8 ± 0.2
P_biocrude_280	3.89 ± 0.35	72.48 ± 1.97	9.6 ± 0.33	0.37 ± 0.06	12.79 ± 1.89	36.59 ± 1.34
P_biocrude_350	3.97 ± 0.29	72.66 ± 2.34	9.62 ± 0.09	0.24 ± 0.1	12.44 ± 2.36	36.96 ± 1.04

*by mass difference

Mineral compositions data for biofilm samples and biochar samples, including Al, As, B, Ba, Ca, Cd, Co, Cr, Cu, Fe, K, Mg, Mn, Mo, Na, Ni, P, Pb, S, Se, Si, Sr, and Zn data, are provided in the sheet labelled “ICPS_analysis” and summarized in Appendix B. Product yields obtained after HTL at 280°C and 350°C are provided in the sheet labelled “HTL_product_yields” and summarized in Table 6. Data on the properties of aqueous products obtained after the HTL reactions are provided in the sheet labelled “Aqueous_phase_analysis” and are summarized in Table 7. Data on the biochemical composition of the laboratory and pilot biofilm samples, including protein, ash, lipid, and carbohydrate content, are provided in the sheet labelled “Biochemical_analysis” and are summarized in Table 8.

Table 6. Yield in each phase after hydrothermal liquefaction, dry basis

	HTL reaction temperature	Biocrude	Gas	Solid	Aqueous*
L_biomass	280°C	28.67 ± 1.78	7.75 ± 1.32	17.59 ± 3.4	45.98
L_biomass	350°C	30.03 ± 1.26	9.88 ± 0.5	14.75 ± 3.47	45.33
P_biomass	280°C	12.74 ± 1.53	4.41 ± 0.69	43.4 ± 2.82	39.45
P_biomass	350°C	13.99 ± 1.04	4.8 ± 0.03	43.69 ± 4.41	37.52

Table 7. Properties of aqueous products obtained after HTL reactions.

	Temperature	pH	TN (mg / L)	NH ₃ (mg / L)	TOC (mg / L)	COD (mg / L)
L_biomass	280°C	8.2 ± 0.14	1836.5 ± 564.98	847.8 ± 138.31	8262 ± 1926.16	28750 ± 565.69
L_biomass	350°C	8.4	4428 ± 25.46	826	6030 ± 25.46	24300 ± 1909.19
P_biomass	280°C	8.07 ± 0.25	5726.67 ± 315.65	1809.17 ± 335.19	5820 ± 1460.72	18510 ± 4656
P_biomass	350°C	8.23 ± 0.06	14613.33 ± 3279.59	2317.5 ± 627.56	5670 ± 450.44	19800 ± 1273.15

Table 8. Biochemical composition of biofilm samples harvested from laboratory- and pilot-scale RABRs.

Characteristic (wt%, dry basis)	L_biomass	P_biomass	T_biomass
Protein (N * 6)	36.66 ± 0.97	24.09 ± 0.35	-
Protein (N * 4.78)	29.21 ± 0.77	19.19 ± 0.28	-
Protein (Bradford method)	14.37 ± 3.08	7.93 ± 3.52	12.41 ± 4.27
Extractable lipid content (chloroform/methanol)	7.40 ± 1.22	9.63 ± 0.97	9.66 ± 2.54
Extractable lipid content (hexane/methanol)	-	2.45 ± 0.02	-
Carbohydrate (MBTH/DTT method)	31.43 ± 6.47	10.69 ± 1.27	20.42 ± 6.66
Ash	9.99 ± 1.19	38.6 ± 3.87	18.26 ± 6.22

3.5 Experimental design, materials and methods

3.5.1 Microalgae feedstock

The biofilm consortium used as the inoculum in this study was collected from trickling filter aeration windows at Central Valley Water Reclamation Facility (CVWRF) in Salt Lake City, Utah. Ongoing 16S/18S/23S/ITS rRNA characterization of this biofilm consortium [76] has identified community members from *Chlorella*, *Pleurocapsa*, *Tychonema*, *Stigeoclonium*, *Oedogonium*, and Nostocales, among others. This consortium was cultivated using a 11,400-liter polyethylene Rotating Algae Biofilm Reactor (RABR)

operating in untreated anaerobic digester effluent at CVWRF and in 10-L RABRs under constant artificial lighting (500 $\mu\text{mol}/\text{m}^2/\text{s}$) at 25°C in Logan, Utah. This anaerobic digester effluent contains approximately 500 mg/L total Kjeldahl nitrogen, 50 mg/L total phosphorus (TP), and 25 mg/L magnesium. Hillman et. al [22] and Goldsberry et al. [78] found that as the 11,400-liter pilot RABR at CVWRF rotates, struvite precipitates from anaerobic digester centrate and collects in the biofilm. In a previous work, we found that phosphorus concentrations in the anaerobic digester effluent used for microalgae cultivation were reduced to 20-30 mg/L after shipping to laboratory RABRs in Logan, Utah, possibly by natural precipitation of supersaturated nutrients in the untreated anaerobic digester effluent (See Chapter II). Biomass samples harvested from the pilot RABR at CVWRF for use in this study were collected in spring and winter 2022. All biomass samples collected in this study were harvested by manual scraping and frozen after harvesting.

3.5.2 Biofilm moisture content

Moisture content in the biofilm samples was measured by drying samples at 60°C until constant weight, as described by Van Wychen and Laurens [100]. Solids content is reported as *solids content (wt%) = (mass after drying (g) – tare) / (mass before drying (g) – tare)*.

3.5.3 Ash content

Ash content in biofilm and biocrude samples was measured by incinerating samples at 550°C for 180 minutes, as described by Van Wychen and Laurens [100]. Briefly, dried biomass samples were heated to 105°C and held for 12 minutes, ramped to

250°C at 10°C/min and held for 30 minutes, ramped to 575°C at 20°C/minute and held for 180 minutes, and then cooled to 105°C and held until samples were removed and weighed. Ash content is reported as *ash content (wt%) = (mass after incinerating (g) – tare) / (mass before incinerating (g) – tare)*.

3.5.4 Hydrothermal Liquefaction

HTL experiments were performed in batch mode using a 500 ml stirred-tank pressure reaction chamber (Parr Instruments, Moline, IL, USA) under a nitrogen atmosphere. First, 30 g dry microalgae were resuspended in distilled water (15% w/w) and added to the pressure chamber at 20°C. The chamber was sealed, sparged and pressurized to 2.0 MPaG with nitrogen, and heated at 7°C / min to the pre-selected reaction temperature (280°C or 350°C). After incubation for 15 minutes at the reaction temperature, the vessel was cooled to 20°C by an internal water coil and the final pressure was recorded. Yield in the gas phase was calculated by pressure difference using the ideal gas law. After venting, the remaining products were rinsed from the pressure vessel with dichloromethane (DCM) and filtered through tared 1.6 µm Whatman filter paper to separate the solid products. After filtration, the biocrude and aqueous phases were separated in a separatory funnel. Yield in the biocrude phase was recorded after vacuum distillation at 40°C for DCM recovery and subsequent drying at 60°C for 12 hours. Yield in the aqueous phase was calculated by mass difference. Aqueous products were characterized using HACH kits to measure chemical oxygen demand (HACH method 8000), total nitrogen (HACH method 10208), total ammonia (HACH method 10301), total phosphorus (HACH method 10209/10210), and total organic carbon

(HACH method 10267). pH was measured using an Orion 8102BNUWP Ross Ultra Combination pH probe (Thermo Scientific Inc, Waltham, MA, USA).

3.5.5 Elemental Analysis

Elemental analysis (CHNS-O) of the dried biofilm and biocrude samples was conducted using a Flash 2000 CHNS-O analyzer (Thermo Scientific Inc, Waltham, MA, USA) as previously described [101]. Briefly, a five-point calibration curve was generated and validated using a 25-(Bis(5-tert-butyl-2-benzo-oxazol-2-yl) thiophene (BBOT) standard (carbon: 72.53%, hydrogen: 6.09%, nitrogen: 6.51%, oxygen: 7.43%, and sulfur: 7.44%). Sample analysis was conducted as follows; 2-3 mg of sample was loaded into a tared tin capsule then loaded into the multi-sample holder. Once the sample was dropped into the quartz reactor (kept at 950°C), the gases produced from its combustion were analyzed using a thermal conductivity detector. Each sample was analyzed in triplicates. The oxygen content was calculated by difference as *Oxygen (wt. %, dry basis) = 100 – Carbon – Hydrogen – Nitrogen – Sulfur – Ash*.

3.5.6 Inductively-coupled plasma spectrophotometry

Analysis of minerals and other elements in the dried biofilm and biochar samples was performed by Utah State University Analytical Laboratories using an inductively-coupled plasma spectrophotometer (Thermo Electron iCAP ICP).

3.5.7 Bomb Calorimetry

Higher heating value (HHV) was measured using an IKA Model C2000 basic bomb calorimeter (IKA Works, Inc., Wilmington, NC, USA). Briefly, 0.5 g samples were loaded into a stainless steel crucible and combusted in a type 2 stainless steel vessel. Acid

correction was performed after combustion by titrating bomb washings with a standard sodium carbonate solution.

3.5.8 Protein content

Protein content was measured using the Bradford assay [102], [103] and estimated from elemental compositions data using a conversion factor of nitrogen * 4.78 [104]. Biomass samples were digested prior to the Bradford reaction by suspending samples in 0.5 M sodium hydroxide, sonicating for 10 minutes in a 40 kHz ultrasonic water bath (Branson 1510, Branson Ultrasonics Corp., Danbury, CT, USA), incubating at 80°C for an additional 10 minutes, and then centrifuging to remove any residual biomass. Protein concentration in the supernatant was estimated by reacting 50 µL sample with 150 µL Bradford Reagent for 5 minutes and comparing absorbance at 595 nm to a bovine serum albumin standard.

3.5.9 Lipid Content

Lipid content was measured using a colorimetric method based on the sulpho-phospho-vanillin (SPV) reaction [105] and gravimetrically after extraction with methanol and hexane [106], [107]. In the SPV method, lipids were first extracted from dry biomass samples using a 2:1 v/v chloroform: methanol extraction. This reaction was performed at room temperature with an extraction ratio of 1 mg dry biomass: 2 ml solvent: 1.5 ml 0.9% NaCl solution. After the extraction, 0.5 ml of the chloroform/lipid phase was transferred to a clean test tube, heated uncapped at 90°C to evaporate the chloroform, and reacted with 100 µL of 98% sulfuric acid at 90°C for 10 minutes. After this reaction, samples were cooled to room temperature, mixed with 2.4 ml of SPV reagent, and

incubated at room temperature for another 10 minutes to allow color development before measuring absorbance at 530 nm. Lipid content was estimated by comparing samples to a standard curve prepared using canola oil. The SPV reagent used in this reaction was prepared by dissolving 750 mg vanillin in 125 ml DI water and 500 ml 85% phosphoric acid.

To quantify hexane/methanol extractable lipids, lipids were first extracted by sonicating 100 mg dry algae in 1 ml of 1:1 v/v hexane: methanol for 15 minutes at 40 kHz and then incubating at room temperature for 1 hour and 45 minutes in a rocking incubator. After incubating, samples were centrifuged for 10 minutes at 12,000 x g and the solvent layer was transferred to a clean tube. Distilled water was added to separate the methanol and hexane layers, and the upper hexane/lipid layer was aspirated into a clean pan and heated at 60°C to evaporate the hexane before weighing. Hexane extractable lipids were recorded as hexane extractable lipids (wt%) = mass in hexane phase (mg) / original mass (mg).

3.5.10 Carbohydrate content

Carbohydrates were measured using a colorimetric 3-methyl-2-benzothiazolinone hydrazone / dithiothreitol (MBTH / DTT) assay [108]. First, MBTH and DTT stock solutions were prepared by dissolving 30 mg MBTH in 10 mL distilled water and 10 mg DTT in 10 mL distilled water, respectively. MBTH/DTT reagent was prepared immediately before sample analysis by mixing 5 mL MBTH stock solution with 5 mL DTT stock solution. Ferric reagent was prepared by dissolving 200 mg ferric ammonium sulfate and 200 mg sulfamic acid in 40 mL of 0.25 M hydrochloric acid. Before the colorimetric reaction, 25 mg dry biomass samples were hydrolyzed in 250 μ L of 72%

sulfuric acid at 30°C for one hour. After this hydrolysis, samples were diluted by the addition of 7 mL distilled water, autoclaved at 121°C for one hour, and filtered through 0.2 µm nylon syringe filters. Samples were further diluted by distilled water as necessary for the colorimetric reaction. For the colorimetric reaction, 50 µL of hydrolyzed sample was vortexed with 500 µL 0.5 M sodium hydroxide, 500 µL MBTH/DTT reagent, and 450 µL distilled water and then incubated in a pre-heated 80°C heat block for 15 minutes. After 15 minutes, 1 mL of ferric reagent was added to each tube in the heat block. Next, samples were removed from the heat block, vortexed, and allowed to cool for 10 minutes. A final volume of 2.5 mL distilled water was added to each sample immediately after the 10-minute cooling period. Carbohydrate content was estimated for these samples by measuring absorbance at 620 nm and comparing to a glucose standard curve.

3.6 Author Contributions

Jacob Watkins: Conceptualization, Methodology, Validation, Formal Analysis, Investigation, Data Curation, Writing – Original Draft, Writing – Review and Editing, Visualization, Supervision, Project Administration; **Hamza Abdellaoui:** Methodology, Validation, Investigation, Writing – Original Draft; **Elise Barton:** Methodology, Investigation; **Clayton Lords:** Methodology, Investigation; **Foster Agblevor:** Resources; **Ronald Sims:** Conceptualization, Methodology, Resources, Writing – Review and Editing, Supervision, Funding Acquisition.

3.7 Acknowledgments

This research was primarily funded by U.S. Department of Energy Bioenergy Technology Office (BETO) [award number DE-EE0009271]. Laboratory space and supplemental funding were provided by the Utah State University Sustainable Waste-to-Bioprocess Engineering Center, the Utah State University Bioenergy Center, and the Huntsman Corporation Endowed Professorship occupied by Dr. Ronald C. Sims. The authors of this paper thank Ben Peterson and Zachary Fica for their help setting up hydrothermal liquefaction equipment and Jaden Storrer, Peter Jeppesen, Davis Haag, Ethan Rico, Adam Martin, Joshua Wintch, and Emma John for their help with biomass cultivation, data collection, and other laboratory operations.

3.8 Declaration of competing interests

The authors declare that they have no known competing financial interests or personal relationships that could have appeared to influence the work reported in this paper.

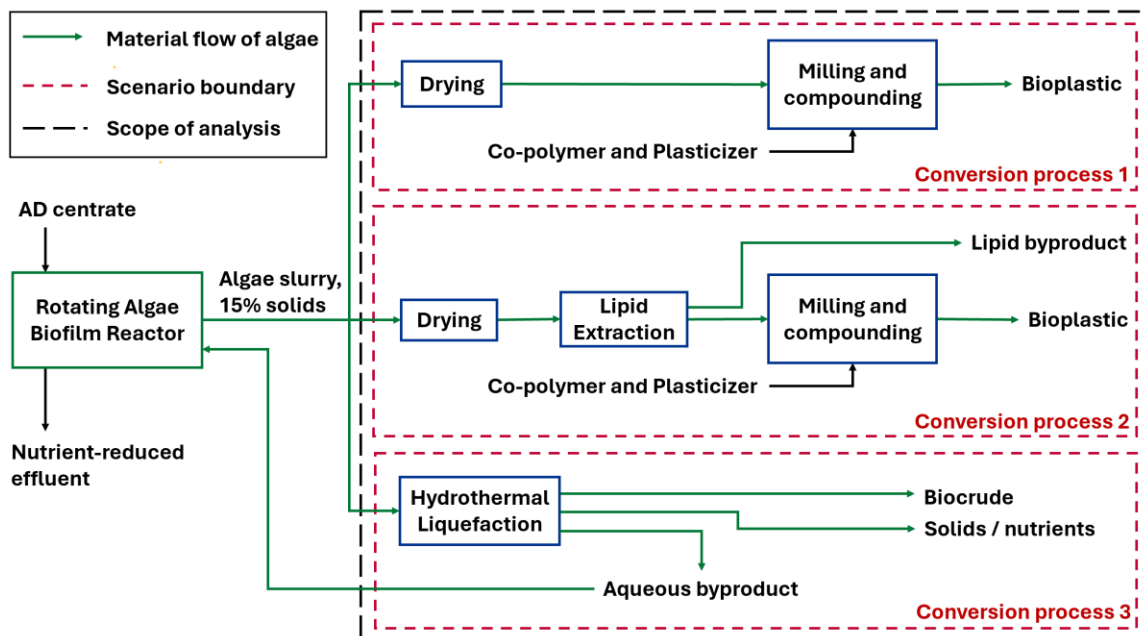
3.9 Data availability

Data are available online at <https://data.mendeley.com/datasets/fjfkhmn24k/1> and <https://doi.org/10.17632/fjfkhmn24k.1>

CHAPTER IV

Techno-economic analysis of biofuel and bioplastic production from a high-ash
microalgae-bacteria biofilm

4.1 Graphical Abstract



4.2 Abstract

Rotating Algae Biofilm Reactors (RABRs) are a promising technology for efficient treatment of wastewater and production of algae-based bioproducts. However, RABR-grown algae can contain a high content of ash (30-60 wt%, dry basis), which influences the technical and economic feasibility of bioproduct conversion processes. In this report, experimental studies and economic analysis were conducted to compare different processes for bioproduct conversion of a high-ash microalgae biofilm grown using a RABR treating 0.6 million gallons per day of anaerobic digestion centrate at the

Central Valley Water Reclamation Facility in Salt Lake City, UT. Process and economic models were developed and compared for three conversion processes: 1) the production of bioplastics, 2) the production of bioplastics with a lipid-extraction pretreatment, and 3) the production of biocrude via hydrothermal liquefaction. Techno-economic analysis was performed for each conversion process, including three cases for algae productivity: 231, 391, and 577 metric tons per year (dry basis). The relatively small production scale and complex processing for hydrothermal liquefaction resulted in a minimum fuel selling price of the biocrude of \$5.32 per gallon of gasoline equivalent. The calculated value for the minimum plastic selling price (MPSP) of bioplastics produced from algae ranges from \$4,050 to \$3,520 per metric ton based on the baseline and final productivity cases of the RABR, respectively. The extraction of lipids in addition to bioplastic production results in an MPSP of \$4,570 to \$4,000 per metric ton for the same productivity cases. The conversion process for bioplastics has the most cost-competitive pricing as well as the highest carbon and energy efficiency compared to the other conversion processes.

4.3 Keywords

Rotating algae biofilm reactor, wastewater reclamation, algae-based thermoplastics, hydrothermal liquefaction

4.4 Highlights

- Process cost models were developed for three conversion processes for high-ash algae biomass
- Bioplastic production from whole cell microalgae biomass had a potential profit margin of 20%

- Bioplastic production with a lipid extraction pretreatment step had a potential profit margin of 2%
- Biocrude production through hydrothermal liquefaction is not profitable at the current state of technology
- Bioplastic production had the highest carbon and energy efficiency

4.5 Introduction

As global populations continue to increase, the need for efficient, economical wastewater management becomes increasingly vital. Poor wastewater management can lead to lake and river eutrophication, toxic algae blooms, contamination of drinking water, and other public health hazards [109], [110]. Well-implemented wastewater management systems avoid these problems and can even reduce groundwater demand through the use of reclaimed water in agricultural and other applications [109]. Existing technologies for wastewater reclamation have improved significantly over the past several decades, and technologies like anaerobic digesters, annamox reactors, and precipitation reactors can recover energy, nitrogen, and phosphorus from wastewater effectively [111], [112]. Bioproducts generated from these processes are valuable but can be limited to methane and soil amendments like compost, digested sludge, and struvite fertilizers. Higher value bioproducts (e.g., biofuels and bioplastics) could make the production of bio-products cost neutral or improve the economics of wastewater reclamation and reduce dependence on non-renewable products such as petroleum-based fuels and plastics.

Developing technologies like microalgae photobioreactors have the potential to improve existing wastewater treatment processes by producing nitrogen- and phosphorus-

rich biomass that can be converted into products like biofuels and compostable bioplastics. Microalgae are of interest for wastewater nutrient recovery for several reasons, including their high biomass productivity, rapid nutrient recovery rates, reduced energy requirements for nitrogen and phosphorus recovery, and ability to be grown on non-arable land [113], [114]. As interest in microalgae technologies continues to grow, a number of techno-economic analyses (TEA) have been published to assess the technical and economic viability of various systems that cultivate microalgae and produce biofuels [115]. The vast majority of the TEA studies have been performed for high-lipid microalgae biomass produced using fresh nutrients (e.g., chemical additives) in open raceway ponds, but a growing body of TEA studies present cultivation and conversion systems for protein-rich biomass [10], [57] and attached-growth microalgae cultivation systems that can be used for wastewater reclamation [116], [117], [118].

Attached-growth systems are particularly promising for wastewater reclamation applications compared to suspended microalgae cultivation systems like open raceway ponds due to their increased areal biomass productivity (e.g. 9.1 g/m²/day vs. 3.2 g/m²/day [119]), increased nutrient recovery rates (e.g. 660 mg TP/m²/day vs 160 mg TP/m²/day [37]), decreased harvesting energy requirements (by excluding centrifugation and filtration steps [118]), and reduced costs of biomass production (e.g. \$510 per metric ton vs. \$673 per metric ton [117]). Microalgae biomass cultivated as a nutrient recovery process from wastewater using attached-growth systems tends to have high ash (30-70 wt%) [45], [116], [117], [120] and high protein (20-50 wt%) [37], [116], [118], [121], [122] concentrations, which can negatively impact the economic viability of biofuel production [116], [123].

To utilize the advantages associated with attached-growth microalgae cultivation systems, there is a need to assess high-value alternatives to biofuels and fertilizer bioproducts for high-ash microalgae feedstocks. Recently, biodegradable bioplastics such as polyurethane and thermoplastic blends have gained significant commercial interest [124]. The viability of processes to co-produce biofuels and bioplastics from high-protein, low-ash microalgae cultivated in nitrogen-replete raceway ponds has been studied previously [57]. Combined revenue from the sale of polyurethanes and protein-rich residual solids sold as a feedstock to bioplastic manufacturers could account for approximately 80% of the total revenue from a nitrogen-replete microalgae cultivation system. For wastewater reclamation applications, production of thermoplastic blends using cross-linked microalgae proteins is particularly appealing because this process can be applied to microalgae feedstocks with relatively high ash content. Compared to other algae-to-bioplastic processes, the ash acts as a “filler” and contributes to the nitrogen, phosphorus, and mineral content available in the final compostable bioplastic. Fillers are already necessary in bioplastic production to reduce feedstock costs, reduce shrinkage during the setting process, and improve the tensile strength and hardness of bioplastics [125]. Thermoplastic blends made using cross-linked microalgae proteins can be sold for a relatively high price [126], but bioplastic production from crossed-linked microalgae proteins has not yet been analyzed by any published TEA.

This study assesses the technical and economic feasibility of producing thermoplastic blends or biofuels from a wastewater-grown microalgae biofilm. Three conversion processes are modeled and compared: the first system models bioplastic production, the second system models bioplastic production with a lipid-extraction

pretreatment, and the third system models biofuel production via hydrothermal liquefaction. Each conversion process is modeled using data from biomass cultivated on a pilot Rotating Algae Biofilm Reactor (RABR) at Central Valley Water Reclamation Facility (CVWRF) in Salt Lake City, Utah. The CVWRF treats 60 million gallons per day (MGD) of municipal wastewater and incorporates a 0.6 MGD nutrient recycle stream of anaerobic digester centrate. The anaerobic digester centrate recycle stream contributes to 16% of the total nutrient load received at the CVWRF headworks and is used directly as the nutrient source for the pilot RABR, where it may eventually supplement or replace existing technologies like ANITA™ Mox and MagPrex. The conversion processes assessed in this study may also be applied to microalgae cultivated on other attached-growth microalgae cultivation technologies, such as Algae Turf Scrubbers [116], [117] and Revolving Algal Bioreactors [37], [59], which produce biomass with similar biochemical compositions to the feedstock assessed in this study.

4.6 Materials and Methods

In this study, three conversion processes are modeled and compared. Each conversion process is assumed to be a small modular system co-located with the RABR cultivation system at a water resource recovery facility (WRRF). The scale of the modeled WRRF is set to match the annual average treatment capacity at the CVWRF. It is assumed that wastewater sludges are treated at the WRRF using anaerobic digestion (AD). The AD centrate, at a daily flow of 600,000 gallons, is the cultivation media for the RABR system. The RABR system removes nutrients (N and P) from the water via algal cultivation producing biomass and treated water. The AD biosolids, at a daily flow of 11

metric tons, on an ash-free, dry weight basis (AFDW), are used as supplemental feedstock for HTL processing.

The first conversion process is direct thermo-mechanical plasticization of microalgae biomass modeled after a commercial process used by Algix, LLC. In this process, microalgae are dried, milled, heated and mixed with a plasticizer (e.g. glycerol), and blended with a co-polymer such as polylactic acid or polyethylene [127], [128], [129].

In the second conversion process, lipids are first extracted from the biomass which can be processed into biofuels or polyurethanes [57], [107], [124], [129], [130], [131], [132], and the residual biomass after extraction is plasticized in the same way as the first conversion process. It is assumed that performance characteristics and economic value of the bioplastic produced from the lipid-extracted biomass is the same as bioplastic produced with the whole biomass.

The third conversion process is hydrothermal liquefaction (HTL) of the whole algal biomass, blended with AD biosolids produced simultaneously at the WRRF. HTL has been demonstrated and modeled for other high-ash microalgae cultivation systems [116], [117], [118] and is modeled herein to compare conversion processes for the RABR-grown algae. In the HTL process, a concentrated slurry (15 wt%) of algae and AD biosolids are heated (280 °C) and pressurized (>6.4 MPaA) to produce biocrude. The produced biocrude is sent to a local refinery for blending with petroleum crude for refinery processing. Solids from hydrothermal liquefaction act as the nutrient sink in this process and are assumed to be sold as a phosphorus-rich soil conditioner. Residual water and water-soluble products are assumed to be sent to the headworks of the RABR

cultivation systems. The economic feasibility of HTL is significantly influenced by facility size, therefore a mixed feed with the AD biosolids is assumed since the flow of algal biomass is only 4% of total flow available from the AD biosolids [123].

The techno-economic analyses (TEA) for each conversion process include three cases for different production rates of algae biomass: baseline, intermediate and final. For the TEA, the costs associated with microalgae cultivation are offset by wastewater reclamation credits, therefore the produced biomass is transferred to each of the conversion processes on a zero-cost basis. The transfer of produced solids at zero-cost may be considered an alternative to landfill disposal, which includes a tipping fee.

Process simulations for HTL and lipid extraction are based on experimental results [98] and are developed in Aspen Plus, version 10. For bioplastic production from whole algae, testing results from Algix's previous and current works are used to develop a simplified process and cost model. Material and energy balances from the process simulation models are used to estimate capital and operating costs for each system.

Variable operating costs are derived from the material and energy balances for each modeled process. Labor costs are minimized due to the labor force already assumed to be present at the WRRF. It is assumed that for the bioplastics process, with and without lipid extraction, 2 additional operators are added to the workforce to attend to weekly operations. For the HTL process, 8 additional operators are added to the workforce to attend to daily operations. Fixed operating costs such as overhead and maintenance are estimated using standard multipliers based on the total capital investment [133].

Base costs for equipment are provided by technical partners at USU, PNNL, Algix, and CVWRF, and the Aspen Process Economic Analyzer and Aspen Capital Cost

Estimator databases and cost formulas. Equipment costs are adjusted by scaling design parameters, such as flow or heat duty, with respect to an exponential scaling factor. The installed cost of equipment is assembled in a Microsoft Excel spreadsheet. A discounted cash flow analysis is used to estimate the minimum product selling price of bioplastic or biofuel by setting the net present value to \$0.

From the TEA results for the three conversion processes, an optimal arrangement and scenario for the algae conversion to biofuels and bioplastic is identified. Life cycle inventory data, including raw materials consumptions (natural gas and chemicals), utility consumptions (electricity and makeup water) and waste generation (solid waste and wastewater) for the optimal case are estimated and reported as efficiency values for carbon and energy utilization. The inventory data can be used for life cycle analysis (LCA), which is outside the scope of this report. The details of process simulation and economic analysis are described in the following sections. Conceptual block diagrams for these conversion processes are shown in the following sections.

4.6.1 Process Inputs and Assumptions for Algae Production

For each conversion process, the feedstock is wastewater-grown algae (WW-algae) harvested from a RABR which is used for side-stream nutrient removal at a municipal WRRF. The scale of the conversion process is scaled to match the availability rate of the feedstock. Three productivity cases labeled as ‘baseline’, ‘intermediate’, and ‘final’ are based on past, present, and future (projected) rates of algal productivity for the RABR system. AD centrate nutrient stream is selected as the growth media for the RABR systems because it has the highest N and P concentrations at CVWRF (500 mg total nitrogen, 50 mg/L total phosphorus) [22], [78], [123]. The nutrient concentrations

increase microalgae biomass productivity per gallon wastewater treated and increase N and P reclamation rates compared to algae grown in primary effluent at the CVWRF. Also, the AD centrate temperature remains elevated and consistent in all seasons (25–35°C) [134], which reduces seasonal variations in microalgae productivity [123]. The annual and seasonal averages of algae throughput for each conversion process in the baseline, intermediate, and final cases are listed in Table 9. The final case has the highest average processing rates and results in the largest plant scale, which is 0.48 metric tons per day on an ash-free dry weight (AFDW) basis. The values for the annual averages for each case of algae production are used in the TEA calculations. The processing throughput for HTL conversion is a combination of the algae flows proposed in Table 9 and anaerobically digested biosolids from the WRRF. The algae feed is supplemented with biosolids to match larger processing scales that are required to meet economic viability for HTL processing [123].

Table 9. Seasonal averages for daily algae production rate (metric ton per day, AFDW)

Case	Summer	Fall	Winter	Spring	Average
Baseline	0.24	0.24	0.06	0.24	0.19
Intermediate	0.45	0.45	0.12	0.30	0.33
Final	0.59	0.59	0.30	0.45	0.48

Measured composition data includes the biochemical content (lipid, carbohydrate, protein, and ash) and elemental content (C, H, N, S, O, and P). Biochemical and elemental compositions of the algae were measured analytically in at least triplicate and are reported as an average value. The elemental composition of the algae was measured

using a Flash 2000 CHNS-O analyzer. Protein content (wt%) was estimated by multiplying the content of N (wt%) by 4.78 [135], [136]. Total lipid content was measured using the sulpho-phospho-vanillin method [137]. Hexane-extractable lipids were measured gravimetrically after extraction with hexane and methanol [107]. Carbohydrate content was measured using the 3-methyl-2-benzothiazolinone hydrazone / dithiothreitol (MBTH / DTT) assay [108]. The elemental and proximate compositions are used in the process model to ensure a closed mass and elemental balance. Seasonal changes in biochemical and elemental content are not considered.

To minimize capital and operating costs, the RABR is harvested weekly for the bioplastic conversion processes and harvested daily for HTL. The conversion processes are designed and scaled to match the harvesting frequency. Therefore, bioplastics production and lipid extraction operate on a semi-continuous basis, only when the algae are harvested. The HTL facility operates continuously to process algae and AD biosolids. The algal slurry harvested from the RABR is 15% biomass solids in water, as demonstrated at the pilot-scale system at CVWRF [98]. The slurry is fed directly into either of the proposed conversion processes without modification.

4.6.2 Production of Bioplastics

The conceptual block diagram for the production of bioplastic, which was developed by Algix, is shown in Figure 6 [127]. The conversion process is co-located at the WRRF to minimize transportation. The harvested slurry (15% solids) is dewatered using a vacuum filter to reduce the moisture content from 85% to 65%. The dewatered microalgal slurry is dried to less than 10% moisture by vacuum drying at 60°C. The purpose of the drying step is to improve the shelf life of the feedstock and reduce the

odor of the final bioplastic product. The dried microalgae are processed in an air jet mill to reduce the particle size of the algae to a desired size for incorporation into composite bioplastics. Milling increases the homogeneity of the composite bioplastic formed from the biomass and increases access to protein constituents in algae for polymerization. During milling, the dried algal agglomerates are reduced in particle size and the cell walls are ruptured. Evaporative water-cooling controls the temperature of the compressed air. After milling, the microalgae are blended with a commercial bioplastic resin at a mass ratio of 45 parts algae to 55 parts resin prior to thermomechanical melting and molding. After melting and molding is performed, the molten bioplastic product is cooled in a water bath. The product can be upgraded further by blending with additional plastic powders and extrusion into a thin film or sheet. Upgrading steps, such as blending with additional plastic powders, adding colorant, and molding into a final product, are excluded in this study.

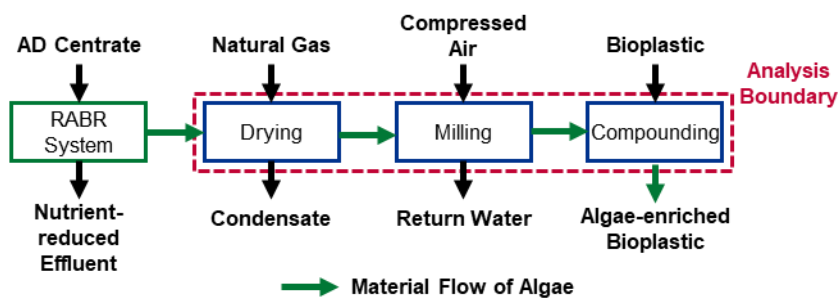


Figure 6. Conceptual block diagram for WW-algae conversion to bioplastic system

Table 10 lists the process parameters that are modeled for bioplastic conversion. Some parameters are proprietary to Algix and therefore are not published. The biodegradable resin pellet used in the bioplastic blending step is assumed to be a commercial polylactic acid (PLA)-based resin. The assumed purchase price of PLA resin is \$4,000 per metric ton. The price for comparable PLA blendstock ranges from \$3,500 to \$5,500 per metric ton [138].

Table 10. Process parameters for the production of bioplastic

Process parameters	Value
Temperature during vacuum drying, °C	60
Heat source during vacuum drying	Combustion of natural gas
Milling Air Pressure, kPaa	700
Milling particle size, μm	100 (average)
Energy consumption during milling (and cooling), MJ/kg product	1.4
Compounding Temperature, °C	110 to 180
Energy consumption during compounding, MJ/kg product	6.3

4.6.3 Production of Bioplastics with Lipid Extraction

A conceptual block diagram for the production of bioplastic with a lipid extraction is shown in Figure 7. Since bioplastics are typically produced by using protein and carbohydrate-based polymers from algae or other biomass [139], lipids can be extracted from whole algae and the lipid-extracted algae (LEA) residues can be used as feedstock for other conversion processes. The design of the lipid extraction process is developed from testing performed with RABR-harvested biomass from the CVWRF [98]. The

testing method is consistent with the experimental work conducted previously [107]. The lipid extraction and bioplastic conversion processes are co-located at the WRRF to minimize transportation. Similar to the conversion process for bioplastic production from whole algae, raw algae are dewatered and dried to a moisture content of less than 10%. The dried algae are milled in the jet mill to disrupt the cell walls and enable the release of lipids and other intracellular contents. Solvent extraction separates lipids from the milled algae. The milled algae are blended with hexane and methanol in a batch extraction. The mixture is filtered to remove the LEA residues. The lipid-containing solvents are mixed with water to separate the hexane and lipids from the methanol and water phase. The hexane-lipid mixture is distilled to recover hexane and separate the extracted lipid. The methanol and water mixture is distilled separately to recover the methanol. Both recovered solvents are recycled in the process. For further treatment and upgrading, the extracted lipid can be sent to a local refinery to be upgraded to transportation fuels or to another processor to produce high-value polyurethanes [57], [107], [124], [129], [130], [131], [132]. The algal lipids are sold as a co-product. The LEA is dried in a gas-fired dryer and is then processed through the conversion process for bioplastic described in the previous section.

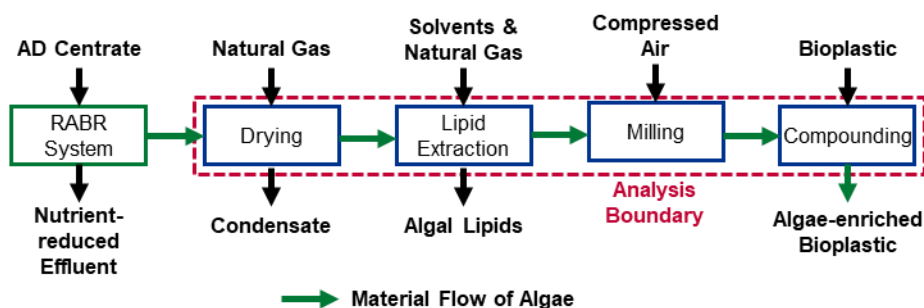


Figure 7. Conceptual block diagram for the WW-algae lipid extraction and bioplastic production system

Table 11 lists the major process parameters for the lipid extraction process. The algal biomass loses 6.9 wt% of its total mass to the extraction steps. 2.8 wt% of the total mass is partitioned to the methanol phase, which includes both lipid and non-lipid material. 4.1 wt% of the total mass is transferred to the hexane phase, which is assumed to be only lipids. Based on discussion with Algix, the process parameters for milling and compounding of LEA into the bioplastic are assumed to be the same as the process parameters described for the whole algae feedstock (Table 10).

Table 11. Process parameters for lipid extraction [98]

Process parameters	Values
Solvent mixture (volume ratio)	1:1 methanol:hexane
Solvent:dry biomass (volume:mass ratio)	10:1
Water:methanol volume (volume ratio)	0.36:1 water:methanol
Mass remaining in solid phase after extraction (AFDW)	93.1 wt%
Total mass extracted from algae solids, (AFDW)	6.9 wt%
Material transfer to the methanol (lipid and non-lipid) (AFDW)	2.8 wt%
Lipids recovered in the hexane (AFDW)	4.1 wt%

4.6.4 Hydrothermal Liquefaction (HTL)

Figure 8 shows the block flow diagram for HTL. The process parameters are based on the HTL testing work performed using the harvested WW-algae from the pilot-scale RABR facility at CVWFR [98] and previous modeling work by Pacific Northwest National Laboratory [123]. Algae harvested from the RABR system and concentrated wet biosolids from anaerobic digestion are processed at an on-site HTL facility with an assumed processing scale of 11 metric tons per day (AFDW). The scale of the facility is adjusted to accommodate the maximum amount of algae biomass that could be provided by the RABR system and the estimated amount for wet biosolids from the anaerobic digester at the 600,000 gallon-per-day effluent flow rate. The cost of algae feedstock is assumed to be \$0 based on the underlying assumption that algae is a solid waste from the RABR system and the credits of wastewater nitrogen (N) and phosphorus (P) removal via RABR system can balance the cost associated with the removal of nutrients via the cultivation of the biomass feedstock. The feedstock cost of the AD biosolids is also assumed to be \$0. The separated HTL products (biocrude, solids, aqueous-phase products, and gas) are isolated for additional processing. The biocrude is assumed to be the final product and it can be sold to a local refinery to be co-processed with petroleum crude via hydroprocessing to produce distillate fuels such as naphtha, diesel, and jet fuels. The solid product is assumed to be returned to CVWRF as an amendment for soil compost due to its content of P. The excess water and aqueous phase is assumed to be recycled into the RABR. Flue gas is assumed to be used within the HTL process for heat integration.

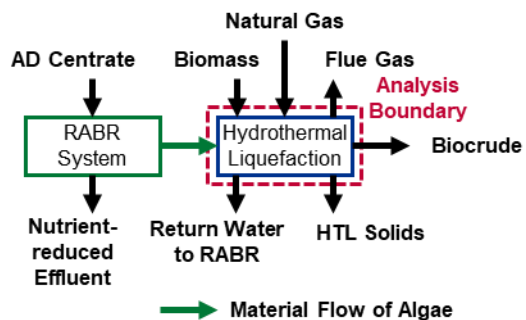


Figure 8. Conceptual block diagram for WW-algae HTL conversion to biocrude system

Table 12 lists the process parameters developed from internal HTL testing results [98]. The processing temperature for HTL is assumed to be 280 °C. Based on the HTL testing results using the RABR algae as feedstock, the biocrude yields at 280 °C and 350 °C are 21% and 23% (AFDW), respectively. The yield at higher temperature is only slightly higher than the one at lower temperature. However, the operating pressure required by 350 °C is about 21 MPa, much higher than the one for 280 °C, and leads to a higher material cost for the HTL equipment. The energy requirements for heat and pressure can also be reduced if operating at a lower temperature for HTL. Therefore, an operating temperature of 280 °C is assumed to minimize equipment and material costs-

Table 12. Process parameters for HTL conversion

Parameters	Values
Temperature, °C	280
Pressure, MPaA	10
Liquid hourly space velocity (LHSV), v/v/h	4
Yield of biocrude, wt% feedstock (AFDW)	21
Yield of aqueous products, wt% feedstock (AFDW)	48
Yield of gas, wt% feedstock (AFDW)	7.2
Yield of solids, wt% feedstock (AFDW)	24
C in the HTL biocrude, wt% (AFDW)	76
H in the HTL biocrude, wt% (AFDW)	9.0
O in the HTL biocrude, wt% (AFDW)	11
N in the HTL biocrude, wt% (AFDW)	3.3
S in the HTL biocrude, wt% (AFDW)	0.37
P in the HTL solids, wt% (AFDW)	9.2

4.6.5 Economic Analysis

Base costs for non-standard equipment, including the RABR system, the HTL reactor, and the bioplastic milling and compounding system are provided by technical partners from USU, PNNL, Algix and CVWRF based on direct experiences. Estimations for labor cost are based on empirical or experiential data for each system. Variable operating costs for raw materials and utilities are obtained from industrial databases. The economic analysis parameters are listed Table 13, and are similar to parameters used in other TEAs [140]. For each of the productivity cases and conversion processes, a potential profit margin value is calculated as the quotient of the difference between potential revenues and cost, and the revenue.

Table 13. Economic parameters for analysis

Parameters	Value
Internal rate of return	10%
Plant financing debt/equity	60% / 40% of total capital investment
Term for debt financing	10 years
Interest rate for debt financing	8% annually
Plant life	30 years
Income tax rate	21%
Working capital cost	5% of fixed capital investment
Depreciation schedule	7 years
Construction period	1 year
Start-up time	3 months
Total indirect cost	55% of total direct cost
Cost year	2020 US\$

A standard reference basis common to conceptual design studies, known as the n^{th} -of-a-kind plant design, is used. These assumptions do not account for additional first-of-a-kind plant costs, including special financing, equipment redundancies, larger cost contingencies, longer startup times, and low capacity utilization. For n^{th} -plant designs, it is assumed that the costs reflect a mature technology.

4.7 Discussion

In this discussion the results for the compositional analysis and economic analysis are reported. In Table 14, the measured elemental and proximate composition of the algae are reported. As anticipated, the ash content of the algae is 39 wt%, which is higher than typical purpose-grown algae (<30 wt% [141]), but typical for wastewater-grown algae. The lipid content is 14 wt%, which is relatively low when compared to algal strains that are optimized for high lipid contents (e.g. 50-80 wt% [142]).

Table 14. Microalgae feedstock composition, AFDW basis [98]

Elemental compositions, wt%	
C	26%
H	4.4%
O	26% (by balance)
N	4%
S	0.54%
Ash	39%
P (included in ash)	4.7%
Biochemical compositions, wt% (normalized to 100%)	
Protein	30%
Lipid	14%
Carbohydrate	17%
Ash	39%

4.7.1 Bioplastic conversion system

The installed equipment costs and the minimum plastic selling price for the conversion of WW-algae to bioplastic is shown in Table 15. The installation cost for the algae dewatering/drying process represents about 61% of the total cost. The bioplastic production cost, including milling and compounding, is about 19% of the total cost. The minimum plastic selling price (MPSP) is estimated to be \$3,520 and 4,050 per metric ton of bioplastic product for final and baseline cases, respectively. This price falls into the average price range of biodegradable plastics between \$3,350 and \$4,690 per metric ton for the North America market for 2022 to 2030 [143].

For the operating costs, 97% of the cost of chemicals is attributed to the purchase of PLA, which is required to sell the blended bioplastic. This first-of-a-kind economic analysis shows that the bioplastic with incorporated WW-algae can be cost competitive with other bioplastic products. For productivity cases beyond the baseline, the potential for higher profit margin is possible due to the decreasing MPSP.

The biochemical fractions of algal biomass can be used to produce polyurethanes from lipids and protein-rich residues for bioplastics. 80% of the total revenue from fractionated algal biomass can be derived from the algal protein and lipid fractions [57]. The direct blending of the algal biomass into bioplastics simplifies processing by avoiding fractionation steps. The direct impacts of biomass composition on the performance of algae-based plastics have not been quantified, however, there are general requirements for the Algix conversion process: less than 40% carbohydrates, less than 40% ash, and at least 30% protein.

Table 15. TEA results of WW-algae conversion to bioplastic system

Cases	Baseline	Intermediate	Final
Algae-based bioplastic production, metric ton/yr	231	391	577
Installation Cost (2020 US \$)			
Algae storage	\$68,000	\$101,000	\$135,000
Algae dewatering/drying	\$780,000	\$1,098,000	\$1,415,000
Plastic production	\$249,000	\$350,000	\$451,000
Balance of Plant	\$186,000	\$260,000	\$333,000
Total Installed Capital Cost	\$1,283,000	\$1,809,000	\$2,334,000
Total Capital Investment	\$2,383,000	\$3,509,000	\$4,434,000
Operating Cost, \$/metric ton bioplastic			
Natural gas	\$10	\$10	\$10
Chemicals	\$2,200	\$2,200	\$2,200
Electricity and other utilities	\$180	\$180	\$180
Fixed Costs	\$310	\$200	\$150
Capital Depreciation	\$330	\$280	\$240
Average Income Tax	\$100	\$80	\$70
Average Return on Investment	\$920	\$770	\$670
Minimum Plastic Selling Price, \$/metric ton	\$4,050	\$3,720	\$3,520

Alternatively, the WRRF could produce dried algae and sell it directly as a supplemental material for bioplastic production. At a minimum the equipment to dry the algae to <10% water content would be needed. We calculate that the minimum product selling price of the algae to break even is \$613 per metric ton. This is competitive with the 2023 benchmark price for farmed algae (\$602 per metric ton [141]), which assumes highly favorable conditions that maximize productivity.

4.7.2 Bioplastic conversion system with lipid extraction pretreatment

Table 15 summarizes the installed equipment costs and the minimum plastic selling price for the lipid extraction and bioplastic conversion process. The most significant contribution to the capital cost is from the lipid extraction process, which represents over 50% of the total capital costs. Similar to the bioplastic-only process, the cost of the commercial bioplastic blendstock dominates the variable costs. The assumption that the LEA performs similar to the whole algae when blended into the final plastic product may be an opportunity for improvement in future studies. Understanding the performance of LEA vs. whole algae will be an important factor to consider when determining if the lipid-extraction process produces comparable economic outcomes. Ultimately, the higher processing costs results in higher MPSP values ranging from \$4,570 to \$4,000 per metric ton for the baseline and final cases, respectively. The higher MPSP is close to or exceeds the average market selling price (\$4,020 per metric ton).

The direct sale of the LEA residue as a bioplastic blendstock rather than a bioplastic product is not economically viable. The breakeven selling price for the LEA residue varies from \$3,300 to \$4,400 per metric ton for the final and baseline cases, respectively. The proposed selling price of LEA residue is much higher than the selling

price for whole algae biomass (\$603 per metric ton). Due to the added investment for lipid extraction, without the sale of the residues as bioplastic, it is more difficult to recover the costs associated with production.

Table 16. TEA results of WW-algae lipid extraction and bioplastic production system

Cases	Baseline	Intermediate	Final
Crude lipid, L/yr	6,400	10,800	16,000
Bioplastic production, metric ton/yr	225	380	561
Installation Cost (2020 US \$)			
Algae storage	\$68,000	\$101,000	\$135,000
Algae dewatering/drying	\$499,000	\$583,000	\$751,000
Lipid extraction	\$1,253,000	\$1,508,000	\$2,009,000
Bioplastic production	\$164,000	\$231,000	\$297,000
Balance of Plant	\$225,000	\$298,000	\$381,000
Total Installed Capital Cost	\$2,209,000	\$2,721,000	\$3,573,000
Total Capital Investment	\$4,183,000	\$5,140,000	\$6,749,000
Operating Cost, \$/metric ton bioplastic			
Natural Gas	\$30	\$30	\$30
Chemicals	\$2,300	\$2,300	\$2,300
Electricity and other utilities	\$160	\$160	\$160
Sales credit for lipids	\$(20)	\$(20)	\$(20)
Fixed Costs	\$290	\$210	\$170
Capital Depreciation	\$490	\$420	\$370
Average Income Tax	\$120	\$100	\$90
Average Return on Investment	\$1,200	\$1,000	\$900
Minimum Plastic Selling Price (MPSP)	\$4,570	\$4,200	\$4,000

4.7.3 Hydrothermal Liquefaction

HTL has been studied for energy recovery and has been demonstrated to produce high fuel yields for similar high-ash microalgae feedstocks [116], [123]. The TEA results

for the HTL conversion system are listed in Appendix C. Economically feasible production of biofuels via HTL is not possible using only the biomass provided by the RABR system modelled in this study. For the final cultivation case, coupled with the biosolids from the anaerobic digester we calculate a MFSP of \$5.32/GGE. Although the MFSP is not cost-competitive with current prices for petroleum fuels, relevant credits for renewable fuel products such as the California Low Carbon Fuel Standard, the EPA Renewable Fuel Standard, and the recent Blending Tax Credit have the potential to reduce the MFSP by several dollars per GGE. The sale of the HTL solids as soil conditioner recovers some cost of operation, contributing \$1.83/GGE to the net MFSP value.

The 2022 annual biosolids production from the CVWRF is 5,700 metric tons per year [144]. When co-feeding this biosolid with WW-algae from RABR to HTL, the plant scale increases to 19 metric tons per day, which is about 24 times of the final case of WW-algae only HTL. The HTL biocrude yield for the biosolid is assumed to be 31% of feedstock at AFDW basis based on the related testing conducted at PNNL [145], which is higher than the 21% for the WW-algae HTL tested in this study.

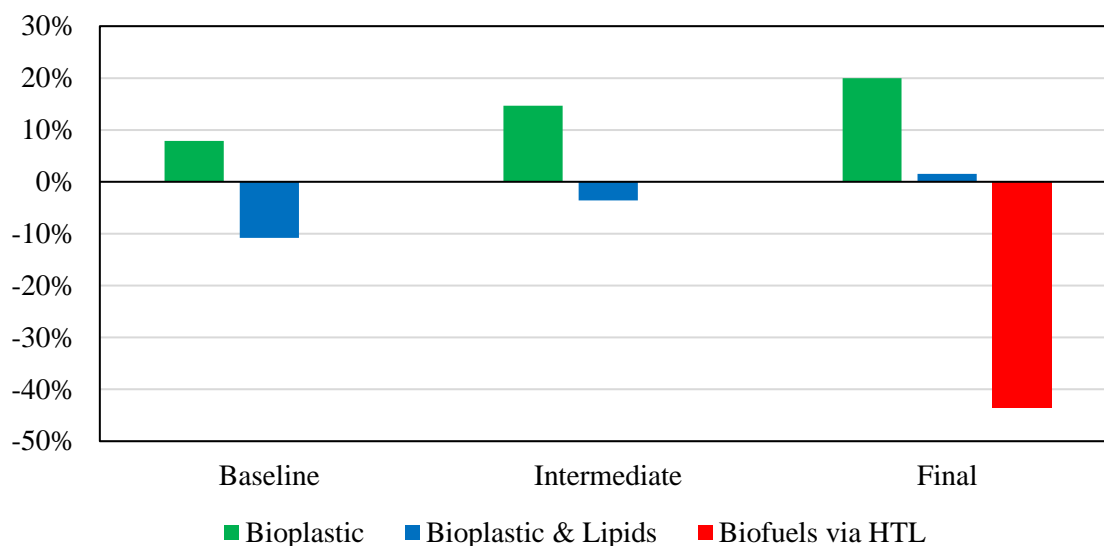


Figure 9. Potential profit margin values for the proposed conversion processes

To compare the economic feasibility of the three conversion processes, we calculated a potential profit margin based on the market prices for bioplastic, crude lipids, and biocrude. Income was estimated using fixed selling prices for the bioplastics, lipids, and HTL biocrude. The price of the bioplastic was selected as \$4,020 per metric ton, which is the estimated average price of bioplastic in North America for 2022 – 2030 [143]. The price of the crude lipid and HTL biocrude was selected as \$0.80/L (\$3.03/GGE), which is the market price for vegetable oils [138]. The results of the income and expense calculations are presented in Figure 9. At current rates of algal productivity, only the conversion process for direct production of bioplastics could be considered profitable, having potential income greater than expenses with a minimum profit margin value of 8%. Only in the final case for algae productivity does the conversion process for bioplastic production with a lipid extraction pretreatment become

profitable with a narrow margin of 2%. Even at the increased production scale, HTL is not profitable, and may only become so if credits through other programs are applied.

4.7.4 Sustainability Metrics

Table 15 lists carbon and energy efficiency metrics for the three conversion processes. The bioplastic conversion process has the highest carbon and energy efficiencies. The lipid extraction and bioplastic production process have higher carbon and energy efficiency than the HTL process. For the bioplastic processes, more of the initial carbon is retained in the final plastic product, whereas carbon is lost during HTL to the aqueous and gas phase products, creating treatment or emission burdens.

Table 17. Conversion sustainability metrics

	HTL	Bioplastic Conversion	Lipid Extraction and Bioplastic Conversion
Carbon Efficiency (C in final products / C in algae)	0.37	0.93	0.75
Energy Efficiency (LHV of products / LHV of algae)	0.31	0.55	0.44

4.8 Conclusions

Process and economic models were developed and compared for three processes for the conversion of microalgae biomass harvested from a rotating algae biofilm reactor: Conversion processes investigated include the production of bioplastic from whole algae biomass, the production of bioplastic from lipid-extracted biomass, and the production of

biocrude via hydrothermal liquefaction (HTL). The calculated value for the minimum plastic selling price (MPSP) of bioplastics produced from algae is within the range of commercial bioplastic products and ranges from \$4,050 to \$3,520 per metric ton based on the baseline and final productivity of the RABR, respectively, with a potential profit margin ranging from 8 to 20%. The extraction of lipids in addition to bioplastic production results in an MPSP of \$4,570 to \$4,000 per metric ton and may be further improved by upgrading the extracted lipids into biofuels or high-value plastics. The relatively small production scale and complex processing for HTL was economically infeasible, and co-feeding other feedstocks is necessary to achieve an economically viable process. Of the three conversion processes modeled in this TEA, bioplastic production from whole algae has the highest carbon and energy efficiency and the highest potential profit margin (20%). Based on the results of this TEA, bioplastic production from whole algae is an economically viable process that can be used to valorize algae biomass harvested from rotating algae biofilm reactors treating anaerobic digester centrate at municipal wastewater reclamation facilities.

4.9 Funding

This research was funded by the U.S. Department of Energy Bioenergy Technology Office under award number DE-EE0009271, with laboratory space and supplemental funding provided by the Utah State University Sustainable Waste-to-Bioprocess Engineering Center and the Huntsman Corporation Endowed Professorship occupied by Dr. Ronald C. Sims. Work performed at the U.S. DOE's Pacific Northwest National Laboratory (PNNL) was done under contract DE-AC05-76RL01830 and the auspices of the WSU-PNNL Bioproducts Institute, which is a joint research collaboration

of Washington State University (WSU) and PNNL. The views expressed in this article do not necessarily represent the views of the U.S. DOE or the United States Government.

Neither the U.S. Government nor any agency thereof, nor any of their employees, makes any warranty, expressed, or implied, or assumes any legal liability or responsibility for the accuracy, completeness, or usefulness of any information, apparatus, product, or process disclosed, or represents that its use would not infringe privately owned rights.

4.10 Declaration of Competing Interests

Ashton Zeller works for BLOOM Sustainable Materials, a technology company which converts algae biomass into thermoplastic compounds for use in consumer products. Ashton Zeller helped determine parameters for use in the techno-economic analysis of the bioplastic conversion process. All other authors declare no conflicts of interest.

4.11 Author Contributions

Jacob Watkins: conceptualization, data curation, investigation, methodology, visualization, writing – original draft, writing – review and editing; **Yunhua Zhu:** conceptualization, data curation, formal analysis, investigation, methodology, visualization, writing – original draft; **Peter Valdez:** conceptualization, data curation, formal analysis, investigation, methodology, validation, visualization, writing – original draft, writing – review and editing; **Ashton Zeller:** investigation, methodology, resources, writing – review and editing; Clayton Lords: investigation, resources, writing – original draft; **Pavlo Bohutskyi:** conceptualization, project administration, supervision;

Ronald C. Sims: conceptualization, funding acquisition, methodology, project administration, resources, supervision, writing – review and editing.

CHAPTER V

Conclusions

In this thesis, (1) the effects of environmental factors on the biomass production rate and nutrient removal efficiency of Rotating Algae Biofilm Reactors (RABRs) treating municipal wastewater were examined, (2) biochemical compositions and hydrothermal liquefaction product yields were characterized for a microalgae biofilm grown in municipal anaerobic digester centrate, and (3) the cost of producing biofuels and bioplastics from the same biofilm was evaluated.

The effects of temperature, light intensity, hydraulic retention time, and harvesting period were within the expected ranges. Several two-way interactions were also present. Optimum values identified in this screening study were applied to a 11,400-liter pilot RABR for further testing. Microalgae biomass cultivated on the pilot RABR at Central Valley Water Reclamation Facility (CVWRF) was characterized and used as the input in a techno-economic analysis of bioplastic and biofuel production from wastewater-grown microalgae biomass. Based on this analysis, direct production of bioplastic composites from dried microalgae biomass was identified as an economically viable upgrading process for wastewater-grown biomass with high ash (38 wt%) and high protein (30 wt%) content.

CHAPTER VI

Recommendations for future work

6.1 Future research pertaining to Chapter II

6.1.1 Bioaugmentation

Bioaugmentation and careful strain selection can improve the biochemical characteristics, growth rate, and phosphorus content of microalgae biofilm cultures [59], [146]. Currently, the individual roles of community members in the CVWRF biofilm are not well-understood. Future work can consider broad-scale bioaugmentation with local biofilm cultures (e.g. [146]) or species specific bioaugmentation with previously-identified phosphorus accumulating species (e.g. [59]). To improve winter productivities, bioaugmentation with cold-tolerant species such as those identified by the DISCOVER program [83] should also be evaluated.

6.1.2 Light intensity

A primary objective of this study was to identify two-way interaction effects which involved light intensity. To achieve this, we used an experimental design which only allowed a rough approximation of the optimal light intensity for biofilm growth. Further optimization should be performed to identify a “minimum acceptable light intensity” which can be used to design a pilot-scale RABR with a packing factor which maximizes photosynthetic efficiency. To avoid the substratum degradation observed in this study, this optimization should be performed on synthetic substrates like polyethylene or polycarbonate.

6.1.3 Harvesting period

Harvesting period had no statistically significant influence on the biomass productivity or nutrient removal efficiency of the CVWRF biofilm community. Other studies have found that harvesting period can influence the relative abundance of species within algae biofilms and that microalgae biofilms harvested every 2 days have higher lipid content than microalgae biofilms harvested every 6 days [147]. Future work should test the influence of harvesting period on the biochemical composition of the CVWRF biofilm.

6.1.4 Hydraulic Retention Time

Hydraulic Retention Time (HRT) has a significant influence on size requirements for full-scale RABR systems. In this study, the fastest phosphorus removal and biomass growth was achieved with a 2-day HRT. These reactors were operated in batch mode, which influences the pH of the liquid media and causes nutrient concentrations to fluctuate more suddenly than the continuous-flow systems used at wastewater reclamation facilities. In addition, only two ratios of growth area to liquid volume were tested in this study. Further optimization of HRT should further optimize HRT using continuous-flow RABRs and should consider interactions between HRT and the ratio of reservoir volume to RABR surface area.

6.2 Future research pertaining to Chapter IV

6.2.1 Production of polyurethanes and high-value lipid products:

In this TEA, the lipid-extraction / bioplastic production conversion process only considered revenue from the protein-based bioplastic composite and the sale of crude

lipids. However, upgrading lipids into high-value products like polyurethanes could increase the viability of this conversion process [57]. Future work should consider the production of high-value products from wastewater-grown microalgal lipids.

6.2.2 Treatment of hydrothermal liquefaction aqueous products:

In this techno-economic analysis (TEA), the scale of biomass production was not large enough for hydrothermal liquefaction to be economically feasible. However, hydrothermal liquefaction of raw municipal solids may be economically viable for large municipalities.

Treating hydrothermal liquefaction aqueous-phase (AP) coproduct contributes significantly to the cost of HTL systems, partially because AP coproduct contains many toxic compounds that must be diluted before biological treatment [148], [149]. In the HTL conversion process modelled in this TEA, the volume of AP coproduct was relatively low compared to the volume of anaerobic digester centrate already being treated by RABRs (less than 900 gallons AP coproduct vs. 600,000 gallons anaerobic digester centrate per day). However, dilution at this scale is not always convenient, and identifying a minimum dilution requirement for AP coproduct reuse is advantageous [148], [149]. Previous studies conducted using planktonic microalgae have increased the maximum tolerable concentration of HTL AP coproduct significantly by using mixtures of multiple algal species and by slowly adapting microalgae cultures to higher and higher AP concentrations [149]. Recently, Haag et al. demonstrated that RABRs could tolerate AP coproduct concentrations up to 25% (v/v) with no adaptation period [150]. Future work should attempt to increase this concentration by adapting the RABR community used by Haag et al. to higher AP coproduct concentrations.

REFERENCES

- [1] D. L. Correll, “The Role of Phosphorus in the Eutrophication of Receiving Waters: A Review,” *J. environ. qual.*, vol. 27, no. 2, pp. 261–266, Mar. 1998, doi: 10.2134/jeq1998.00472425002700020004x.
- [2] B. E. Lapointe, L. W. Herren, D. D. Debortoli, and M. A. Vogel, “Evidence of sewage-driven eutrophication and harmful algal blooms in Florida’s Indian River Lagoon,” *Harmful Algae*, vol. 43, pp. 82–102, Mar. 2015, doi: 10.1016/j.hal.2015.01.004.
- [3] A. Y. Ugya, H. A. Ari, and X. Hua, “Microalgae biofilm formation and antioxidant responses to stress induce by *Lemna minor* L., *Chlorella vulgaris*, and *Aphanizomenon flos-aquae*,” *Ecotoxicology and Environmental Safety*, vol. 221, p. 112468, Sep. 2021, doi: 10.1016/j.ecoenv.2021.112468.
- [4] F. Kessouri *et al.*, “Coastal eutrophication drives acidification, oxygen loss, and ecosystem change in a major oceanic upwelling system,” *Proc. Natl. Acad. Sci. U.S.A.*, vol. 118, no. 21, p. e2018856118, May 2021, doi: 10.1073/pnas.2018856118.
- [5] S. Fossen Johnson, “Methemoglobinemia: Infants at risk,” *Current Problems in Pediatric and Adolescent Health Care*, vol. 49, no. 3, pp. 57–67, Mar. 2019, doi: 10.1016/j.cppeds.2019.03.002.
- [6] L. Knobeloch, B. Salna, A. Hogan, J. Postle, and H. Anderson, “Blue babies and nitrate-contaminated well water,” *Environmental Health Perspectives*, vol. 108, no. 7, pp. 675–678, Jul. 2000, doi: 10.1289/ehp.00108675.
- [7] M. Preisner, E. Neverova-Dziopak, and Z. Kowalewski, “An Analytical Review of Different Approaches to Wastewater Discharge Standards with Particular Emphasis on Nutrients,” *Environmental Management*, vol. 66, no. 4, pp. 694–708, Oct. 2020, doi: 10.1007/s00267-020-01344-y.
- [8] M. Ha, G. Gutenberger, L. Ou, H. Cai, and T. Hawkins, “Opportunities for Recovering Resources from Municipal Wastewater,” ANL/ESD-21/11, 1876441, 176194, Jul. 2022. doi: 10.2172/1876441.
- [9] U. S. DOE, “National Algal Biofuels Technology Roadmap. US Department of Energy, Office of Energy Efficiency and Renewable Energy,” *Biomass Program*, vol. 14, 2010.
- [10] B. D. Beckstrom, M. H. Wilson, M. Crocker, and J. C. Quinn, “Bioplastic feedstock production from microalgae with fuel co-products: A techno-economic and life cycle impact assessment,” *Algal Research*, vol. 46, p. 101769, Mar. 2020, doi: 10.1016/j.algal.2019.101769.
- [11] M. A. Alam and Z. Wang, Eds., *Microalgae Biotechnology for Development of Biofuel and Wastewater Treatment*, 1st ed. 2019. Singapore: Springer Singapore : Imprint: Springer, 2019. doi: 10.1007/978-981-13-2264-8.
- [12] C. Torri *et al.*, “Biological treatment of Hydrothermal Liquefaction (HTL) wastewater: Analytical evaluation of continuous process streams,” *Journal of Water Process Engineering*, vol. 40, p. 101798, Apr. 2021, doi: 10.1016/j.jwpe.2020.101798.

- [13] J. Parkinson, “Methane Emission Treatment and Potential Upcycling using *Methylobacterium alcaliphilum*,” 2021, doi: 10.26076/04C4-7AA9.
- [14] A. S. Reshetnikov, V. N. Khmelena, I. I. Mustakhimov, and Y. A. Trotsenko, “Genes and Enzymes of Ectoine Biosynthesis in Halotolerant Methanotrophs,” in *Methods in Enzymology*, vol. 495, Elsevier, 2011, pp. 15–30. doi: 10.1016/B978-0-12-386905-0.00002-4.
- [15] P. J. Strong, M. Kalyuzhnaya, J. Silverman, and W. P. Clarke, “A methanotroph-based biorefinery: Potential scenarios for generating multiple products from a single fermentation,” *Bioresource Technology*, vol. 215, pp. 314–323, Sep. 2016, doi: 10.1016/j.biortech.2016.04.099.
- [16] R. B. Levine, T. Pinnarat, and P. E. Savage, “Biodiesel Production from Wet Algal Biomass through in Situ Lipid Hydrolysis and Supercritical Transesterification,” *Energy Fuels*, vol. 24, no. 9, pp. 5235–5243, Sep. 2010, doi: 10.1021/ef1008314.
- [17] B. L. Peterson, “Development and Optimization of a Produced Water, Biofilm Based Microalgae Cultivation System for Biocrude Conversion with Hydrothermal Liquefaction,” 2018, doi: 10.26076/8751-95AB.
- [18] C. J. López Rocha, E. Álvarez-Castillo, M. R. Estrada Yáñez, C. Bengoechea, A. Guerrero, and M. T. Orta Ledesma, “Development of bioplastics from a microalgae consortium from wastewater,” *Journal of Environmental Management*, vol. 263, p. 110353, Jun. 2020, doi: 10.1016/j.jenvman.2020.110353.
- [19] L. Christenson and R. Sims, “Production and harvesting of microalgae for wastewater treatment, biofuels, and bioproducts,” *Biotechnology Advances*, vol. 29, no. 6, pp. 686–702, Nov. 2011, doi: 10.1016/j.biotechadv.2011.05.015.
- [20] M. Wiatrowski and Ryan Davis, “Algal Biomass Conversion to Fuels via Combined Algae Processing (CAP): 2022 State of Technology and Future Research,” National Renewable Energy Laboratory, Golden, CO, NREL/TP-5100-85662, 2023. [Online]. Available: <https://www.nrel.gov/docs/fy23osti/85662.pdf>
- [21] J. W. R. Chong *et al.*, “Advances in production of bioplastics by microalgae using food waste hydrolysate and wastewater: A review,” *Bioresource Technology*, vol. 342, p. 125947, Dec. 2021, doi: 10.1016/j.biortech.2021.125947.
- [22] K. M. Hillman, “Observation of Struvite in the Mixed Microalgae Biofilm Matrix of a Rotating Algal Biofilm Reactor During Nutrient Removal from Municipal Anaerobic Digester Filtrate,” Master’s Thesis, Utah State University, 2020. Accessed: Dec. 04, 2021. [Online]. Available: <https://digitalcommons.usu.edu/etd/7796>
- [23] A. Kumar and J. S. Singh, “Microalgal bio-fertilizers,” in *Handbook of Microalgae-Based Processes and Products*, Elsevier, 2020, pp. 445–463. doi: 10.1016/B978-0-12-818536-0.00017-8.
- [24] X. You, L. Yang, X. Zhou, and Y. Zhang, “Sustainability and carbon neutrality trends for microalgae-based wastewater treatment: A review,” *Environmental Research*, vol. 209, p. 112860, Jun. 2022, doi: 10.1016/j.envres.2022.112860.
- [25] R. B. Chowdhury, G. A. Moore, A. J. Weatherley, and M. Arora, “Key sustainability challenges for the global phosphorus resource, their implications for global food security, and options for mitigation,” *Journal of Cleaner Production*, vol. 140, pp. 945–963, Jan. 2017, doi: 10.1016/j.jclepro.2016.07.012.

- [26] D. L. Childers, J. Corman, M. Edwards, and J. J. Elser, "Sustainability Challenges of Phosphorus and Food: Solutions from Closing the Human Phosphorus Cycle," *BioScience*, vol. 61, no. 2, pp. 117–124, Feb. 2011, doi: 10.1525/bio.2011.61.2.6.
- [27] B. Stürmer and M. Waltner, "Best Available Technology for P-Recycling from Sewage Sludge—An Overview of Sewage Sludge Composting in Austria," *Recycling*, vol. 6, no. 4, p. 82, Dec. 2021, doi: 10.3390/recycling6040082.
- [28] T. Li, M. Strous, and M. Melkonian, "Biofilm-based photobioreactors: their design and improving productivity through efficient supply of dissolved inorganic carbon," *FEMS Microbiology Letters*, vol. 364, no. 24, Dec. 2017, doi: 10.1093/femsle/fnx218.
- [29] M. Gross, W. Henry, C. Michael, and Z. Wen, "Development of a rotating algal biofilm growth system for attached microalgae growth with in situ biomass harvest," *Bioresource Technology*, vol. 150, pp. 195–201, Dec. 2013, doi: 10.1016/j.biortech.2013.10.016.
- [30] N. C. Boelee, H. Temmink, M. Janssen, C. J. N. Buisman, and R. H. Wijffels, "Balancing the organic load and light supply in symbiotic microalgal–bacterial biofilm reactors treating synthetic municipal wastewater," *Ecological Engineering*, vol. 64, pp. 213–221, Mar. 2014, doi: 10.1016/j.ecoleng.2013.12.035.
- [31] N. C. Boelee, M. Janssen, H. Temmink, R. Shrestha, C. J. N. Buisman, and R. H. Wijffels, "Nutrient Removal and Biomass Production in an Outdoor Pilot-Scale Phototrophic Biofilm Reactor for Effluent Polishing," *Appl Biochem Biotechnol*, vol. 172, no. 1, pp. 405–422, Jan. 2014, doi: 10.1007/s12010-013-0478-6.
- [32] V. Loomba, G. Huber, and E. von Lieres, "Single-cell computational analysis of light harvesting in a flat-panel photo-bioreactor," *Biotechnol Biofuels*, vol. 11, no. 1, p. 149, Dec. 2018, doi: 10.1186/s13068-018-1147-3.
- [33] F. Gao, Z.-H. Yang, C. Li, G.-M. Zeng, D.-H. Ma, and L. Zhou, "A novel algal biofilm membrane photobioreactor for attached microalgae growth and nutrients removal from secondary effluent," *Bioresource Technology*, vol. 179, pp. 8–12, Mar. 2015, doi: 10.1016/j.biortech.2014.11.108.
- [34] Z. Zhao, K. Muylaert, A. Szymczyk, and I. F. J. Vankelecom, "Enhanced microalgal biofilm formation and facilitated microalgae harvesting using a novel pH-responsive, crosslinked patterned and vibrating membrane," *Chemical Engineering Journal*, vol. 410, p. 127390, Apr. 2021, doi: 10.1016/j.cej.2020.127390.
- [35] T. Li, B. Podola, L. K. P. Schultze, and M. Melkonian, "Design scenario analysis for porous substrate photobioreactor assemblies," *J Appl Phycol*, vol. 31, no. 3, pp. 1623–1636, Jun. 2019, doi: 10.1007/s10811-018-1700-2.
- [36] R. J. Wicker, E. Kwon, E. Khan, V. Kumar, and A. Bhatnagar, "The potential of mixed-species biofilms to address remaining challenges for economically-feasible microalgal biorefineries: A review," *Chemical Engineering Journal*, vol. 451, p. 138481, Jan. 2023, doi: 10.1016/j.cej.2022.138481.
- [37] X. Zhao, K. Kumar, M. A. Gross, T. E. Kunetz, and Z. Wen, "Evaluation of revolving algae biofilm reactors for nutrients and metals removal from sludge thickening supernatant in a municipal wastewater treatment facility," *Water Research*, vol. 143, pp. 467–478, Oct. 2018, doi: 10.1016/j.watres.2018.07.001.

- [38] Y. T. Cheah and D. J. C. Chan, "Physiology of microalgal biofilm: a review on prediction of adhesion on substrates," *Bioengineered*, vol. 12, no. 1, pp. 7577–7599, Jan. 2021, doi: 10.1080/21655979.2021.1980671.
- [39] R. M. Donlan, "Biofilms: Microbial Life on Surfaces," *Emerg. Infect. Dis.*, vol. 8, no. 9, pp. 881–890, Sep. 2002, doi: 10.3201/eid0809.020063.
- [40] Y. T. Cheah and D. J. C. Chan, "A methodological review on the characterization of microalgal biofilm and its extracellular polymeric substances," *Journal of Applied Microbiology*, vol. 132, no. 5, pp. 3490–3514, May 2022, doi: 10.1111/jam.15455.
- [41] D. Li and H. Xi, "Layered Extraction and Adsorption Performance of Extracellular Polymeric Substances from Activated Sludge in the Enhanced Biological Phosphorus Removal Process," *Molecules*, vol. 24, no. 18, p. 3358, Sep. 2019, doi: 10.3390/molecules24183358.
- [42] J. Wang, Q. Li, M.-M. Li, T.-H. Chen, Y.-F. Zhou, and Z.-B. Yue, "Competitive adsorption of heavy metal by extracellular polymeric substances (EPS) extracted from sulfate reducing bacteria," *Bioresource Technology*, vol. 163, pp. 374–376, Jul. 2014, doi: 10.1016/j.biortech.2014.04.073.
- [43] R. Wang, Y. Peng, Z. Cheng, and N. Ren, "Understanding the role of extracellular polymeric substances in an enhanced biological phosphorus removal granular sludge system," *Bioresource Technology*, vol. 169, pp. 307–312, Oct. 2014, doi: 10.1016/j.biortech.2014.06.040.
- [44] B. D'Acunto, G. Esposito, L. Frunzo, M. R. Mattei, and F. Pirozzi, "Mathematical Modeling of Heavy Metal Biosorption in Multispecies Biofilms," *Journal of Environmental Engineering*, vol. 142, no. 9, p. C4015020, 2016, doi: 10.1061/(ASCE)EE.1943-7870.0001052.
- [45] J. Peng, K. Kumar, M. Gross, T. Kunez, and Z. Wen, "Removal of total dissolved solids from wastewater using a revolving algal biofilm reactor," *Water Environ Res*, vol. 92, no. 5, pp. 766–778, May 2020, doi: 10.1002/wer.1273.
- [46] A. Hodges, Z. Fica, J. Wanlass, J. VanDarlin, and R. Sims, "Nutrient and suspended solids removal from petrochemical wastewater via microalgal biofilm cultivation," *Chemosphere*, vol. 174, pp. 46–48, May 2017, doi: 10.1016/j.chemosphere.2017.01.107.
- [47] K. Zhou, Y. Hu, L. Zhang, K. Yang, and D. Lin, "The role of exopolymeric substances in the bioaccumulation and toxicity of Ag nanoparticles to algae," *Sci Rep*, vol. 6, no. 1, p. 32998, Dec. 2016, doi: 10.1038/srep32998.
- [48] M. Morales, H. Bonnefond, and O. Bernard, "Rotating algal biofilm versus planktonic cultivation: LCA perspective," *Journal of Cleaner Production*, vol. 257, p. 120547, Jun. 2020, doi: 10.1016/j.jclepro.2020.120547.
- [49] H. Ennaceri, T. Ishika, V. O. Mkpuma, and N. R. Moheimani, "Microalgal biofilms: Towards a sustainable biomass production," *Algal Research*, vol. 72, p. 103124, May 2023, doi: 10.1016/j.algal.2023.103124.
- [50] L. B. Christenson and R. C. Sims, "Rotating algal biofilm reactor and spool harvester for wastewater treatment with biofuels by-products," *Biotechnol. Bioeng.*, vol. 109, no. 7, pp. 1674–1684, Jul. 2012, doi: 10.1002/bit.24451.

- [51] M. Gross and Z. Wen, “Yearlong evaluation of performance and durability of a pilot-scale Revolving Algal Biofilm (RAB) cultivation system,” *Bioresource Technology*, vol. 171, pp. 50–58, Nov. 2014, doi: 10.1016/j.biortech.2014.08.052.
- [52] A. Ozkan, K. Kinney, L. Katz, and H. Berberoglu, “Reduction of water and energy requirement of algae cultivation using an algae biofilm photobioreactor,” *Bioresource Technology*, vol. 114, pp. 542–548, Jun. 2012, doi: 10.1016/j.biortech.2012.03.055.
- [53] E. P. Bennion, D. M. Ginosar, J. Moses, F. Agblevor, and J. C. Quinn, “Lifecycle assessment of microalgae to biofuel: Comparison of thermochemical processing pathways,” *Applied Energy*, vol. 154, pp. 1062–1071, Sep. 2015, doi: 10.1016/j.apenergy.2014.12.009.
- [54] U. Jena, K. C. Das, and J. R. Kastner, “Effect of operating conditions of thermochemical liquefaction on biocrude production from *Spirulina platensis*,” *Bioresource Technology*, vol. 102, no. 10, pp. 6221–6229, May 2011, doi: 10.1016/j.biortech.2011.02.057.
- [55] E. A. Couto, F. Pinto, F. Varela, A. Reis, P. Costa, and M. L. Calijuri, “Hydrothermal liquefaction of biomass produced from domestic sewage treatment in high-rate ponds,” *Renewable Energy*, vol. 118, pp. 644–653, Apr. 2018, doi: 10.1016/j.renene.2017.11.041.
- [56] K. M. Hillman and R. C. Sims, “Struvite formation associated with the microalgae biofilm matrix of a rotating algal biofilm reactor (RABR) during nutrient removal from municipal wastewater,” *Water Science and Technology*, vol. 81, no. 4, pp. 644–655, Feb. 2020, doi: 10.2166/wst.2020.133.
- [57] M. Wiatrowski *et al.*, “Techno-economic assessment for the production of algal fuels and value-added products: opportunities for high-protein microalgae conversion,” *Biotechnol Biofuels*, vol. 15, no. 1, p. 8, Dec. 2022, doi: 10.1186/s13068-021-02098-3.
- [58] M. Molazadeh, H. Ahmadzadeh, H. R. Pourianfar, S. Lyon, and P. H. Rampelotto, “The Use of Microalgae for Coupling Wastewater Treatment With CO₂ Biofixation,” *Front. Bioeng. Biotechnol.*, vol. 7, p. 42, Mar. 2019, doi: 10.3389/fbioe.2019.00042.
- [59] E. Schaedig *et al.*, “Isolation of phosphorus-hyperaccumulating microalgae from revolving algal biofilm (RAB) wastewater treatment systems,” *Front. Microbiol.*, vol. 14, p. 1219318, Jul. 2023, doi: 10.3389/fmicb.2023.1219318.
- [60] Y. Luo, P. Le-Clech, and R. K. Henderson, “Characterisation of microalgae-based monocultures and mixed cultures for biomass production and wastewater treatment,” *Algal Research*, vol. 49, p. 101963, Aug. 2020, doi: 10.1016/j.algal.2020.101963.
- [61] G. Padmaperuma, R. V. Kapoore, D. J. Gilmour, and S. Vaidyanathan, “Microbial consortia: a critical look at microalgae co-cultures for enhanced biomanufacturing,” *Critical Reviews in Biotechnology*, vol. 38, no. 5, pp. 690–703, Jul. 2018, doi: 10.1080/07388551.2017.1390728.
- [62] F. Meng *et al.*, “Effects of light intensity on oxygen distribution, lipid production and biological community of algal-bacterial granules in photo-sequencing batch reactors,” *Bioresource Technology*, vol. 272, pp. 473–481, Jan. 2019, doi: 10.1016/j.biortech.2018.10.059.

- [63] R. Mu *et al.*, “Advances in the use of microalgal–bacterial consortia for wastewater treatment: Community structures, interactions, economic resource reclamation, and study techniques,” *Water Environment Research*, vol. 93, no. 8, pp. 1217–1230, Aug. 2021, doi: 10.1002/wer.1496.
- [64] S. Iman Shayan, F. A. Agblevor, L. Bertin, and R. C. Sims, “Hydraulic retention time effects on wastewater nutrient removal and bioproduct production via rotating algal biofilm reactor,” *Bioresource Technology*, vol. 211, pp. 527–533, Jul. 2016, doi: 10.1016/j.biortech.2016.03.104.
- [65] G. B. Jones, R. C. Sims, and J. Zhao, “Experimental and theoretical investigations of rotating algae biofilm reactors (RABRs): Areal productivity, nutrient recovery, and energy efficiency,” *Biotech & Bioengineering*, p. bit.28451, Jun. 2023, doi: 10.1002/bit.28451.
- [66] G. Jones, D. Ellis, Z. Zhang, J. Zhao, and R. Sims, “Optimizing algae biofilm growth in wastewater treatment using predictive mathematical models,” in *Contemporary Research in Mathematical Biology: Modeling, Computation and Analysis*, in Contemporary Mathematics and Its Applications: Monographs, Expositions and Lecture Notes. , World Scientific, 2025. doi: 10.1142/12639.
- [67] B. Polizzi, A. Fanesi, F. Lopes, M. Ribot, and O. Bernard, “Understanding photosynthetic biofilm productivity and structure through 2D simulation,” *PLoS Comput Biol*, vol. 18, no. 4, p. e1009904, Apr. 2022, doi: 10.1371/journal.pcbi.1009904.
- [68] W. K. Dodds, B. J. F. Biggs, and R. L. Lowe, “Photosynthesis-irradiance patterns in benthic microalgae: variations as a function of assemblage thickness and community structure,” *J Phycol*, vol. 35, no. 1, pp. 42–53, Feb. 1999, doi: 10.1046/j.1529-8817.1999.3510042.x.
- [69] E. Erickson, S. Wakao, and K. K. Niyogi, “Light stress and photoprotection in *Chlamydomonas reinhardtii*,” *The Plant Journal*, vol. 82, no. 3, pp. 449–465, May 2015, doi: 10.1111/tpj.12825.
- [70] Z. T. Fica and R. C. Sims, “Algae-based biofilm productivity utilizing dairy wastewater: effects of temperature and organic carbon concentration,” *J Biol Eng*, vol. 10, no. 1, p. 18, Dec. 2016, doi: 10.1186/s13036-016-0039-y.
- [71] Y. Wang *et al.*, “The self-adaption capability of microalgal biofilm under different light intensities: Photosynthetic parameters and biofilm microstructures,” *Algal Research*, vol. 58, p. 102383, Oct. 2021, doi: 10.1016/j.algal.2021.102383.
- [72] S. L. Meng *et al.*, “Interaction Effects of Temperature, Light, Nutrients, and pH on Growth and Competition of *Chlorella vulgaris* and *Anabaena* sp. Strain PCC,” *Front. Environ. Sci.*, vol. 9, p. 690191, Jul. 2021, doi: 10.3389/fenvs.2021.690191.
- [73] Z. Yang, L. Geng, W. Wang, and J. Zhang, “Combined effects of temperature, light intensity, and nitrogen concentration on the growth and polysaccharide content of *Microcystis aeruginosa* in batch culture,” *Biochemical Systematics and Ecology*, vol. 41, pp. 130–135, Apr. 2012, doi: 10.1016/j.bse.2011.12.015.
- [74] D. Mu, R. Ruan, M. Addy, S. Mack, P. Chen, and Y. Zhou, “Life cycle assessment and nutrient analysis of various processing pathways in algal biofuel production,” *Bioresource Technology*, vol. 230, pp. 33–42, Apr. 2017, doi: 10.1016/j.biortech.2016.12.108.

- [75] J.-H. Wang, L.-L. Zhuang, X.-Q. Xu, V. M. Deantes-Espinosa, X.-X. Wang, and H.-Y. Hu, "Microalgal attachment and attached systems for biomass production and wastewater treatment," *Renewable and Sustainable Energy Reviews*, vol. 92, pp. 331–342, Sep. 2018, doi: 10.1016/j.rser.2018.04.081.
- [76] R. C. Sims, "Synergistic Municipal Wastewater Treatment Using a Rotating Algae Biofilm Reactor (RABR): SWIM Project EE0009271," presented at the DOE Bioenergy Technologies Office (BETO) 2023 Project Peer Review, Apr. 03, 2023. [Online]. Available: <https://www.energy.gov/sites/default/files/2023-04/beto-04-project-peer-review-algae-a-apr-2023-sims%20.pdf>
- [77] J. L. Wood, J. Y. Takemoto, and R. C. Sims, "Rotating Algae Biofilm Reactor for Management and Valorization of Produced Wastewater," *Front. Energy Res.*, vol. 10, p. 774760, Jan. 2022, doi: 10.3389/fenrg.2022.774760.
- [78] P. R. Goldsberry, "RABRs for Use in Biologically Enhanced Precipitation of Struvite in Anaerobic Digester Effluent (Municipal Wastewater)," Master's Thesis, Utah State University, 2023. Accessed: Oct. 19, 2023. [Online]. Available: <https://digitalcommons.usu.edu/etd2023/5>
- [79] H. Wickham, *ggplot2: Elegant Graphics for Data Analysis*, 2nd ed. 2016. in Use R! Cham: Springer International Publishing : Imprint: Springer, 2016. doi: 10.1007/978-3-319-24277-4.
- [80] R Core Team, *R: A Language and Environment for Statistical Computing*. Vienna, Austria: R Foundation for Statistical Computing, 2020. [Online]. Available: <https://www.R-project.org>
- [81] M. Zhang, K.-T. Leung, H. Lin, and B. Liao, "The biological performance of a novel microalgal-bacterial membrane photobioreactor: Effects of HRT and N/P ratio," *Chemosphere*, vol. 261, p. 128199, Dec. 2020, doi: 10.1016/j.chemosphere.2020.128199.
- [82] S. C. Foo, C. Y. Mok, S. Y. Ho, and N. M. H. Khong, "Microalgal culture preservation: Progress, trends and future developments," *Algal Research*, vol. 71, p. 103007, Apr. 2023, doi: 10.1016/j.algal.2023.103007.
- [83] M. Huesemann *et al.*, "DISCOVR strain pipeline screening – Part I: Maximum specific growth rate as a function of temperature and salinity for 38 candidate microalgae for biofuels production," *Algal Research*, vol. 71, p. 102996, Apr. 2023, doi: 10.1016/j.algal.2023.102996.
- [84] Y. Maltsev, K. Maltseva, M. Kulikovskiy, and S. Maltseva, "Influence of Light Conditions on Microalgae Growth and Content of Lipids, Carotenoids, and Fatty Acid Composition," *Biology*, vol. 10, no. 10, p. 1060, Oct. 2021, doi: 10.3390/biology10101060.
- [85] X. Li, S. Slavens, D. W. Crunkleton, and T. W. Johannes, "Interactive effect of light quality and temperature on *Chlamydomonas reinhardtii* growth kinetics and lipid synthesis," *Algal Research*, vol. 53, p. 102127, Mar. 2021, doi: 10.1016/j.algal.2020.102127.
- [86] E. Sforza, M. Pastore, S. M. Franke, and E. Barbera, "Modeling the oxygen inhibition in microalgae: An experimental approach based on photorespirometry," *New Biotechnology*, vol. 59, pp. 26–32, Nov. 2020, doi: 10.1016/j.nbt.2020.06.003.
- [87] M. Plöhn, K. Scherer, S. Stagge, L. J. Jönsson, and C. Funk, "Utilization of Different Carbon Sources by Nordic Microalgae Grown Under Mixotrophic

- Conditions,” *Front. Mar. Sci.*, vol. 9, p. 830800, Mar. 2022, doi: 10.3389/fmars.2022.830800.
- [88] R. Sekar, V. P. Venugopalan, K. Nandakumar, K. V. K. Nair, and V. N. R. Rao, “Early stages of biofilm succession in a lentic freshwater environment,” *Hydrobiologia*, vol. 512, no. 1–3, pp. 97–108, Jan. 2004, doi: 10.1023/B:HYDR.0000020314.69538.2c.
- [89] Y.-N. Wang *et al.*, “Growth and nutrients removal characteristics of attached *Chlorella* sp. using synthetic municipal secondary effluent with varied hydraulic retention times and biomass harvest intervals,” *Algal Research*, vol. 61, p. 102600, Jan. 2022, doi: 10.1016/j.algal.2021.102600.
- [90] N. C. Boelee *et al.*, “The effect of harvesting on biomass production and nutrient removal in phototrophic biofilm reactors for effluent polishing,” *J Appl Phycol*, vol. 26, no. 3, pp. 1439–1452, Jun. 2014, doi: 10.1007/s10811-013-0178-1.
- [91] B. Siville and W. J. Boeing, “Optimization of algal turf scrubber (ATS) technology through targeted harvest rate,” *Bioresource Technology Reports*, vol. 9, p. 100360, Feb. 2020, doi: 10.1016/j.biteb.2019.100360.
- [92] D. Dermoun, D. Chaumont, J.-M. Thebault, and A. Dauta, “Modelling of growth of *Porphyridium cruentum* in connection with two interdependent factors: Light and temperature,” *Bioresource Technology*, vol. 42, no. 2, pp. 113–117, Jan. 1992, doi: 10.1016/0960-8524(92)90069-A.
- [93] L. Pastor, D. Mangin, R. Barat, and A. Seco, “A pilot-scale study of struvite precipitation in a stirred tank reactor: Conditions influencing the process,” *Bioresource Technology*, vol. 99, no. 14, pp. 6285–6291, Sep. 2008, doi: 10.1016/j.biortech.2007.12.003.
- [94] X. Liu, G. Wen, Z. Hu, and J. Wang, “Coupling effects of pH and Mg/P ratio on P recovery from anaerobic digester supernatant by struvite formation,” *Journal of Cleaner Production*, vol. 198, pp. 633–641, Oct. 2018, doi: 10.1016/j.jclepro.2018.07.073.
- [95] A. M. Ibekwe, S. E. Murinda, M. A. Murry, G. Schwartz, and T. Lundquist, “Microbial community structures in high rate algae ponds for bioconversion of agricultural wastes from livestock industry for feed production,” *Science of The Total Environment*, vol. 580, pp. 1185–1196, 2017, doi: <https://doi.org/10.1016/j.scitotenv.2016.12.076>.
- [96] S. Chen *et al.*, “Lighting the way to sustainable development: Physiological response and light control strategy in microalgae-based wastewater treatment under illumination,” *Science of The Total Environment*, vol. 903, p. 166298, Dec. 2023, doi: 10.1016/j.scitotenv.2023.166298.
- [97] K. Sukačová, M. Trtílek, and T. Rataj, “Phosphorus removal using a microalgal biofilm in a new biofilm photobioreactor for tertiary wastewater treatment,” *Water Research*, vol. 71, pp. 55–63, Mar. 2015, doi: 10.1016/j.watres.2014.12.049.
- [98] J.D. Watkins, H. Abdellaoui, E. Barton, C. Lords, and R.C. Sims, “Dataset: compositional analysis and hydrothermal liquefaction of a high-ash microalgae biofilm,” *Data Br*, 2024.
- [99] J. D. Watkins *et al.*, “Techno-economic analysis of bioplastic production from a high-ash microalgae biofilm cultivated in municipal anaerobic digester effluent,” p. Manuscript in preparation, 2024.

- [100] S. Van Wychen and L. M. L. Laurens, "Determination of Total Solids and Ash in Algal Biomass: Laboratory Analytical Procedure (LAP)," NREL/TP-5100-60956, 1118077, Jan. 2016. doi: 10.2172/1118077.
- [101] H. Abdellaoui, "Catalytic Pyrolysis of Olive Mill Wastewater Sludge," 2015, doi: 10.26076/0609-916F.
- [102] M. M. Bradford, "A rapid and sensitive method for the quantitation of microgram quantities of protein utilizing the principle of protein-dye binding," *Analytical Biochemistry*, vol. 72, no. 1–2, pp. 248–254, May 1976, doi: 10.1016/0003-2697(76)90527-3.
- [103] A. Noyes, R. Godavarti, N. Titchener-Hooker, J. Coffman, and T. Mukhopadhyay, "Quantitative high throughput analytics to support polysaccharide production process development," *Vaccine*, vol. 32, no. 24, pp. 2819–2828, May 2014, doi: 10.1016/j.vaccine.2014.02.034.
- [104] L. M. L. Laurens, M. Quinn, S. Van Wychen, D. W. Templeton, and E. J. Wolfrum, "Accurate and reliable quantification of total microalgal fuel potential as fatty acid methyl esters by in situ transesterification," *Anal Bioanal Chem*, vol. 403, no. 1, pp. 167–178, Apr. 2012, doi: 10.1007/s00216-012-5814-0.
- [105] J. Park, H. J. Jeong, E. Y. Yoon, and S. J. Moon, "Easy and rapid quantification of lipid contents of marine dinoflagellates using the sulpho-phospho-vanillin method," *ALGAE*, vol. 31, no. 4, pp. 391–401, Dec. 2016, doi: 10.4490/algae.2016.31.12.7.
- [106] A. Tsigirika, M. Ntola, K. N. Kontogiannopoulos, A. J. Karabelas, and S. I. Patsios, "Optimization of Solvent Extraction of Lipids from *Yarrowia lipolytica* towards Industrial Applications," *Fermentation*, vol. 9, no. 1, p. 35, Dec. 2022, doi: 10.3390/fermentation9010035.
- [107] H.-Y. Shin, S.-H. Shim, Y.-J. Ryu, J.-H. Yang, S.-M. Lim, and C.-G. Lee, "Lipid Extraction from *Tetraselmis* sp. Microalgae for Biodiesel Production Using Hexane-based Solvent Mixtures," *Biotechnol Bioproc E*, vol. 23, no. 1, pp. 16–22, Feb. 2018, doi: 10.1007/s12257-017-0392-9.
- [108] S. Van Wychen and L. M. L. Laurens, "Determination of Total Carbohydrates in Algal Biomass: Laboratory Analytical Procedure (LAP)," NREL/TP-5100-60957, 1118073, Jan. 2016. doi: 10.2172/1118073.
- [109] K. K. Kesari *et al.*, "Wastewater Treatment and Reuse: a Review of its Applications and Health Implications," *Water Air Soil Pollut*, vol. 232, no. 5, p. 208, May 2021, doi: 10.1007/s11270-021-05154-8.
- [110] A. Igwaran, A. J. Kayode, K. M. Moloantoa, Z. P. Khetsha, and J. O. Unuofin, "Cyanobacteria Harmful Algae Blooms: Causes, Impacts, and Risk Management," *Water Air Soil Pollut*, vol. 235, no. 1, p. 71, Jan. 2024, doi: 10.1007/s11270-023-06782-y.
- [111] M. N. Hasan *et al.*, "Recent technologies for nutrient removal and recovery from wastewaters: A review," *Chemosphere*, vol. 277, p. 130328, Aug. 2021, doi: 10.1016/j.chemosphere.2021.130328.
- [112] J. L. Campos *et al.*, "Nitrogen and Phosphorus Recovery From Anaerobically Pretreated Agro-Food Wastes: A Review," *Front. Sustain. Food Syst.*, vol. 2, p. 91, Jan. 2019, doi: 10.3389/fsufs.2018.00091.

- [113] M. I. Khan, J. H. Shin, and J. D. Kim, "The promising future of microalgae: current status, challenges, and optimization of a sustainable and renewable industry for biofuels, feed, and other products," *Microb Cell Fact*, vol. 17, no. 1, p. 36, Dec. 2018, doi: 10.1186/s12934-018-0879-x.
- [114] F. G. Acién Fernández, C. Gómez-Serrano, and J. M. Fernández-Sevilla, "Recovery of Nutrients From Wastewaters Using Microalgae," *Front. Sustain. Food Syst.*, vol. 2, p. 59, Sep. 2018, doi: 10.3389/fsufs.2018.00059.
- [115] A. Bhatt, M. Khanchandani, M. S. Rana, and S. K. Prajapati, "Techno-economic analysis of microalgae cultivation for commercial sustainability: A state-of-the-art review," *Journal of Cleaner Production*, vol. 370, p. 133456, Oct. 2022, doi: 10.1016/j.jclepro.2022.133456.
- [116] K. DeRose, C. DeMill, R. W. Davis, and J. C. Quinn, "Integrated techno economic and life cycle assessment of the conversion of high productivity, low lipid algae to renewable fuels," *Algal Research*, vol. 38, p. 101412, Mar. 2019, doi: 10.1016/j.algal.2019.101412.
- [117] J. Hoffman, R. C. Pate, T. Drennen, and J. C. Quinn, "Techno-economic assessment of open microalgae production systems," *Algal Research*, vol. 23, pp. 51–57, Apr. 2017, doi: 10.1016/j.algal.2017.01.005.
- [118] J. Barlow, R. C. Sims, and J. C. Quinn, "Techno-economic and life-cycle assessment of an attached growth algal biorefinery," *Bioresource Technology*, vol. 220, pp. 360–368, Nov. 2016, doi: 10.1016/j.biortech.2016.08.091.
- [119] S.-H. Lee *et al.*, "Higher Biomass Productivity of Microalgae in an Attached Growth System, Using Wastewater," *Journal of Microbiology and Biotechnology*, vol. 24, no. 11, pp. 1566–1573, Nov. 2014, doi: 10.4014/jmb.1406.06057.
- [120] M. Audu *et al.*, "Ash-pretreatment and hydrothermal liquefaction of filamentous algae grown on dairy wastewater," *Algal Research*, vol. 57, p. 102282, Jul. 2021, doi: 10.1016/j.algal.2021.102282.
- [121] A. Alavianghavanini, N. R. Moheimani, and P. A. Bahri, "Producing protein-based products from microalgae cultivated on anaerobically digested abattoir effluent: Process integration and techno-economic analysis," *Bioresource Technology Reports*, vol. 25, p. 101734, Feb. 2024, doi: 10.1016/j.biteb.2023.101734.
- [122] S. S. Bulynina, E. E. Ziganshina, and A. M. Ziganshin, "Growth Efficiency of *Chlorella sorokiniana* in Synthetic Media and Unsterilized Domestic Wastewater," *BioTech*, vol. 12, no. 3, p. 53, Aug. 2023, doi: 10.3390/biotech12030053.
- [123] Y. Zhu, Schmidt, P. Valdez, L. Snowden-Swan, and S. Edmundson, "Hydrothermal Liquefaction and Upgrading of Wastewater-Grown Microalgae: 2021 State of Technology," Pacific Northwest National Laboratory, Richland, Washington, 99354, PNNL-32695, Mar. 2022. [Online]. Available: https://www.pnnl.gov/main/publications/external/technical_reports/PNNL-32695.pdf
- [124] Y. Arora, S. Sharma, and V. Sharma, "Microalgae in Bioplastic Production: A Comprehensive Review," *Arab J Sci Eng*, vol. 48, no. 6, pp. 7225–7241, Jun. 2023, doi: 10.1007/s13369-023-07871-0.
- [125] A. Safitri *et al.*, "The role of various plastisizers and fillers additions in improving tensile strength of starch-based bioplastics: A mini review," *IOP Conf. Ser.: Earth*

- Environ. Sci.*, vol. 1115, no. 1, p. 012076, Dec. 2022, doi: 10.1088/1755-1315/1115/1/012076.
- [126] A. A. Corcoran and R. W. Hunt, “Capitalizing on harmful algal blooms: From problems to products,” *Algal Research*, vol. 55, p. 102265, May 2021, doi: 10.1016/j.algal.2021.102265.
- [127] M. A. Zeller, R. Hunt, A. Jones, and S. Sharma, “Bioplastics and their thermoplastic blends from *Spirulina* and *Chlorella* microalgae,” *J of Applied Polymer Sci*, vol. 130, no. 5, pp. 3263–3275, Dec. 2013, doi: 10.1002/app.39559.
- [128] F. Lombardi *et al.*, “Chemical-Physical Characterization of Bio-Based Biodegradable Plastics in View of Identifying Suitable Recycling/Recovery Strategies and Numerical Modeling of PLA Pyrolysis,” *Waste Biomass Valor*, May 2023, doi: 10.1007/s12649-023-02159-8.
- [129] S. Onen Cinar, Z. K. Chong, M. A. Kucuker, N. Wiecek, U. Cengiz, and K. Kuchta, “Bioplastic Production from Microalgae: A Review,” *IJERPH*, vol. 17, no. 11, p. 3842, May 2020, doi: 10.3390/ijerph17113842.
- [130] T. A. Phung Hai *et al.*, “Flexible polyurethanes, renewable fuels, and flavorings from a microalgae oil waste stream,” *Green Chem.*, vol. 22, no. 10, pp. 3088–3094, 2020, doi: 10.1039/D0GC00852D.
- [131] S. Zhang, L. Zhang, G. Xu, F. Li, and X. Li, “A review on biodiesel production from microalgae: Influencing parameters and recent advanced technologies,” *Front. Microbiol.*, vol. 13, p. 970028, Jul. 2022, doi: 10.3389/fmicb.2022.970028.
- [132] T. Mutanda, D. Naidoo, J. K. Bwapwa, and A. Anandraj, “Biotechnological Applications of Microalgal Oleaginous Compounds: Current Trends on Microalgal Bioprocessing of Products,” *Front. Energy Res.*, vol. 8, p. 598803, Dec. 2020, doi: 10.3389/fenrg.2020.598803.
- [133] M. S. Peters, K. D. Timmerhaus, R. E. West, and R. E. West, *Plant design and economics for chemical engineers*, 5. ed, International ed. 2004. in McGraw-Hill chemical engineering series. Boston: McGraw-Hill, 2004.
- [134] R. Lemaire and M. Christensson, “Lessons Learned from 10 Years of ANITA Mox for Sidestream Treatment,” *Processes*, vol. 9, no. 5, p. 863, May 2021, doi: 10.3390/pr9050863.
- [135] S. O. Lourenço, E. Barbarino, P. L. Lavín, U. M. Lanfer Marquez, and E. Aidar, “Distribution of intracellular nitrogen in marine microalgae: Calculation of new nitrogen-to-protein conversion factors,” *European Journal of Phycology*, vol. 39, no. 1, pp. 17–32, Feb. 2004, doi: 10.1080/0967026032000157156.
- [136] L. M. L. Laurens *et al.*, “Algal Biomass Constituent Analysis: Method Uncertainties and Investigation of the Underlying Measuring Chemistries,” *Anal. Chem.*, vol. 84, no. 4, pp. 1879–1887, Feb. 2012, doi: 10.1021/ac202668c.
- [137] S. K. Mishra *et al.*, “Rapid quantification of microalgal lipids in aqueous medium by a simple colorimetric method,” *Bioresource Technology*, vol. 155, pp. 330–333, Mar. 2014, doi: 10.1016/j.biortech.2013.12.077.
- [138] *Process Economics Program (PEP) Yearbook*. IHS Markit, 2020.
- [139] W. Y. Chia, D. Y. Ying Tang, K. S. Khoo, A. N. Kay Lup, and K. W. Chew, “Nature’s fight against plastic pollution: Algae for plastic biodegradation and bioplastics production,” *Environmental Science and Ecotechnology*, vol. 4, p. 100065, Oct. 2020, doi: 10.1016/j.ese.2020.100065.

- [140] Y. Zhu *et al.*, “Microalgae Hydrothermal Liquefaction and Biocrude Upgrading: 2022 State of Technology,” PNNL-34032, 1962867, Mar. 2023. doi: 10.2172/1962867.
- [141] B. Klein and R. Davis, “Algal Biomass Production via Open Pond Algae Farm Cultivation: 2022 State of Technology and Future Research,” National Renewable Energy Laboratory, Golden, CO, NREL/TP-5100-85661. [Online]. Available: <https://www.nrel.gov/docs/fy23osti/85661.pdf>
- [142] K. S. Khoo, I. Ahmad, K. W. Chew, K. Iwamoto, A. Bhatnagar, and P. L. Show, “Enhanced microalgal lipid production for biofuel using different strategies including genetic modification of microalgae: A review,” *Progress in Energy and Combustion Science*, vol. 96, p. 101071, May 2023, doi: 10.1016/j.pecs.2023.101071.
- [143] Yahoo Finance, “North America Biodegradable Plastic Market Size, Share & Trends Analysis Report By Product, By Application, By Country And Segment Forecasts, 2022 – 2030,” Dec. 2022. [Online]. Available: <https://finance.yahoo.com/news/north-america-biodegradable-plastic-market-165400794.html>
- [144] Central Valley Water Reclamation Facility, “2022 Annual Biosolids Report,” South Salt Lake, UT., Feb. 2023.
- [145] L. Snowden-Swan *et al.*, “Wet Waste Hydrothermal Liquefaction and Biocrude Upgrading to Hydrocarbon Fuels: 2021 State of Technology,” PNNL-32731, 1863608, Apr. 2022. doi: 10.2172/1863608.
- [146] A. F. Miranda *et al.*, “Applications of microalgal biofilms for wastewater treatment and bioenergy production,” *Biotechnol Biofuels*, vol. 10, no. 1, p. 120, Dec. 2017, doi: 10.1186/s13068-017-0798-9.
- [147] T. Abrantes Silva *et al.*, “Enhancing microalgae biomass production: Exploring improved scraping frequency in a hybrid cultivation system,” *Journal of Environmental Management*, vol. 355, p. 120505, Mar. 2024, doi: 10.1016/j.jenvman.2024.120505.
- [148] Y. Zhu, S. B. Jones, A. J. Schmidt, K. O. Albrecht, S. J. Edmundson, and D. B. Anderson, “Techno-economic analysis of alternative aqueous phase treatment methods for microalgae hydrothermal liquefaction and biocrude upgrading system,” *Algal Research*, vol. 39, p. 101467, May 2019, doi: 10.1016/j.algal.2019.101467.
- [149] C. M. Godwin, D. C. Hietala, A. R. Lashaway, A. Narwani, P. E. Savage, and B. J. Cardinale, “Algal polycultures enhance coproduct recycling from hydrothermal liquefaction,” *Bioresource Technology*, vol. 224, pp. 630–638, Jan. 2017, doi: 10.1016/j.biortech.2016.11.105.
- [150] D. R. Haag, “Testing the resilience of microalgae biofilms when exposed to hydrothermal liquefaction aqueous phase,” Undergraduate Honors Capstone Project, Utah State University, 2024.

APPENDIXES

Appendix A: Statistical design, biomass productivity data, and effluent phosphorus data
for Chapter I

RABR	DW	AFDW	P_OUT	Trial	Temp	LightInt	HydRetTime	HarvFreq
1	8.38	7.62	4.81	0	2	1	1	0
2	6.15	5.62	4.86	0	2	1	1	2
3	5.99	5.41	2.49	0	2	1	2	2
4	5.91	5.25	3.77	0	2	1	2	2
5	6.28	5.67	3.68	0	2	1	2	0
6	4.89	4.25	1.40	0	2	1	2	1
7	9.56	8.24	2.92	0	2	1	0	1
8	6.26	5.47	3.03	0	2	1	1	2
9	6.05	5.43	2.69	0	2	1	2	2
10	4.72	4.10	2.24	0	2	2	2	1
11	5.14	4.50	3.90	0	2	2	2	2
12	6.24	5.48	4.17	0	2	2	2	0
13	4.70	4.03	8.22	0	2	2	2	1
14	5.97	5.27	11.09	0	2	2	0	0
15	5.89	5.13	10.20	0	2	2	1	2
16	5.62	4.71	9.79	0	2	2	1	1
17	7.08	6.07	4.60	0	2	2	1	1
18	6.22	5.45	3.87	0	2	2	1	2
19	6.14	5.64	2.54	0	2	0	1	1
20	5.53	4.99	2.91	0	2	0	1	1
21	4.27	3.78	1.78	0	2	0	1	2
22	2.90	2.57	2.29	0	2	0	2	1
23	3.97	3.60	3.18	0	2	0	2	0
24	4.30	3.94	1.50	0	2	0	2	1
25	4.17	3.78	6.11	0	2	0	2	0
26	4.53	4.09	3.70	0	2	0	1	2
27	11.46	10.58	4.85	0	2	0	0	2
28	2.75	2.33	2.65	0	1	0	2	1
29	2.75	2.47	2.30	0	1	0	2	2
30	5.05	4.46	8.86	0	1	0	1	0
31	5.42	4.90	7.39	0	1	0	0	0
32	5.66	5.07	6.28	0	1	0	0	2
33	1.97	1.64	3.35	0	1	0	2	2
34	3.13	2.83	3.74	0	1	0	2	1
35	2.21	1.99	4.51	0	1	0	2	2
36	2.87	2.59	14.68	0	1	0	0	0
37	2.90	2.51	11.96	0	1	1	1	2
38	7.46	6.82	4.78	0	1	1	0	0
39	1.92	1.64	17.34	0	1	1	0	2
40	3.97	3.44	2.14	0	1	1	1	0
41	5.16	4.62	5.46	0	1	1	0	2
42	2.04	1.81	12.81	0	1	1	0	1
43	6.74	6.05	4.11	0	1	1	0	1
44	3.71	3.19	5.38	0	1	1	1	1

45	2.08	1.81	17.42	0	1	1	0	1
46	7.49	6.56	3.94	0	1	2	0	0
47	8.32	7.18	3.60	0	1	2	1	0
48	5.30	4.45	6.60	0	1	2	0	0
49	5.37	4.60	7.88	0	1	2	1	0
50	3.91	3.36	4.85	0	1	2	1	1
51	5.44	4.61	9.02	0	1	2	0	2
52	5.74	4.93	2.90	0	1	2	1	0
53	3.84	3.14	7.43	0	1	2	1	2
54	7.70	6.54	5.78	0	1	2	0	0
55	4.52	4.04	6.52	0	0	2	1	1
56	7.64	6.77	6.63	0	0	2	0	1
57	7.39	6.48	8.31	0	0	2	0	2
58	6.26	5.74	6.41	0	0	2	0	0
59	7.60	6.65	4.99	0	0	2	0	1
60	6.96	6.29	5.95	0	0	2	0	1
61	3.71	3.35	2.40	0	0	2	2	0
62	3.79	3.40	2.73	0	0	2	2	2
63	3.53	3.27	5.33	0	0	2	1	0
64	5.04	4.49	4.74	0	0	1	1	1
65	5.19	4.68	4.68	0	0	1	0	2
66	4.10	3.70	2.56	0	0	1	2	0
67	3.64	3.31	4.70	0	0	1	0	2
68	3.56	3.27	1.45	0	0	1	2	1
69	2.74	2.46	7.70	0	0	1	2	0
70	3.19	2.76	6.15	0	0	1	1	0
71	2.94	2.66	6.55	0	0	1	1	0
72	4.85	4.41	3.53	0	0	1	0	1
73	4.59	4.25	8.17	0	0	0	0	2
74	3.33	3.05	1.42	0	0	0	2	2
75	4.21	3.90	5.61	0	0	0	0	1
76	2.93	2.62	5.43	0	0	0	1	1
77	4.52	4.21	7.37	0	0	0	0	0
78	2.88	2.64	3.72	0	0	0	2	0
79	4.01	3.63	2.75	0	0	0	2	1
80	4.34	3.93	3.41	0	0	0	1	2
81	3.41	3.20	1.79	0	0	0	2	0
1	3.39	2.18	8.87	1	0	1	0	2
2	0.94	0.67	6.23	1	0	2	2	2
3	5.30	4.63	0.85	1	1	2	2	1
4	0.61	0.42	6.84	1	0	2	2	2
5	8.00	7.24	17.84	1	2	1	0	2
6	5.20	4.70	17.61	1	2	0	0	1
7	3.71	3.02	1.37	1	2	2	2	0
8	7.25	6.61	12.53	1	2	0	1	0
9	1.38	0.93	8.51	1	0	1	1	1
10	6.25	5.01	3.45	1	2	2	1	0
11	3.41	2.90	4.24	1	1	1	2	2
12	6.94	6.04	5.96	1	0	1	2	0
13	1.77	1.33	8.61	1	0	2	0	1
14	7.56	5.97	6.33	1	2	1	1	2
15	0.18	0.10	6.57	1	0	0	2	1
16	4.99	4.10	5.51	1	1	2	1	2

17	9.98	8.90	12.38	1	1	1	0	1
18	1.31	0.95	6.41	1	0	1	1	1
19	6.74	5.90	9.33	1	1	2	0	0
20	3.16	2.82	25.00	1	1	0	0	2
21	1.50	1.28	4.23	1	1	1	1	0
22	2.33	1.90	28.68	1	1	0	1	1
23	2.48	2.05	2.25	1	1	1	2	0
24	13.26	11.88	7.56	1	2	2	0	2
25	0.60	0.31	8.42	1	0	0	0	0
26	1.69	1.13	6.83	1	0	0	1	2
27	7.10	5.56	5.22	1	2	0	2	1
28	5.56	4.34	1.84	1	2	1	2	1
29	5.55	4.70	8.39	1	1	0	2	0
30	9.02	7.44	11.69	1	2	0	2	2
31	2.71	1.76	9.18	1	0	0	0	0
32	3.36	2.52	11.14	1	1	0	1	2
33	3.93	3.44	6.72	1	0	2	1	0
34	11.10	9.06	3.88	1	2	2	1	1
35	4.02	3.33	11.84	1	2	1	0	0
36	6.30	5.43	8.53	1	1	2	0	1
1	12.29	10.79	7.51	2	1	0	2	0
2	5.22	4.18	2.73	2	1	2	1	0
3	1.26	0.80	6.99	2	0	0	2	1
4	6.17	5.16	8.06	2	2	1	2	1
5	2.11	1.84	9.25	2	0	2	1	0
6	10.59	9.57	14.66	2	1	1	0	2
7	6.77	5.55	2.99	2	1	1	1	0
8	0.53	0.43	7.66	2	0	1	1	1
9	13.75	11.85	3.78	2	2	2	0	2
10	3.06	2.25	13.66	2	1	0	1	1
11	7.72	5.99	1.99	2	2	2	2	0
12	17.66	16.35	7.37	2	2	1	0	0
13	11.95	10.81	6.84	2	1	1	0	1
14	7.57	6.24	3.15	2	1	2	1	2
15	6.32	5.05	8.97	2	2	0	1	2
16	8.48	7.14	3.67	2	1	0	2	1
17	1.77	1.44	10.57	2	0	0	0	0
18	4.34	2.85	8.14	2	0	1	0	2
19	6.09	5.67	18.49	2	1	0	0	2
20	10.94	9.75	2.98	2	1	1	2	2
21	3.30	2.76	5.99	2	0	1	1	1
22	11.96	10.42	6.92	2	2	1	1	2
23	0.65	0.44	7.17	2	0	0	0	0
24	16.25	15.15	3.50	2	2	2	1	1
25	11.95	10.36	7.20	2	1	2	0	0
26	2.89	2.14	7.91	2	0	0	1	2
27	1.11	0.90	9.75	2	0	2	2	2
28	1.44	0.93	8.04	2	0	1	2	0
29	8.68	8.09	8.72	2	2	0	2	2
30	8.39	7.80	15.94	2	2	0	0	1
31	13.28	12.11	8.99	2	2	0	1	0
32	3.39	2.88	4.16	2	1	2	2	1
33	1.89	1.76	6.05	2	0	2	2	2

34	6.61	5.65	4.11	2	2	1	2	0
35	1.16	0.89	9.24	2	0	2	0	1
36	11.07	10.13	3.47	2	2	2	0	1

Appendix B: Mineral compositions data for microalgae biofilm and biochar samples.

	Ca	P	S	K	Mg	Al	As	B	Ba	Cd	Co	Cr
	%					mg / kg						
L_biomass	3.47	0.74	0.76	0.8	0.51	91	3.48	26.1			0.9	1.5
P_biomass	5.75 ± 0.03	4.74 ± 1.12	0.67 ± 0.04	0.39 ± 0.06	1.96 ± 1.08	2382.93 ± 6.42	2.98 ± 4.18	39.4 ± 3.08	504.76 ± 22.8	3.6 ± 0.35	3.05 ± 0.11	34.02 ± 1.06
L_biochar_2 80	8.22	0.1	1.07	2.94	1.01	1340	0.03	27.15	142.95	1	4.3	24.85
L_biochar_3 50	24.65	0.08	2.94	7	1.02	2734.23	0.47	6.55	297.48	2.88	2.8	55.36
P_biochar_2 80	12.17 ± 1.37	0.24 ± 0.05	3.44 ± 1.42	9.24 ± 0.9	0.57 ± 0.13	6968.38 ± 816.53	1.47 ± 2.5	22.22 ± 1.74	1120.94 ± 127.84	8.28 ± 0.86	6.34 ± 0.58	77.61 ± 12.99
P_biochar_3 50	12.46 ± 1.33	0.26 ± 0.02	3.95 ± 1.83	9.8 ± 1.56	0.57 ± 0.14	7523.82 ± 633.93	2.82 ± 1.67	21.59 ± 1.24	1134.09 ± 119.67	8.54 ± 1.28	6.36 ± 0.71	78.66 ± 9.78

	Cu	Fe	Mn	Mo	Na	Ni	Pb	Se	Si	Sr	Zn
	mg / kg										
L_biomass	46.3	879.2	18.6	2.2	4887	1	3			236.1	36.5
P_biomass	381.41 ± 12.17	19938.82 ± 770.58	218.27 ± 4.84	4.69 ± 0.32	5922.23 ± 387.93	30.74 ± 0.59	16.63 ± 0.24	3.92 ± 4.66	1702.47 ± 253.35	611.12 ± 10.26	1451.94 ± 32.68
L_biochar_ 280	583	7725	137.6	14.5	1000	34.15	8.8	0.03	2797.5	542	492.45
L_biochar_ 350	912.46	11904.57	335.57	18.69	1062.3	95.39	23.94	0.03	4956.62	1523.66	863.17
P_biochar_ 280	805.05 ± 101	44971.82 ± 5191.96	468.46 ± 41.61	9.37 ± 1.2	4168.09 ± 2443.4	67.27 ± 10.07	38.94 ± 4.94	10.18 ± 8.29	4084.34 ± 1233.6	1277.51 ± 139.21	3044.77 ± 386.92
P_biochar_ 350	830.45 ± 117.18	45700.61 ± 5079.14	483.14 ± 29.57	10.65 ± 0.89	4759.92 ± 1618.91	68.16 ± 9.14	42.11 ± 3.51	11.99 ± 1.56	4669.36 ± 540.46	1303.27 ± 136.47	3092.01 ± 372.4

Appendix C: Techno-economic analysis results for the hydrothermal liquefaction
conversion process

Case	Baseline	Intermediate	Final	Final + AD solids
Biocrude production, GGE/yr	3,644	6,167	9,111	302,124
Biocrude yield, GGE/ton algae AFDW	51.8	51.8	51.8	72.6
Installation Cost (2020 US \$)				
Algae storage	\$68,000	\$101,000	\$135,000	\$0
HTL biocrude production	\$372,000	\$527,000	\$682,000	\$4,399,000
Balance of plant	\$44,000	\$62,000	\$80,000	\$221,000
Total Installed Capital Cost	\$484,000	\$690,000	\$897,000	\$4,620,000
Total Capital Investment	\$884,000	\$1,290,000	\$1,697,000	\$8,620,000
Operating Cost, \$/GGE				
Natural gas	0.33	0.33	0.33	0.23
Electricity and other utilities	0.09	0.09	0.09	0.06
Byproduct credit	-3.21	-3.21	-3.21	-1.83
Fixed costs	52.6	31.7	21.9	3.55
Capital depreciation	7.96	6.65	5.82	0.9
Average income tax	2.37	1.97	1.73	0.27
Average return on investment	16.7	15	13.7	2.04
Minimum fuel selling price (MFSP)	76.8	52.6	40.4	5.32

Appendix D: Considerations for future research based on observations during experimental testing of laboratory RABR productivity

This appendix describes additional analysis that was performed for the Trial 1 RABRs described in chapter II. Biomass samples collected from these RABRs were quantified weekly and analyzed on an average-productivity basis (total g biomass / total cultivation period) and on a productivity-over-time basis (total produced in harvesting period n / length of harvesting period, where n is 1, 2, 3, etc. and spans the full cultivation period). To determine whether there was a relationship between biomass productivity and time since inoculation, productivity was measured over time and plotted in Excel (Table 18). These differences may be related to changes in the relative abundance of various biofilm community members over time and to increased cellulolytic activity and degradation of the cotton substrate.

Table 18. Harvest-harvest productivity variations for Rotating Algae Biofilm Reactors in Trial 1 (Excel Sparklines).

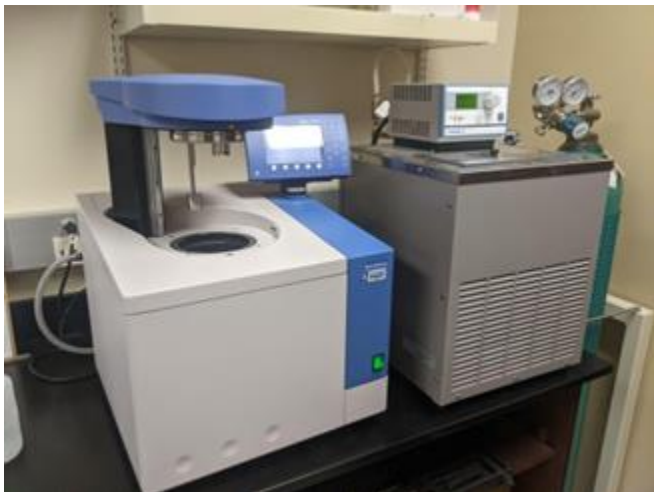
RABR	Temp	LightInt	HarvFreq	HRT	Sparkline
1	2	2	1	0	1
2	2	2	1	2	1
3	2	2	1	2	2
4	2	2	1	2	2
5	2	2	1	0	2
6	2	2	1	1	2
7	2	2	1	1	0
8	2	2	1	2	1
9	2	2	1	2	2
10	2	2	2	1	2
11	2	2	2	2	2
12	2	2	2	0	2
13	2	2	2	1	2
14	2	2	2	0	0
15	2	2	2	2	1
16	2	2	2	1	1
17	2	2	2	1	1
18	2	2	2	2	1
19	2	2	0	1	1
20	2	2	0	1	1
21	2	2	0	2	1
22	2	2	0	1	2
23	2	2	0	0	2
24	2	2	0	1	2
25	2	2	0	0	2
26	2	2	0	2	1
27	2	2	0	2	0
28	1	2	0	1	2
29	1	2	0	2	2
30	1	2	0	0	1
31	1	2	0	0	0
32	1	2	0	2	0
33	1	2	0	2	2
34	1	2	0	1	2
35	1	2	0	2	2
36	1	2	0	0	0
37	1	2	1	2	1
38	1	2	1	0	0
39	1	2	1	2	0
40	1	2	1	0	1

Table 1 continued

RABR	Temp	LightInt	HarvFreq	HRT	Sparkline
41	1	1	1	2	0
42	1	1	1	1	0
43	1	1	1	1	0
44	1	1	1	1	1
45	1	1	1	1	0
46	1	1	2	0	0
47	1	1	2	0	1
48	1	1	2	0	0
49	1	1	2	0	1
50	1	1	2	1	1
51	1	1	2	2	0
52	1	1	2	0	1
53	1	1	2	2	1
54	1	1	2	0	0
55	0	0	2	1	1
56	0	0	2	1	0
57	0	0	2	2	0
58	0	0	2	0	0
59	0	0	2	1	0
60	0	0	2	1	0
61	0	0	2	0	2
62	0	0	2	2	2
63	0	0	2	0	1
64	0	0	1	1	1
65	0	0	1	2	0
66	0	0	1	0	2
67	0	0	1	2	0
68	0	0	1	1	2
69	0	0	1	0	2
70	0	0	1	0	1
71	0	0	1	0	1
72	0	0	1	1	0
73	0	0	0	2	0
74	0	0	0	2	2
75	0	0	0	1	0
76	0	0	0	1	1
77	0	0	0	0	0
78	0	0	0	0	2
79	0	0	0	1	2
80	0	0	0	2	1
81	0	0	0	0	2

Appendix E: Standard Operating Procedures

E.1 Bomb Calorimetry



Equipment

Bomb Calorimeter

Water Bath

Sodium Benzoate Standard

Methyl Orange

Sodium Carbonate (3.76 g/L)

Nitrile gloves

Oxygen gas

Protocol

1. Turn on water bath and bomb calorimeter. Wait for the water bath to reach 19C.
2. Find the bomb vessel and accessories in the box labelled DV #1 or bomb chamber #1. Wear gloves when handling the bomb chamber and the crucible to prevent contamination with oil from your hands.
3. Attach thread to the bomb calorimeter's sparking wire and check that the connections are secure.
4. Add 0.5g sample to the crucible. Before using your test samples, verify that the bomb calorimeter is working correctly using a 0.5g sample of sodium benzoate.
5. Place crucible in bomb with thread in contact with the sample. Submerging or placing the thread underneath the sample can help ensure that the thread won't lose contact with the sample.

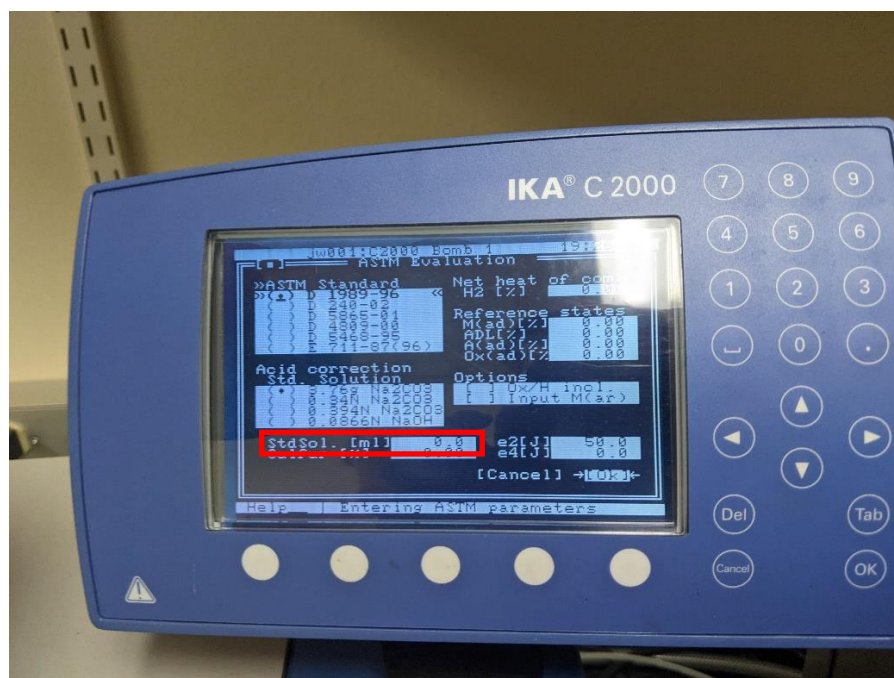


6. Close the bomb chamber and place in the calorimeter.
7. Enter the sample's mass and provide a label for the sample. This can be your initials and an identifier to help you keep track of the sample.
8. Evaluate the sample ("Start").
9. Record the sample's raw HHV.
10. Remove the crucible from the bomb chamber.
11. Release pressure from the bomb chamber in a fume hood, remove the threaded ring, and open chamber using the cap release tool. Don't use pliers or other non-standard tools to open the bomb chamber or remove the threaded ring.



Image: pressure release tool (left) and cap release tool (right)

12. Rinse the sample remnants into a small beaker using DI water.
13. Add a spatula-sized piece of methyl orange to the solution.
14. Titrate with Sodium Carbonate (Na_2CO_3).
15. Record titration volume as the standard solution.



16. Record sample's adjusted HHV.
17. Clean the bomb and the crucible with ethanol and paper towels.
18. Drain and close the bomb calorimeter water chamber before turning the bomb calorimeter and water bath off.

Menu -> Maintenance -> Drain IV

Menu -> System -> Exit or Menu -> Maintenance -> close MC

E.2 Parr Pressure Vessel



Equipment

500ml Parr pressure vessel

PTFE or graphite gaskets

Adjustable torque wrench with $\frac{3}{8}$ " spline adapter

High temperature - high pressure grease and anti-seize lubricant

Nitrogen tank

Fume Hood

Goggles

Lab coat

Nitrile Gloves

Ear protection

Setting up the pressure vessel:

This protocol is used for loading and pressurizing a 500ml Parr stirred-tank pressure vessel. This pressure vessel is used for high-temperature, high-pressure reactions, such as hydrothermal liquefaction, subcritical transesterification, and hydrolysis by subcritical water. *Note: don't turn on the heater until all setup steps have been completed.*

1. *Ensure that all vent ports on top of the pressure vessel are connected to vent to a fume hood.* Byproducts of reaction processes may be toxic or otherwise harmful to health.
2. *Ensure that the water line is connected to a flowing water source.* A failure to cool the vessel properly will result in an over pressurized vessel that will expel contents in the vessel at high speed into the immediate area which can cause severe injury.
3. *Ensure that the solenoid for the water line is working properly.* The solenoid can be tested by pressurizing the solenoid with tap water and plugging the solenoid into the wall. Alternatively, set the controller temperature to below 20C (room temp). When the solenoid is triggered, water should be released simultaneously from the motor cooling line and from the reaction cooling line. When the solenoid has not been triggered, water should only flow from the motor cooling line. Plug the solenoid back into the temperature controller after testing the solenoid.
4. *Ensure that the propeller on the vessel is turning without issue.* If it isn't turning or doing so with great difficulty, apply high pressure / high temperature lubricant to the joints of the upper motor and verify that no vent attachments have been over torqued. If attachments are screwed in too far, they can prevent motor rotation. If the reaction proceeds without stirring, the temperature controller will overheat the vessel and may build pressure beyond the safety rupture disc's capacity.
5. *Check the PTFE or Graphite gasket for signs of wear.* Graphite gaskets should be replaced every 1-2 uses and PTFE gaskets should be replaced every 4-6 uses.



6. *Load biomass into the steel pressure vessel and lift the vessel into place.* To raise the vessel, pull the arm pin and raise the arm until it locks in position under the pressure vessel top. Next, turn the knob on the top right of the machine to raise the arm until the steel container is seated on the upper portion of the vessel. For sensitive samples, line the vessel with a clean glass liner before adding your sample.
7. *Attach the fastening sleeves to seal the pressure vessel.* After clipping the sleeves together, tighten all bolts by hand. Next, tighten bolts in 10 ft-lbs increments until all screws are torqued to 35 ft-lbs. Use a star pattern to avoid uneven loading on the gasket.



8. *Pressurize the vessel to 2 MPaG and check for leaks.* Leaks can be detected by listening closely for a hissing sound and by watching the pressure gauge for a decrease in pressure. Check closely for loose fittings and partially-open valves.

A second technician must verify the following points:

- a. All vent ports are connected to a fume hood
- b. All bolts are tightened to 35 ft-lbs.
- c. No leaks are audible after pressurization with nitrogen and tank pressure appears constant.
- d. The water-cooling line is connected to an active water source and the solenoid is functioning properly.
- e. The motor impeller is rotating properly.

Both technicians must be present for the entire pressurizing/depressurizing process.

E.3 Hydrothermal Liquefaction

Prior to starting this protocol, complete all steps in “setting up the pressure vessel” and ensure that a second technician has verified that the vessel is set up correctly. This protocol can be modified for other pressurized processes by modifying the initial pressure, operating temperature, and reaction time.

Operating conditions:

2 MPaG initial pressure (nitrogen atmosphere)
300 ml biomass slurry (approx. 20% solids content)
350°C operating temperature
15 MPaG operating pressure
30-minute reaction time

1. *Flush the pressure vessel with pure nitrogen.* This is done by pressurizing and depressurizing the vessel three times using pure nitrogen gas.
2. *Pressurize the vessel to 2 MPaG, disconnect the pressure vessel from the nitrogen tank, and check for leaks.* Also verify that the impeller attached to the motor and rotating and that water is running through the cooling line.
3. *Lift the heating sleeve into place and begin heating the vessel.* Use the Parr controller to set the reaction temperature. This is done by using the up and down arrow keys to adjust the value.
4. *Monitor the pressure and temperature during the heating process.* Final pressure should be 12-15 MPaG. Record the start and end time of the heating process to calculate an average temperature change per minute. Expect temperature to increase at approximately 10°C per minute.
 - If pressure exceeds 20 MPaG, turn off the heating unit and set the cooling solenoid to “ALWAYS ON”. Leave the room while the pressure vessel returns to a safe pressure.
 - Wear ear protection, safety goggles, and a lab coat for the entire pressurization / depressurization process.
5. *Allow the reaction to proceed for 30 minutes.* If there are no pressurization issues, start a timer when the internal vessel temperature reaches 350°C. After 30 minutes, turn off the heater and set the solenoid to remain open. This can be done manually or by programming the Parr 3148 controller as described in the controller manual.
6. *Allow the internal vessel temperature to reach 20°C.* Lower the heating unit to allow the vessel to cool more quickly. Use heat-resistant gloves when handling the heating unit. Leave the impeller motor on during the cooling process.

E.4 Analyzing HTL Products

Solid phase

1. *Prepare a vacuum filter with a clean, tared, 1.6 μ m filter.* This will be used to separate the HTL solid phase from the aqueous and non-polar phases. Record the mass of the clean filter.
2. *Transfer the contents of the pressure vessel to the vacuum filter.* Use dichloromethane or chloroform to rinse residual oil and aqueous solutes from the pressure vessel and the impeller. Use a metal brush to remove residual char from the interior walls of the pressure vessel and the impeller. If a secondary container is used when transferring the sample to the vacuum filter, this container should also be rinsed with dichloromethane or chloroform. All steps which involve solvents should be performed in a fume hood.
3. *Filter the biocrude and aqueous phase products using the vacuum filter.* Rinse the cake with dichloromethane or chloroform until the filtrate is clear.
4. *Dry the solid phase and filter overnight at 60°C.* After drying, weigh the filter and solids until a constant weight is achieved. Analysis of the aqueous and biocrude fractions can be performed while the solid phase dries.
5. *After drying, measure the following properties:*

Elemental composition (CHNS-O)

Mineral and heavy metal content (e.g. Phosphorus, Calcium, Selenium, etc.)

Biocrude phase

1. *Transfer the filtered liquid into a separatory funnel and separate the aqueous and biocrude phases.* Mix the two phases in the vacuum filter using a magnetic stir bar before transferring.
2. *Distill solvents from the biocrude phase using a rotary evaporator.* Once the volume of biocrude has been sufficiently reduced (e.g. 10-20 ml remain in the evaporator flask), transfer the biocrude phase into tared aluminum pans for drying. Rinse the rotovap flask with fresh DCM to collect all residual oil from the flask (usually 3-5 rinses). Evaporate the remaining DCM from the samples overnight in the fume hood and then again at 40°C.

The following rotovap settings can be used to recover dichloromethane and chloroform:

100 mbar vacuum pressure

40°C water bath

-10°C cooling coil (50/50 glycol/water mixture)

120 RPM

E.5 Lyophilization

Materials:

-80°C freezer
Lyophilizer
Filter paper
Vacuum pump oil

Protocol:

1. Freeze samples overnight at -80°C. For large samples, lyophilization can be accelerated by freezing samples in a shape with a high surface area to volume ratio.
2. Prepare the lyophilizer:
 - a. Check the vacuum pump oil level.
 - b. Place a protective filter in the sample vessel attachment piece.



- c. Rotate all unused sample valves to the closed position.



Image: open (right) and closed (left) sample valves

3. Switch lyophilizer power to “ON.” Vacuum and temperature settings can be adjusted using the “menu” and “selection” buttons on the lyophilizer display.
4. Place your frozen sample in the sample holder and attach the sample holder to the lyophilizer. Rotate the sample valve to the open position.
5. Lyophilize for 24-72 hours or until your sample is dry.

E.6 Dry Weight - 60°C

<https://www.nrel.gov/docs/fy16osti/60956.pdf>
Section 10.1.6-10.1.7

Protocol:

1. Place samples on tared aluminum weighing pans in a thin layer.
2. Place samples in oven at 60°C.
3. Allow samples to dry for at least 18h and until a constant weight is achieved.

Solids content in each sample can be calculated using the following equation:

$$\text{solids content (wt\%)} = (\text{mass after drying (g)} - \text{tare}) / (\text{mass before drying (g)} - \text{tare})$$

E.7 Ash Free Dry Weight with a ramp-capable muffle furnace

<https://www.nrel.gov/docs/fy16osti/60956.pdf>
Section 10.2.2 through 10.2.2.4

Ramping program:

- Ramp from room temp to 105°C
- Hold at 105°C for 12 minutes
- Ramp to 250°C at 10°C/minute
- Hold at 250°C for 30 minutes
- Ramp to 575°C at 20°C/minute
- Hold at 575°C for 180 minutes
- Allow temperature to drop to 105°C
- Hold at 105°C until samples are removed

Ramping Protocol:

1. Place samples on tared aluminum weighing pans.
2. Dehydrate sample by lyophilization or by drying at 60°C until a stable weight is achieved.
3. Place samples in the muffle furnace and start the ramping program.
4. Remove the ashed samples from the muffle furnace and allow to cool to room temperature in a desiccator.
5. Weigh the pan and ashed sample and record the weight in a lab notebook to the nearest 0.1 mg to constant weight.

Ash content in each sample can be calculated using the following equation:

$$\text{ash content (wt\%)} = (\text{dry mass after ashing (g)} - \text{tare}) / (\text{dry mass before ashing (g)} - \text{tare})$$

E.8 Ash Free Dry Weight in a non-ramping muffle furnace

<https://www.nrel.gov/docs/fy16osti/60956.pdf>
Section 10.2.1 - 10.2.1.6

NOTE: If a muffle furnace with a ramping program is not available, samples must be pre-ignited to avoid starting a fire in the furnace.

Non-ramping Protocol:

1. Using an ashing burner and a clay triangle on a stand, heat the crucible containing the oven-dry sample until smoke appears.
2. Immediately ignite the smoke and allow the sample to burn (reignite the smoke if necessary) until no more smoke or flame appears.
3. Allow the crucible to cool on a suitable surface before placing it in the muffle furnace.
4. Place the cool sample in the muffle furnace at $575^{\circ}\text{C} \pm 25^{\circ}\text{C}$ for 24 ± 6 hours. Handle the pre-ignited samples with care while placing them in or taking them out of the furnace to prevent sample loss.
5. Remove the ashed samples from the muffle furnace and allow them to cool to room temperature in a desiccator.
6. Weigh the crucible and ashed sample and record the weight in a lab notebook to the nearest 0.1 mg to constant weight (section 3.5).

Ash content in each sample can be calculated using the following equation:

$$\text{ash content (wt\%)} = (\text{dry mass after ashing (g)} - \text{tare}) / (\text{dry mass before ashing (g)} - \text{tare})$$